UNIVERSITY OF SOUTHAMPTON

FACULTY OF ENGINEERING, SCIENCE & MATHEMATICS

School of Engineering Sciences

Effects of Varying Strain-Rate on the Behaviour of FRP Yacht Hull Structure under Slam Load Conditions

by

Corrado Labriola

Thesis for the degree of Master of Philosophy

September 2006

UNIVERSITY OF SOUTHAMPTON

ABSTRACT

FACULTY OF ENGINEERING, SCIENCE & MATHEMATICS
SCHOOL OF ENGINEERING SCIENCES

Master of Philosophy

EFFECTS OF VARYING STRAIN-RATE ON THE BEHAVIOUR OF FRP YACHT HULL STRUCTURE UNDER SLAM LOAD CONDITIONS

by Corrado Labriola

The recent progress of the performance of sailing yachts has been driven by the continuing use and development of lightweight sandwich structures made of polymeric composite materials. So far the structural design of sailing yachts has relied on static or quasi-static approaches which usually lead to conservative design. Sailing yachts undergo several diverse dynamic loads in a seaway. Rigs and rigging, deck and hull have to be designed to withstand local and distributed loads whose entity is always difficult to determine. In this respect, the phenomenon of slamming, namely the impact of the hull bottom against the water surface in a rough sea, and its effects on the structure represent a crucial issue.

This implies that when structural optimisation is required it is necessary to better define the external loads and the strain-rate properties of the material utilized.

With this in mind, this thesis explores the dynamic response of a FRP (fibre reinforced plastics) sandwich hull panel subject to slam loads.

This is achieved initially by investigating experimentally the dynamic properties of FRP under rates of strain typically experienced by sailing yacht structures. A systematic methodology is then proposed to describe the strain-rate behaviour of the material by LS-DYNA explicit finite element code. This methodology is subsequently applied to examine the response of a hull panel to a slam load.

It is shown that the ALE (Arbitrary Lagrangian-Eulerian) method, within LS-DYNA code, is suitable to model the fluid-structure interaction slam problem and to assess the relative entity of the load to be used in the panel analysis.

A static finite element analysis of the panel is also carried out based on standard design rules. Results are compared with the dynamic approach presented and the conservativeness of the static method is underpinned.

Developing the knowledge of both the dynamic properties of the materials and the use of tools such as explicit finite element codes is shown to be a valid approach to optimise the design of sailing structures under slam load.

LIST OF CONTENTS

LIST OF FIGURES

LIST OF TABLES

DECLARATION OF AUTHORSHIP

I, Corrado Labriola, declare that the thesis entitled "**Effects of Varying Strain-Rate on the Behaviour of FRP Yacht Hull Structure under Slam Load Conditions**" and the work presented in it are my own. I confirm that:

- This work was done wholly or mainly while in candidature for a research degree at this University;
- Where any part of this thesis has previously been submitted for a degree or any other qualification at this University or any other institution, this has been clearly stated;
- Where I have consulted the published work of others, this is always clearly attributed;
- Where I have quoted from the work of others, the source is always given. With the exception of such quotations, this thesis is entirely my own work;
- I have acknowledged all main sources of help;
- Where the thesis is based on work done by myself jointly with others, I have made clear exactly what was done by others and what I have contributed myself;
- None of this work has been published before submission.

Signed: …….

Date: …….

ACKNOWLEDGEMENTS

First of all I would like to thank the EPSRC for funding my research and Professor R.A. Shenoi for his patience and valuable advice throughout.

This M.Phil. is an important achievement for me. It is not just the title itself that I value rather the emotions I have experienced during this chapter of my life. I came to the UK in 2001, speaking broken English but full of enthusiasm and keen to face this new challenge. I have met so many people, from every part of the world, with cultural and religious backgrounds similar or completely different from mine. These people have enriched my ego and my soul and made me learn to understand myself better. I hope I have left good memories in their minds too. Probably in the Ship Science department somebody will miss the Italian coffee aroma travelling from the pantry all along the corridor of the upper floor. Many colleagues and professors were attracted and often joined to taste the golden liquid or just to share a relaxed laugh. Facing the afternoon, or even better, every day of your life with a smile on your face always helps. That's why since I met Kate I started feeling even more smiley than I usually am. She brightened up my life and made me feel so good. She helped me to achieve this M.Phil. more than anyone else. She knows what I went through as two months earlier she achieved her Ph.D. We went through a difficult time, academia apart, but we understood how strong we are as individuals and that together we can be even stronger. Life has tested and will always test us presenting always new challenges that we will face with a smile on our faces. It would be boring otherwise. These words probably come from the DNA my "mamma" passed me. She is such a strong woman and she has always supported me. She has taught me so many things, first of all to smile and to be optimistic; then she taught me on the phone lots of recipes which have been useful when I invited Kate for dinner. My mamma is the real lighthouse of my life.

Also thanks for being always there to my brother Giuseppe and my best friend Francesco. If my mum is the lighthouse you two are the red and green buoy at the entrance of the harbour! Grazie.

NOMENCLATURE

A	Strain-rate dependent coefficient
ABS	American Bureau of Shipping
ALE	Arbitrary Lagrangian Eulerian
CAD	Computer Aided Design
E_{ij}	Young's Moduli in the i-j plane
F.E.M.	Finite Element Method
f.s.i	Fluid structure interaction
FGRP	Fibre Glass Reinforced Plastics
FRP	Fibre Reinforced Plastics
f_w	Design category factor
G_{ij}	Shear Moduli in the i-j plane
k_l	Longitudinal impact factor
k_s	Sailing craft hull pressure reduction factor
L_H	Length of the hull
L_{WL}	Length of water line
m	Experimental parameter
n	Experimental parameter
NAFEMS	National association of finite element methods and standards
P_{bsbase}	Sailing craft bottom pressure
P_{eq}	Equivalent static pressure
P_{max}	Maximum pressure
PVC	Polyvinyl Chloride
q_l	Stiffness modulus under dynamic loading
q_o	Stiffness modulus under quasi-static loading
SAN	Styrene Acrilo-Nitrile
SR	Strain-Rate
T_C	Draft of canoe body
u.d.	Unidirectional
U_v	Impact velocity

β	Experimental parameter
ε_{ij}	Strain in the i-j plane
$\varepsilon_{u\ STATIC}$	Static ultimate strain
ε_{u}	Ultimate strain
λ	Experimental parameter
ν_{12}	Poisson Ratio
ρ	Water density
σ_{D}	Dynamic component of the stress
σ_{ij}	Stress in the i-j plane
σ_{S}	Static component of the stress
$\sigma_{u\ STATIC}$	Static ultimate strength
σ_{u}	Ultimate strength
ψ	Impact dead-rise angle
$[\theta]_{n}$	Unidirectional ply made of n layers forming an angle θ with the principal direction

1 Introduction

1.1 Motivation

This thesis explores the structural response of a sailing-yacht sandwich hull panel subject to slam loads, namely those loads generated during the impact of the hull bottom against the water surface in a rough sea (figure 1-1), by means of a strain-rate approach. In other words, stresses and deformations are evaluated considering their dependence on the velocity at which materials strain.

Figure: 1-1 Racing Boat made of FRP undergoing slamming

The motivation comes from the formidable progress of the performance of sailing-yachts, owing to new possibilities opened by the use of polymeric composite materials. Better understanding of the mechanical phenomena and new tools such as finite element analysis have contributed to this development. Accurate predictions of dynamic loads and structural response are the challenge designers have to face in their daily jobs. In this respect, the phenomenon of slamming and its effects on the structure represent a crucial issue. So far, this problem has been treated by empirical approaches which usually lead to conservative design.

Recently, the belief that minor structural failures initiated by slamming loads are common has stimulated researchers to look into the phenomena more accurately (Manganelli et al., 2003; Le Sourne et al., 2003; Ojeda et al., 2004; Sebastiani et al., 2001; Thomas et al., 2001; Hentinen and Holm, 1994).

The aim of this research is to promote the knowledge of the dynamic response of cored hull structures undergoing slamming.

A sandwich panel is one made of two stiff strong skins, usually FRP (fibre-reinforced plastics) in marine applications, separated by a lightweight core material, usually polymeric foam or cellular materials. It is well established that the dynamic properties of the constituent materials of a sandwich panel can equally play a significant role with respect to the general response of the panel, at certain rates of deformation (Vinson, 1999). Consequently, the dynamic properties of both core and skins have to be known in order to perform a strain-rate analysis. However, polymeric foams do not show significant strain-rate sensitivity in the strain-rate ranges concerned with boats applications (Mahfuz et al., 2000; Saha et al., 2005; Zhao, 1997). This suggests that more attention has to be paid in investigating the dynamic properties of the composite skins when studying the response of sandwich structures where such cores are used.

In the past decades, composites have become among the most preferred materials in design where a combination of lightness and strength is required. Unlike other materials, the properties of composites can be designed according to the application. This can be achieved by altering variables such as volume fraction of each component, lay-up sequence, shape of the reinforcing and manufacturing procedure. As a result, the uniqueness of the material properties is obtained. Hence the overall behaviour of each composite material depends on several factors and this entails a very difficult task in determining and interpreting their properties. The task becomes even harder when the dynamic properties are sought.

The aeronautical, naval and automotive industries' progress in designing ever more sophisticated composite structures has generated a great deal of interest in understanding the dynamic properties of composite materials. In order to meet the requirements of these industries, several research works have been carried out on diverse composite materials, mainly at high-strain rate. Due to the complexity of the phenomena involved and the diversity of variables concerned with these materials, the results obtained are few and uncertain. Besides, very little experimental data are available on composite materials at low-medium strain-rate

ranges typical of boats applications (0-80s^{-1}) (Riber, 1997). This makes the strain-rate behaviour of composite materials a relatively unexplored area and a challenging task for designers.

As stated before, the ultimate goal of this work is to assess the structural response of a sailing-yacht sandwich hull panel subject to slam loads. Both the knowledge of the dynamic properties of the materials and the characterization of the slam loads are required for this purpose.

It has been established that the influence of the dynamic properties of the skin material plays a key role on the response of sandwich panels to slam phenomena. With this in mind, the first step of this thesis is to investigate experimentally the strain-rate behaviour of E-glass/epoxy, a widely adopted FRP material in marine sandwich constructions.

E-glass/epoxy is one of the most used materials in the boat industry where a compromise between costs and performances is required. With this in mind, a theoretical study is conducted on an E-glass/epoxy sandwich panel using the DK46 sailing-yacht as a case study. A novel experimental approach to investigate E-glass/epoxy dynamic properties is conducted and data are presented in the strain-rate range of interest which has not been previously investigated.

Subsequently, numerical modelling of the experiments is proposed to establish a systematic methodology aimed at describing the strain-rate behaviour of E-glass/epoxy material. Once the modelling has been demonstrated to be valid, the same methodology is applied to the investigation of more general problems where the same type of material is deployed, in particular, the behaviour of the skins of the panel under examination.

Slam loads depend on a multitude of factors related to the boat dimensions, performance, and sea conditions, which make it practically impossible to identify two similar slamming events. A numerical modelling approach is used to evaluate slam loads by means of a fluid-structure interaction simulation. The time-pressure distribution on the area of the hull subject to the impact is obtained and it is then applied in the strain-rate based analysis of the sandwich panel.

In chapter two, a review on the slam loads dynamics of sailing yachts hulls is presented and discussed. The past and present approaches used to assess slam loads on sailing yachts are examined, and the issues involved in evaluating the loads are highlighted. Chapter three presents a review of the latest development in strain-rate in composite materials.

Table 1 shows the most investigated composite materials and the relative strain-rate range concerned with each application. The highlighted area in table 1 shows the material glass-epoxy and the strain-rate range (0-80s^{-1}) relative to the applications of interest in this research. It also shows a lack of data between 40s^{-1} and 80s^{-1} which is examined in this research.

Table 1-1: Strain-Rate investigation of Composite Structures

Structural Applications	Aeronautical (object impact), Marine, military applications (blast waves)	Automotive (crash worthiness)	Marine, fast power boats ,ocean sailing yachts (slamming)
			
Strain rate ranges concerned [s^{-1}]	up to 1000	up to 500	up to 80
Materials investigated			
Glass/epoxy	covered	covered	covered up to 40 s^{-1}, lack of data 40-80 s^{-1}
Carbon/epoxy	covered	covered	covered up to 40 s^{-1}, lack of data 40-80 s^{-1}
Kevlar/epoxy	covered	covered	covered up to 40 s^{-1}, lack of data 40-80 s^{-1}

2 Critical Review on the Slam Loads Dynamics of Sailing Yachts Hull

2.1 Introduction

The following review presents the current state of the art in the slam loads dynamics of a sailing-yacht hull. Previous studies have focused on static consideration on the materials' properties and on experimental evaluation of the slamming loads.

Up to now, yacht structures have been designed according to empirical rules, coming from the experience and static considerations, which accounted for the dynamic effects by considering coefficients of ignorance (Hobbs and McEwen, 2002). This is mainly because of costs-benefits assessments which suggested that a conservative design is more convenient than an analytical one (Curry, 1987; Marchant, 1994; Larsson and Eliasson, 2000). The different classing societies have formulated scantling rules to be followed. The most accredited standards are provided by ABS which proposes a specific guide for Ocean Racing Yachts (ORY, 1994).

For pleasure boats, a new ISO Standard is being developed that will replace the standards for boats below 24 m in length. It is largely based on ABS standards, the ORY 1994 and the High Speed Craft Guide (HSC, 1997) together with NBS-VTT extended rule, 1997.

A sailing yacht undergoes several diverse dynamic loads in a seaway. Rigs and rigging, deck and hull have to be designed to withstand local and distributed loads whose entity is always difficult to determine. This is especially the case for the loads on the hull due to slamming effects which lead to significant strain-rates in the hull if compared to other structural components of the yacht. As a consequence, the design of the hull becomes a critical issue. Few examples of damages have been reported in the literature due to slamming. It is also true that most of the existing yachts are cruising-yachts, which statistically are unlikely to encounter rough sea in their life time and moreover their structures are designed adopting high safety factors. Most of failures reported regarded racing-yachts, for example

Boomerang VII 42 ft, and were concerned mainly with composite sandwich structures. The failure happens as a delamination initiation and propagation along the slamming area as shown in figure 2-1. Consequences can be dramatic irrespective of where the failure happens, e.g. in the middle of an ocean race miles away from the coast.

Figure 2-1: Delamination initiation due to slamming in a 42 ft racing sailing yacht. Source: Larson and Eliasson, 2000

The formidable progress of the performance of sailing yachts has highlighted the need of designing lighter yet still reliable structures. Better understanding of the mechanical phenomena, the material properties and new tools such as finite element analysis, have contributed to this development. Accurate predictions of dynamic loads and structural response are the challenge designers have to face in their jobs. In this respect, the phenomenon of slamming and its effects on the structure represent a crucial issue. This motivated researchers to look into the phenomena more accurately. However, there remains much more research to be done in this field.

2.2 Structural and Design Considerations

Fibre-reinforced plastic (FRP) composites are the most commonly used building materials for sailing yachts and high speed light craft hulls. This is mainly because of the high strength to weight ratio of the material, which is ideal for construction of ship hulls and makes it a cost efficient material. Besides, FRP are corrosion resistant and have a low maintenance cost.

A structural hull design is primarily based on the knowledge of the ultimate load conditions the particular vessel will encounter during its life time. The

dimensioning loads for the hull of fast sailing yachts are mainly impact loads due to vertical acceleration of the hull penetrating the water surface, i.e. slamming. From these design loads the preliminary hull layout can begin and each structural member can be dimensioned. The approach to the structural design of sailing yachts relies somewhat traditionally on static or quasi-static consideration regarding loading aspects.

This is primarily due to the difficulties concerning the determination of the dynamic loads involved and the lack of knowledge on the dynamic properties of the materials adopted, especially if the latter are composites. Therefore designers have always dimensioned their structures according to empirical assessments.

The state of the art of sailing yacht structures design can be found in Larsson and Eliasson, 2000 and Claughton et al., 1998. In chapter 11 of the Claughton et al., 1998 Belgrano and McFarlan, designers at SP technologies and one of the most advanced companies on the market with regard to yacht design and manufacturing, describe the key aspects involved in design. In their structural analysis they use the pressure suggested by the ABS (American Bureau of Shipping) guide 1994 but rather than using the flexural properties coming from the simplistic rule of mixture approach adopted in classification guides, they use the ones obtained by means of an in-house made panel laminate code. They also made the following considerations about core material issues with regard to sandwich structures' design. They formulated a core shear strength database of about fifty crafts ranging in overall length from 6.6-45m, which included designs that either failed in core or which were proven to be safe. Subsequently, a program was created to account for the previous information on materials and geometry and the specifications of the new boat to be designed. This program gives a dimensionless constant F to be utilized for the current design. It can be seen that for a matter of costs and time a simplistic empirical approach is preferred to an optimization by means of experimental and fem technique which account for strain-rate effects.

As a consequence, these considerations lead to conservative designs which often result in heavier and more expensive structures. These reasons have encouraged researchers in looking into the dynamics of the phenomena involved in slamming

both from the fluid-structure interaction and the structure response point of view. Most previous works aimed at determining the loads acting on ships structures and fast motor crafts while very little has been done on sailing yachts.

2.3 Investigation of Slamming Loads

As stated before, slamming loads are crucial loads to be considered in dimensioning boats' structures. These are modelled by pressure over the hull. More precisely the slamming pressure represents an irregular load acting on the hull of fast sailing yachts, which is due to the impact of the bottom of the hull against the water surface. As a result a sudden change of the relative acceleration of the boat is caused. Typically, as the forward sections of the boat strike the water surface, the hull panels in the slamming area are affected by a highly non-uniform pressure distribution with peak values that can reach a thousand times the order of magnitude of the hydrostatic pressure. These peaks only act on a very limited area (smaller than the average panel size) and for a very short time period (less 50 ms). In designing FRP hull panels, the slamming pressure is generally the dimensioning load. This is why in the past decades many efforts have been made in order to better understand the phenomenon and achieve advances in design.

2.3.1 Experimental approaches

A simple way to model a hull slamming pressure is to consider the problem of a wedge penetrating a liquid surface. Several two dimensional analyses of this type have been published. Pioneering works have been made by von Karman, 1929 while investigating the impact of seaplane floats during landing. He presented a simple solution to the impact problem based on the conservation of the momentum. In his theory, a wedge-shaped body of mass M and of a dead-rise angle ? strikes a horizontal surface of water with the velocity U? and generates a two-dimensional flow (figure 2-2). The maximum pressure is found at the moment of first contact and given by $p_{\max} = \left(rU_v^2/2\right)\cdot p \cdot \cot y$. The wedge is considered to be rigid and to enter the liquid with a velocity normal to the liquid surface. Neither hull flexibility nor forward speed is taken into account.

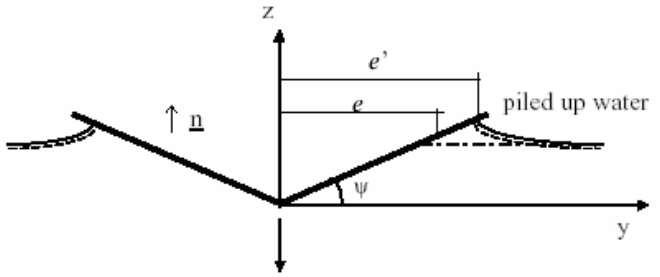

Figure 2-2: Wedge shaped body for slamming analysis approach by von Karman, 1929

A later contribution by Allen and Jones, 1978 proposed a simplified method for determining structural design limit pressures on fast crafts by assessing the momentary pressure distribution over a planning hull in head sea. This method is based on extensive full-scale trials conducted on 65-ft and 95-ft slender planning V-shaped hull and on large scale structural models in the laboratory. The hull is subjected to highest pressure in the region where the combined effects of incident velocity and relative geometry is worst (figure 2-3).

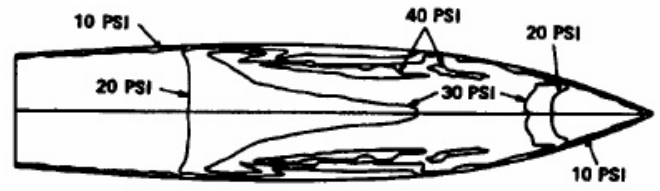

Figure 2-3: Example of momentary pressure distribution on a planning hull according to Allen and Jones, 1978

Savitsky, 1964 synthesised large amounts of experimental data on planning craft in calm water into design formulas for prediction of lift, running attitude, resistance and stability. He also derived semi-empirical equations for prediction of impact acceleration of planning craft on waves.

Based on the approaches followed by the pioneers of slamming investigations, several works have been proposed in the literature aimed at determining the loads acting on the hull of ships and fast motor boats. Hagiwara and Yuhara, 1976 investigated the characteristics of wave impact pressure acting on the bows of very large ships and their structural response by means of drop tests on three-dimensional semi-cylindrical 1/3 scale bow models. From the results, they

concluded that the maximum impact pressure as measured on the model plating was not distributed uniformly and simultaneously and was not considered to directly contribute to the structural response of the plating. Many agree that since the time duration of the phenomenon is very short, it can be argued that the peak pressures have little importance for the overall panel response. For design purposes, it is therefore convenient to average the pressure over a period of time and a given area in order to ease the correlation between slamming and strain response, in other words to represent these loads by an equivalent static pressure uniformly distributed over the panel. When the duration of the pressure pulse is considerably longer than the natural periods of the panel, this pressure can simply be taken as the spatial average of the real hydrodynamic load. Accordingly, they defined an equivalent static pressure as P_{eq}, which was converted from the maximum transient strain of the panel into uniformly distributed static pressure. In the severest conditions, the magnitude of P_{eq} was of the order of one third of P_{max}.

A more recent work on slamming has been produced by Vredeveldt at al., 2001. Their approach consisted of considering a slam as an impact introducing vibrations in the ship structure. The response of a shell subjected to a slam can be described by a set of natural vibrations modes. They showed that the natural frequencies yield a base for damage prediction. In light of these considerations they instrumented a model with an appropriately designed transducer to measure the impact loads.

As can be inferred, for obvious economic reasons dictated by industries needs, most of research works have been focused on large ships. Only recently, the formidable progress of the performance of sailing yachts has stimulated the interest of some researchers in investigating slamming in the sailing boats field. A very interesting and unique research work has been presented by Manganelli et al., 2001. They instrumented a $1/7^{th}$ model of an Open 60 class boat with slam patches in order to measure the hydrodynamic forces acting on the hull as a result of slamming loads (figure 2-4). Manganelli et al., 2001 took into account the forward speed of the yacht as well as the influence of the heel angle by testing different configurations, reproducing in this way a realistic slamming of the yacht sailing upwind. This particular measurement technique provided an evaluation of

equivalent "static" loads for a specific sailing yacht, but offered a valid reference for qualitative consideration applied to similar yachts. The following figure shows the crucial areas where slamming has its effects on a sailing boat and where the patches have consequently been placed.

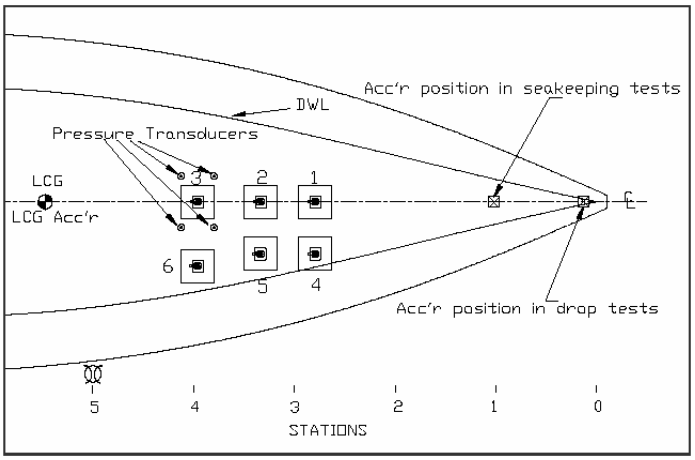

Figure 2-4: Model instrumented with patches for pressure measurement by Manganelli et al., 2001

Hentinen and Holm, 1994 conducted load measurements due to slamming on a 9.4m sailing yacht. They stated that slamming loads are independent on the hull structure but dependent on the hull geometry. According to their results, they found that the measured slamming pressures exceeded the design pressures that are normally used. However, this does not seem to damage the majority of the existing structures, since these are built by use of very conservative safety factors. Another reason why this is so can be found in the non linear response of the hull panels when these are made of single skin FRP. As a matter of fact, most of the stresses and deflections of hull panels are usually calculated with linear theories. In fact, the bending behaviour of FRP is characterized by remarkable geometric nonlinearities due to the large panel's size and relatively low stiffness of the plate thickness. This is especially so for structures designed for the maximum stress rather than for the maximum deflection. In this paper Hentinen and Holm, 1994 pointed out the need to investigate both slam loads and structural response more accurately in order to improve the current scantling rules.

2.3.2 Numerical Approaches

Most experimental works have not been confirmed by numerical simulation due to the lack of suitable tools. Recently, advances have been made by Souli, 2001 and Le Sourne et al., 2003 in the simulation of slamming loads by means of finite element method figure 2-5. They managed to accurately simulate experimental drop tests on a scaled model of a ship through a numerical code which accounted for the dynamic interaction fluid structures. For this purpose, the ALE method (arbitrary Lagrangian-Eulerian) within LS-DYNA explicit finite element code was used. The feature of this method is to adopt two mesh types in the analysis. The Lagrangian mesh, associated with the typical finite element analysis, is used to model the material impacting the fluid. This mesh deforms as it responds to the loading and the boundary conditions in the analysis. The Eulerian mesh is used to model the fluids (water and air), and remains fixed throughout the analysis tracking material as it moves through the mesh.

Olovsson and Souli, 2000, 2001 worked on the development of a new ALE algorithm to be implemented in LS-DYNA which allowed very accurate slam load predictions to be perfrormed. They validated this method by simulating the experimental drop test of a V-shaped cylinder conducted by Zhao et al., 1997. The numerical force-time plots' comparison confirmed the accuracy and reliability of the method.

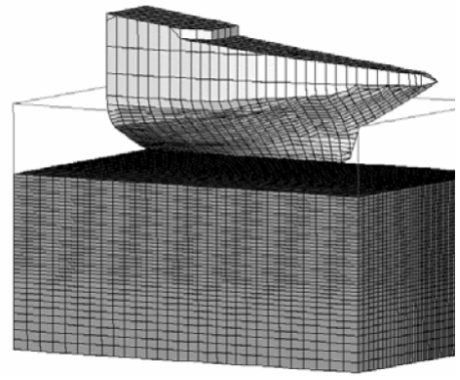

Figure 2-5: F.e.m. Ship Slamming Simulation by Le Sourne et al., 2003

Cappello and Mancuso, 2001 conducted an interesting research work on the optimization of the lay-up for the hull of a racing sailing yacht (figure 2-6). They performed an FE structural analysis in three different sailing configurations with the aim of obtaining the fibre directions that allow the minimization of the yacht deformability due to the slam effects. This study did not consider either the dynamic loads coming from typical slamming pressures or the dependence of the mechanical properties on the strain-rate.

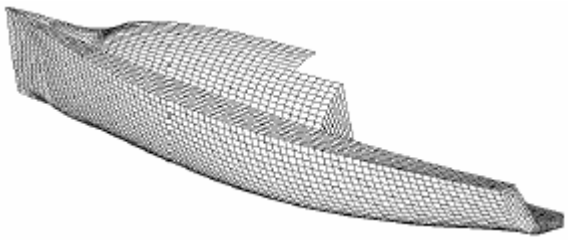

Figure 2-6: Finite element mesh of the hull by Cappello and Mancuso, 2001

Ojeda et al., 2004 carried out a finite element investigation on the response of a composite catamaran under slamming loads (figure 2-7). They investigate the response of the structure to quasi-static slamming loads according to "Det Norske Veritas High Speed and Light Craft" crest landing and hollow landing rules. In addition, they carried out an optimisation study for the structural response by changing the ply orientation in the vessel. The whole study was conducted using a static linear approach which cannot be satisfactory when an optimisation of the strength and weight of the structure is required.

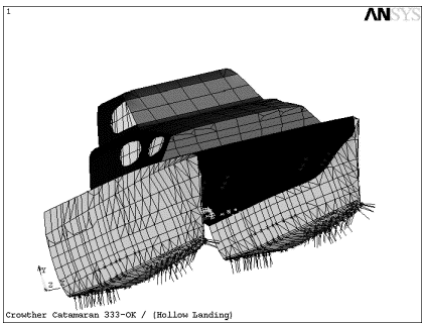

Figure 2-7: Load application in the f.e.m. model Ojeda et al., 2004

All the research works reviewed so far aim mainly at determining the loads acting on hulls undergoing slamming. Few investigations of the hull structural response have been conducted and most of them are concerned with metal structures. Besides, none of them are based on a strain-rate analysis approach.

2.4 Dynamic Response of Sandwich plates

The concept of sandwich construction for boat structures and other marine applications is not new. As known, a sandwich panel is one made of two stiff strong skins separated by a lightweight core material. The primary advantage of using the sandwich concept in a FRP hull instead of a stiffened single-skin structure is the built-in flexural stiffness of the sandwich, which makes the stiffener system unnecessary. The bending and the in-plane stresses are mainly carried by the faces, whereas the shear stresses are taken by the core (Zenkert, 1995).

Stresses and deflections of hull panels are usually calculated with linear theories. In fact, the bending behaviour of FRP hull panels can be characterized by remarkable geometric nonlinearities depending on the size of the panel. Pronounced lateral deflections introduce in-plane displacements and membrane strains in the faces, as well as shear deformation in the core. Thus, the classical Kirchhoff plate theory is not sufficient to describe this kind of response. Several researchers attempted to develop non-linear calculation methods to describe the response of hull panels, to be consequently used in hull design.

A recent work by Riber, 1997 outlines a geometrical nonlinear theory based on the classical sandwich plate theory expanded by the higher-order terms in the strain displacement relations, including shear deformation. By use of the principle of minimum potential energy, Riber, 1997 derived two different analytical solutions for the simply supported and the clamped cases. The solutions were then presented as simple design formulae.

Another key advantage of sandwich structures is their shock resistance capacity. This is particularly of interest to the navy and many other applications, such as the aerospace, automotive and sporting industries. Structures in these applications are often subjected to high strain-rates due to impact by hard objects, mine blast, projectile impact, collision, etc.

Many research projects have been funded mainly by the defence industry in order to explore the behaviour of sandwich structures at a high rate of strain. The approach followed by several researchers is to investigate at first the strain-rate response of the constituent materials separately and subsequently of the whole sandwich assembly (Mahfuz et al., 2002, 2006; Saha et al., 2005; Chacravarty et al., 2004). Between the two constituents, the core material is believed to play a more crucial role, in high strain-rate applications, especially those concerned with shock loads. As a consequence, more attention is paid in analyzing the core material rather than the skins.

The core materials tested, which are also deployed in the leisure boat industry, are usually polymeric foams, such as PVC (polyvinyl chloride), PUR (polyurethane) and cellular material such as end-grain balsa wood. Polymeric foams were found to be strain-rate sensitive with their elastic region and ultimate strength to failure recording up to a 30% improvement at 1300 s^{-1}. Their elastic modulus was not affected by the strain-rate (Mahfuz et al., 2000, 2006; Saha et al., 2005; Zhao, 1997; Walley et al., 1991) (figure 2-8). For balsa wood, it was noticed that the ultimate strength improved with the strain-rate and the improvement grew as the density increased (Vural and Ravichandran, 2003).

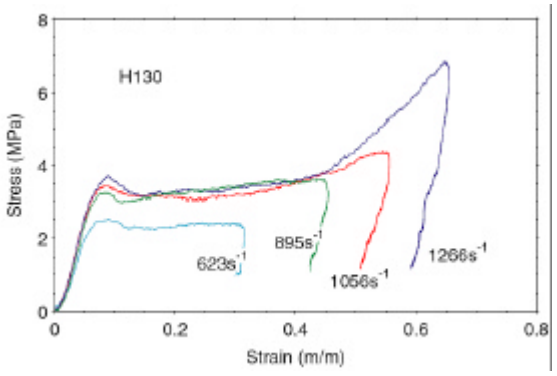

Figure 2-8: Strain-rate response of PVC foam (130 kg/m3) by Mahfuz et al., 2001

2.5 Summary

Generally, most research works regarding slamming focus on the investigation of the loads acting on the hull rather than with their structural response. Furthermore the works investigating the structural response of hull panels often follow a static approach and when a dynamic approach is considered, the materials strain-rate dependence is neglected. In addition, very little attention has been paid to sailing-yachts made of FRP. Strain-rate studies on sandwich structures and their core have usually been based on high strain-rate applications where more weight is given to the influence of the core. Data on the dynamic properties of composites are limited or not available especially at low-medium strain rates. This is the case for E-glass/epoxy composite material, which is commonly deployed in boat hulls, and it is the material of interest for the case study discussed in this thesis. Table 2-1 summarises the works conducted on slamming so far, underpinning the lack of studies led by considering strain-rate effects.

This chapter establishes that for the study of the dynamic response of a sandwich hull panel under slamming loads, the strain-rate properties of the face material are needed. The next chapter of this thesis reviews the progress made in the investigation of the dynamic properties of composite materials.

Table 2-1: Works Conducted on Slamming

Works Conducted on HSC (High Speed Craft)				
Author	**Loads Identification**	**Structural Response**	**Strain-Rate approach**	**Material Investigated**
Hagiwara & Yuhara, 1976	Exp. Model drop tests	Experimental Strain measurements	no	Steel
Sebastiani et al., 2001	Exp. Model drop tests	Experimental and theoretical investigation	no	Steel
Ojeda et al., 2004	no	Static FEA investigation. Loads applied from the standards	no	Composite (no strain-rate approach).
Olovsson and Souli, 2001; Le Sourne, 2003	FSI numerical simulation	no	no	Steel
Thomas et al., 2001	Exp. full scale slam	Experimental and FEA	no	Aluminium
Works Conducted on Sailing Yachts				
Author	**Loads Identification**	**Structural Response**	**Strain-Rate approach**	**Material Investigated**
Hentinen and Holm, 1994	Exp. Measurement of loads on full scale	Experimental measurement	no	Composite
Ward, 1985	no	Dynamic stresses assessed by use of an unsteady model of a pressure loading traveling across a beam	no	Composite
Manganelli et al., 2001	Exp. Measurements of loads on a $1/7^{th}$ scale open 60 model.	no	no	Composite

3 Literature Review on Strain-Rate in Composite Materials

3.1 Introduction

Generally, it is accepted that the dynamic mechanical behaviour of many materials depends on the strain-rate. This is especially so for composite materials with polymeric matrices. However, the constitutive equations for composite materials under dynamic loading are not easily obtained and the mechanical properties must be determined experimentally over a wide range of strain-rates.

Much of the research in strain-rate behaviour in materials relates primarily to the dynamic behaviour of metals. Some of the early studies in strain-rate behaviour for metals date back to the turn of the century and include the measurement of transient impulsive stresses by Hopkinson (Meyers et al., 1990). The study of the behaviour of composite materials at impact strain-rates is still relatively new and reliable data on strain-rate effects is very scarce (Hamouda and Hashmi, 1998). Although the problem of obtaining reliable data is accentuated by difficulties encountered in the design and conduct of impact tests on composites, the increasing importance and use of composites in commercial and military applications ensures continued interest in overcoming such problems. Several experimental studies investigating the response of composite materials at impact strain-rates have been recently reported, and are reviewed and discussed in the following paragraphs.

3.2 Experimental Standards and Procedure

Unlike static tests in strain-rate testing several factors have to be considered due to the dynamics of the phenomena involved. As a consequence of the impact loads applied to test materials at high rate of strains, stress waves are generated and travel back and forth through the material. These waves cause a time dependent stress and strain rate distribution, which vary from section to section of the material under investigation (Clements et al., 1996). Factors that influence the behaviour include the geometry of the specimen, the type of test machine and

hence how the load is transferred, and other factors related with the general set-up of the experiment that are discussed in more detail in chapter 5. It can be said that the experimental method chosen to determine the mechanical properties of materials is dictated by the strain-rate range concerned and the load case. It is therefore not easy to optimise and standardise the experimental procedure, since the general set-up and arrangements of the test might be a complicate function of the particular results needed. This is why many researchers preferred to devise tailor made testing set-up in order to get the best results from the experiment. ASTM suggests some general rules to be followed, aimed to ease the comparison between different works.

3.2.1 Research works led according to Standards

Few works have been done according to the standard rules. Among these, Okoli and Ainullotfi, 2002 carried out tensile tests by use of a servo-hydraulic machine to investigate the properties of glass/epoxy fabrics. As a matter of fact their experiments were led at low strain, with the purpose in mind to infer the properties at high strain rate by extrapolating the data obtained with those coming from intermediate strain-rate tests from other works. As long as the testing is performed at low rates of strain, it may be convenient to follow the standards advised by ASTM. This is because at low strain-rates, the dynamic effects do not play a predominant role and the strain-rate distribution is likely to be constant along the specimen length making the measurement easier. The advantages may be found also in an easier comparison with static testing.

3.2.2 Research works led according to experimental needs

As stated before, the need to devise a tailor made testing set-up and specimen geometry is strictly linked to the effect of the dynamic phenomena involved. In fact, several works have been done by using specifically designed equipment and specimens but, few researchers have either shown the details of their facilities or justified the reasons for their choices. A general overview on the experimental standards and procedures is discussed. More attention is paid to research works led by the use of servo-hydraulic machines since this type of machine was adopted in this work.

Agbossou et al., 1995 adopted a servo-hydraulic machine fitted with a special viscoelastic material to transmit the load to the specimen. A more detailed analysis on the importance of a proper designed test set-up in high strain-rate testing was carried out by Beguelin et al., 1991. They showed that by adopting the so called "pick-up unit" to damp the load transmission, significant benefits in terms of smoother load and strain versus time curves can be obtained in tensile tests conducted by servo-hydraulic machine. Figure 3-1 reports a scheme of the solution adopted, pointing out the benefits of the damping effect in terms of displacement signal acquisition.

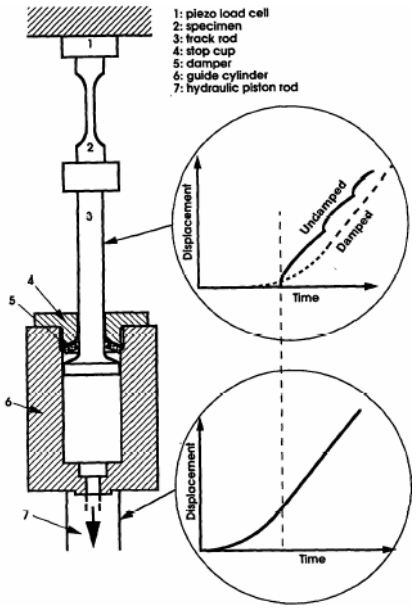

Figure 3-1: Solution adopted by Beguèlin et al., 1991 and Barrè et. al, 1996 for tensile tests

Barrè et al., 1996 also used a similar set-up rearranging the load transmission unit, but not eliminating damping of the vibrations by means of a proper damper. Rotem and Lifshitz, 1971 were pioneers to test u.d. fibrous composites considering the facilities available at the time of their work. They envisaged a thin and narrow specimen to be broken with relatively low loads adopting a drop weight system with a particular jaws assembly design. Pardo et al., 2002 used a similar test set-up to test quasi-unidirectional E-glass/polyester composite by a tensile servo-

hydraulic machine. They concluded that the use of a damper unit is fundamental in order to get reliable data free from noise due to impact waves.

For very high strain-rates, the Hopkinson Bar system has been widely used both for tensile and compressive tests in the past decades (Harding, 1983, 1987; Peterson et al., 1991; Ninan et al., 2001; Tsai and Sun, 2004; Gilat et al., 2002; Jadhav et al., 2003; Vinson and Woldesenbet, 1999). This mechanism is made of an impacting bar hitting an incident bar transmitting the load to the specimen placed in between the transmitting bar and a terminal bar at the opposite end (figure 3-2). The strain and stress measurements are obtained by placing some strain gauges on the incident and output (terminal bar). The data obtained depend on several factors and the strain and load measurements are not detected directly on the specimen but must be inferred.

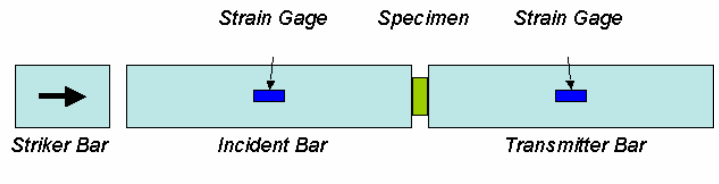

Figure 3-2: Scheme of the Hopkinson Bar

The result is that the data available on materials properties at very high strain-rates are quite speculative. Indeed, most of the results obtained from works at very high strain-rate are often conflicting. This is because the higher the strain-rate range investigated, the more complicated the phenomena involved and the test procedure are.

In this research, a servo-hydraulic machine was preferred to investigate the strain-rate properties of composite materials as the most adequate test apparatus to investigate the strain-rate range of interest in this research. Table 3-1 resumes the system used, the type of test, and the material and strain rate range investigated, and the relative referenced works.

Table 3-1 : Summary of systems used to apply dynamic loads to composite materials

System	Test	SR range [s^{-1}]	Material (Reference)
Charpy Pendulum	Tensile	<100	**S-Glass/epoxy** (Rotem and Lifshitz, 1971; Hayes and Adams, 1982) **Carbon/epoxy** (Sohn and Hu, 1996; Hsiao and Daniel, 1998) **Kevlar/epoxy** (Hayes and Adams, 1982)
Hydraulic Machine	Tensile, Shear	0.001-100	**S-Glass/epoxy** (Thiruppukuzhi and Sun, 2001; Daniel and Liber, 1978) **Carbon/epoxy** (Gilat et al., 2002) **E-Glass/Phenolic** (Barré et al., 1996) **E-Glass/Polyester** (Barré et al., 1996; Pardo et al., 2002; Rotem and Lifshitz, 1971) **E-Glass/epoxy** (Wang et al., 2005; Rozicky, 2000; Rotem and Lifshitz, 1971; Tay et al., 1995) **G-Glass/epoxy** (Harding,1993; Okoli, 2001; Okoli and Smith, 2000a,b) **E-Glass/polyamide** (Todo et al., 2000) **Carbon/polyamide** (Todo et al., 2000) **Graphite/epoxy** (Daniel and Liber, 1978) **Kevlar/epoxy** (Daniel and Liber, 1978) **Boron/epoxy** (Daniel and Liber, 1978) **UD IM6/Peek** (Baguelin et al., 1991)
Hopkinson Bar	Tensile, Shear, Compr.	100-3000	**S2-Glass/8553-40** (Thiruppukuzhi and Sun,1998, 2001; Ninan et al., 2001) **S2-Glass/epoxy** (Tsai and Sun, 2004) **S2-Glass/vynilester** (Akil et al., 2003) **E-Glass/epoxy** (Thiruppukuzhi and Sun,1998; Harding, 1983,1987; Harding and Welsh, 1992; Tay et al., 1995; Armenakas, 1995) **Carbon/epoxy** (Gilat et al., 2002; Hosur et al., 2001; Hsiao and Daniel, 1998; Hiley et al., 1997) **Graphite/epoxy** (Jadhav et al., 2003; Vinson and Woldesenbet, 1999) **Glass-S/MA** (Peterson et al., 1991)

3.3 Geometry variables

The geometry of the specimen represents one of the key aspects for a good understanding of strain-rate testing. Woldesenbet and Vinson, 1999, Harding, 1993, and Tsai and Sun, 2002 paid particular attention to this problem. Tsai and Sun investigated the behaviour of S2-Glass/epoxy systems. Compression tests revealed that the result obtained with a coupon specimen was different from that obtained with a block specimen (figure 3-3). They attributed this discrepancy to the slightly different resin content in the two specimens.

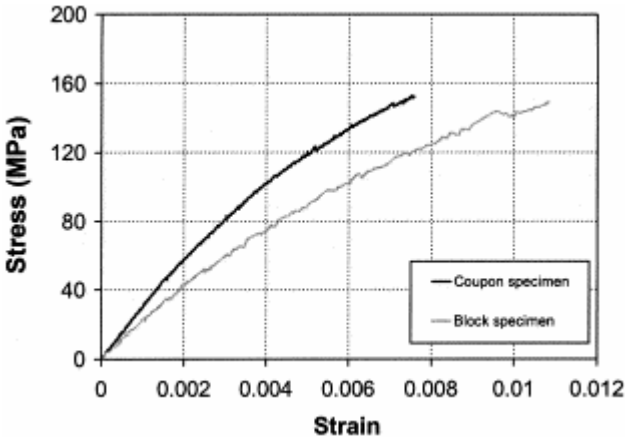

Figure 3-3: Stress-Strain plots for two different type of specimens by Tsai and Sun, 2002

Similar results were found from tests conducted on graphite/epoxy specimens by Woldesenbet and Vinson, 1999. Harding, 1993 conducted high strain-rate compression tests on woven glass/epoxy laminates utilizing two different shapes. Generally, a strain-rate dependence on the strain rate was found. However significant discrepancies were noticed between the two specimen geometries adopted, namely cylindrical and thin stripe, respectively. Harding, 1993 concluded that in considering strain rate effects it is necessary to distinguish clearly between material response, the response of the material unaffected by the geometry of test piece or by the method of load application, and the structural response, where the mechanical behaviour is determined as much by the geometry of the test piece as by its fundamental material properties. Ultimately of course, for the engineer, it is the final structural response of the component he is designing which is important but in the design process it is the material properties that will be needed. It is

therefore commonly agreed that in the design of experiments for studying composite materials, a clear distinction needs to be made between material and structural response as already stated in the previous paragraph.

3.4 Materials' issues

Generally it is accepted that the dynamic mechanical behaviour of many materials depends on the strain-rate. There is now a considerable body of data available on the mechanical performance of metallic materials at diverse strain-rates and some well defined principles governing their general behaviour. However, for composites the situation still remains unresolved. There are many reasons for which this is so. In the first instance compared to metals, interest in polymeric and fibre-reinforced composite materials was developed relatively recently. In composites, the complex interactions between fibres and matrix and the many parameters involved in determining the mechanical response (for instance the effect of strain-rate in the fibre-matrix interfacial bond strength for different fibre surface finishes) make a fundamental interpretation of the experimental data very difficult. These problems are highlighted by the added difficulty of designing strain-rate testing methods suitable for composite specimens which give information on the basic material behaviour rather than on the impact response of a structural element.

One of the approaches used to tackle the problem is to investigate the strain rate properties of the single constituent materials. If the strain-rate behaviour of fibres and matrix are known separately, the strain-rate behaviour of a composite assembly can be subsequently investigated. The main difficulty encountered is in finding a correlation between the behaviour of the separate materials and the resulting assembly.

3.4.1 Polymeric Resin Matrix Materials

Goldberg and Stouffer, 1998a,b, 1999 attempted to describe the dynamic properties of resins by use of modified equations developed for metals. The study showed satisfactory results in computing the deformation response of a thermoplastic matrix. The matrix constitutive equation was implemented into a composite

micromechanical model allowing to describe reasonably well the response of carbon/peek composites at low strain-rates.

The study of Gilat et al., 2002 is more relevant to this work, as they tested epoxy resins to assess the role played in the overall material behaviour. They carried out tests at very low strain-rates (less than 1 s^{-1}) and high strain rates (400 s^{-1}). The results showed that the resin stiffens and improves its ultimate strain and strength as the strain-rate increases. By subsequently testing carbon/epoxy specimens with a tensile split Hopkinson bar technique, they showed that the rate of deformation significantly affects the response of the overall material and its strain and strength for off-axis loads. For 45º laminate specimens, the highest dependence of the maximum stress and strain on the strain rate was observed. These observations suggested that composite sensitivity on the strain-rate is driven by the resin behaviour for off-axis configurations, which needs to be studied further at different rates and load conditions.

3.4.2 Reinforcing Fibres

In view of the experimental difficulties involved in testing individual fibre tows or dry fibre bundles, particularly at high rates of strain, it is not surprising that little information is available on the rate dependence of the reinforcing fibres. However Rotem and Lifshitz carried out tensile tests on glass fibres at moderate strain, in the range 5-30 s^{-1} by use of a drop weight impact tester. For dry bundle E-glass specimens, prepared from a single-end E-glass roving, it was found the tensile failure strength was found to be nearly three times that determined at quasi-static rates.

3.4.3 Fibre-reinforced Composites

The complex interaction between the reinforcing fibres, the matrix and the additional effects associated with the interface between them, prevent any simple or direct correlation between the rate dependence of the individual constituent phases and that of the composite material incorporating each of these phases. This is why most researchers preferred to focus their attention on the whole material rather than on its constituents.

3.4.4 Unidirectional reinforced composites

For unidirectional reinforced specimens under tensile load applied parallel to the direction of reinforcement, most of studies presented in literature agree that the composite mechanical response is determined mainly by the fibres, which are known to have a much higher stiffness and strength than the matrix. The rate dependence of the matrix therefore is relatively unimportant.

For unidirectional glass FRP an increase in ultimate strain and strength was generally found (Barré et al., 1996; Pardo et al., 2002; Wang et al., 2005; Daniel and Liber, 1978; Tay et al., 1995; Rozicky, 2000; Harding, 1987). Wang et al., 2005 observed that in tensile tests at low and intermediate strain rate (up to 50 s^{-1}), an increase of the ultimate strength and strain up to the 40% of the static value was observed for unidirectional glass/epoxy. At higher strain-rates, an increase of the strain rate up to 900 s^{-1} was noted not to lead to any further increase in strength as pointed out by Harding, 1987. Instead there was change in the failure mode. The fibres pull-out became the controlling process. This suggests that while at low strain-rates the epoxy resin has a tensile strain to failure greater than that of the composite, at high strain-rates this is no longer true. At high strain-rate it is the failure strain of the resin which limits the tensile strength of the composite. The resin properties play a more important role in unidirectional reinforced specimens under compression, where the shear modulus of the matrix should be great enough to support the fibres against buckling failure.

For unidirectional carbon FRP a lack of any significant effect of strain-rate was observed and attributed to the lack of rate dependence of the carbon fibres (Harding, 1987).

3.4.5 Woven-Reinforced Composites

Akil et al., 2003 found that for woven-reinforced composites, there is likely to be a greater interaction between the fibre and the matrix, with significantly increased localised strains in the matrix. This is because the fibres straighten under tensile loading or buckle under compressive loading. As a result, the FRP rate dependency of both compressive and tensile strength is increased. In Carbon FRP, an

improvement of the strength has been noticed by Todo et al., 2000 along with a noticeable improvement of the stiffness up to 55%. The latter may be explained looking at the increased interaction between the fibres and the matrix. By observing the strain rate response of three different specimens, carbon, kevlar, and glass FRP, all with the same satin weave reinforcement geometry and the same polyester matrix, they noticed that the rate dependence of the elastic modulus is remarkably similar. This supports the idea that in woven the rate dependence of the modulus derives from the elastic interaction between the axially aligned fibre tows and the matrix and depends on the rate sensitivity of the matrix. In contrast a study by Belingardi and Vadori, 2002 did not note any strain-rate sensitivity for woven E-glass/epoxy at low-medium rates of strain.

3.5 Theoretical Modelling Approaches

Modelling approaches can be distinguished firstly in a macroscopic approach, where the composite material is modelled as an anisotropic and homogenous material, without any attention being paid to the individual constituents, and secondly in a micromechanics approach where the effective properties and response are computed based on the properties and response of the individual constituents. These main methods may be reformulated and therefore a variety of methods exist to model the strain-rate deformation of composite material. In macroscopic techniques, the nonlinearity and rate dependence of the deformation are accounted for at the ply level. In micromechanical techniques, the rate dependence and nonlinearity of the polymer matrix is modelled at the constituent level. The homogenization techniques then compute the effective deformation response of the composite based on the response of the individual constituents.

3.5.1 Constitutive Models

The most developed models can be grouped in:

a) Linear viscoelastic models. For very small strain response; springs and dashpots in series may be used to capture the rate dependent behaviour.

b) Non linear viscoelastic models. When the strains are large enough that the response is no longer linear, non linear dashpots have to be incorporated into the

model. Empirical equations are also used to capture the rate dependent response, in which the yield stress is scaled as a function of strain rate.

c) Molecular approach. This assumes that the deformation of a polymer is due to the motion of molecular chains over potential energy barriers. The molecular flow is due to applied stress, and the internal viscosity is assumed to decrease with applied stress. The yield stress is defined as the point where the internal viscosity decreases to the point where the applied strain-rate is equal to the plastic strain-rate. Internal stresses can also be defined which represent the resistance to molecular flow which tends to drive the material back towards its original configuration.

Among the works led on glass fibre composite, Agbossou et al., 1995 proposed a Bingham-Norton's model group with Eyring's dashpot to describe the experimental failures which seemed to be suitable in first approximation to describe the failure stress as a function of the strain-rate. A schematic diagram is represented in figure 3-4.

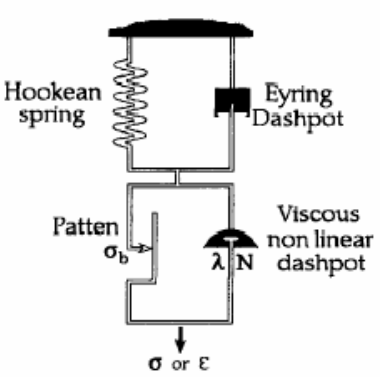

Figure 3-4: Model proposed by Agbossou et al., 1995

According to Agbossou et al., 1995 their experiment the failure stress increased significantly as deformation rate increased. To take into account this observation in their model they distinguished two regions of behaviour according to the strain rate. In the first region, corresponding to strain rates ranging between 10^{-3} and 1 s^{-1} (quasi-static domain), the evolution of stress could be described by the following equation:

$$s = s_i + b \log(\dot{e}) \qquad \text{(eq. 3.1)}$$

In the second region corresponding to the high strain-rate domain (1-300 s^{-1}) the equation used was:

$$s = s_b + l e^{1/N} \qquad \text{(eq.3.2)}$$

With σ_i, σ_b, ß , ?, experimental parameters to be determined.

A viscoplasticity and rate dependent model was developed by Thiruppukuzhi and Sun, 2001 for unidirectional S2-glass/epoxy in off-axis configurations based on experimental observations at very low strain-rate (0-1 s^{-1}). The general form of the viscoplasticity model proposed was:

$$e = A(s)^n \qquad \text{(eq.3.3)}$$

With

$$A = c(\dot{e})^m \qquad \text{(eq.3.4)}$$

a strain-rate dependent coefficient. The coefficients were obtained from the experiments.

Wang et al., 2005 proposed a visco-elastic model composed of an elastic element connected in parallel with a generalized Maxwell model to describe the behaviour of unidirectional glass and carbon epoxy. The viscoelastic parameters in the model were determined by the experiment with a non linear least square fitting method being used to analyse the test data. The theoretical results based on the model showed good coincidence with the experimental results.

Tay et al., 1995 developed an empirical rate-dependent constitutive relationship for glass-fibre reinforced epoxy and pure epoxy. The proposed relationship was a function of both the strain-rate and the strain magnitude. They assumed that the stress induced in the material comprises a static and a dynamic component, as expressed by the equation:

$$s = s_S + s_D \qquad \text{(eq.3.5).}$$

The static component is directly related to the uniaxial strain by Hooke's law. The linear dependence of stress on strain means that the static component can be

expressed as $\sigma_S = q_0 \varepsilon$ where q_0 is the stiffness modulus of the material under unidirectional quasi-static loading. The dynamic component accounts for the deviation from quasi-static behaviour.

$$\sigma_D = q_1 \varepsilon^n (\dot{\varepsilon})^p \qquad \text{(eq. 3.6)}$$

The final constitutive equation obtained is:

$$\sigma_D = q_0 \varepsilon + q_1 \varepsilon^n (\dot{\varepsilon})^p \qquad \text{(eq.3.7)}$$

They concluded that the model was adequate to describe the stress strain behaviour at various strain rates. A significant observation was that the mechanical response of both GFRP and pure epoxy can be described by equations of the same form.

3.5.2 Micromechanical models

Attempts to predict the effective properties and deformation response of the individual plies in a composite laminate have been carried out by use of micromechanical techniques (Chandra et al., 2002; Goldberg et al., 2003). In these techniques, the effective properties and deformation response are computed based on the properties of the individual constituent. Lamination theory can then be used to compute the effective deformation response of the entire composite. In the model proposed by Goldberg et al. the unit cell was defined to consist of a single fibre and its surrounding matrix.

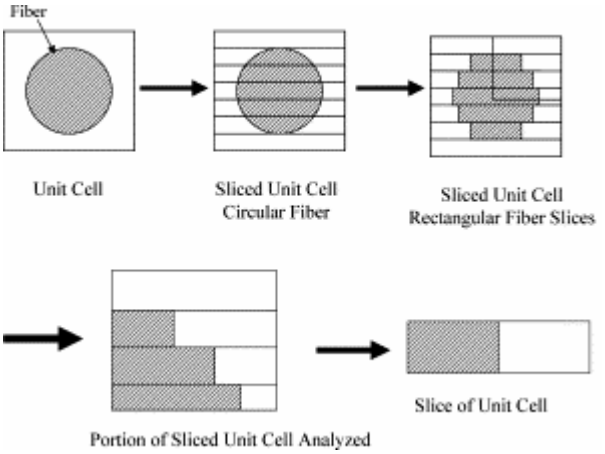

Figure 3-5: Scheme of the micromechanical model by Goldberg et al., 2003

The composite is assumed to have a periodic, square fibre packing and perfect interfacial bond is specified. The fibres are assumed to be transversely isotropic and linear elastic with circular cross section. The matrix is assumed to be isotropic, with a rate dependent, non linear deformation response computed using appropriately developed constitutive equations. The latter have been integrated in the micromechanics equations allowing the whole response of the material to be described. Good accordance was found from comparisons between computed and experimental results, but the ability of the model to analyze the deformation response was limited to carbon/epoxy laminates.

3.6 Numerical Modelling

Some attempts to simulate strain-rate experimental observations using numerical modelling may be found in the literature (Zheng et al., 2003; Coutellier and Rozicky, 2000; Rozicky, 2000). Unlike numerical modelling of static problems, some key issues have to be taken into account while modelling strain-rate phenomena in order to get reliable results from the simulation. These are as follows:

a) The f.e.m. code has to be chosen in order to guarantee computational stability and efficiency. An explicit finite element code response is usually preferred for analyzing the dynamic of materials. This is explained in detail in chapter 7.

b) Boundary conditions have to be chosen such that a strain-rate similar to the one recorded in the experiment is simulated.

c) Material model with strain-rate dependency parameters option has to be considered and at the occurrence built.

3.6.1 Type of test simulated and Material types investigated

Thiruppukuzhi and Sun, 2001 simulated S2glass/epoxy material under tensile loading finding good results for strain-rates below 1 s^{-1}. The laminate was modelled in ABAQUS by using 4 noded layered shell. A load in terms of displacement-time history was imposed at one end of the specimen while the other edge was clamped to model the gripping of the specimen at the load cell. The

experimental material constitutive response was implemented through the software.

Okoli and Ainullotfi, 2002 simulated a three point bend impact test to predict the behaviour of woven glass laminates by use of LS-DYNA. The results were limited since no constitutive model which took into account strain-rate effects was adopted.

3.6.2 Summary of the f.e.m. approaches adopted

Table 3.2 summarizes the numerical simulation studies carried out in the literature. Details such as material tested, geometry and software used are reported, where applicable, along with the relative references. E-Glass/epoxy specimens in tensile tests have not been analysed so far and consequently no direct comparison with the literature can be done. In this work a numerical modelling of the experimental testing carried out on u.d. specimens is presented. Once established that the numerical model is suitable to describe the strain-rate behaviour of E-Glass/epoxy, this is used to investigate the strain-rate response of a sailing yacht hull panel made of similar materials.

Table 3-2: Summary of the Numerical Simulation Works Available in Literature

Material Type	**Type of test simulated**	**Specimen's Shape and Dimensions l/w/t [mm]**	**Boundary conditions applied**	**Software and Element used**		**Material model**	**Strain Rate range investigated [s^{-1}]**	**Ref.**
Steel X2CrNiMo 1810	tension	Hour-glass	Velocity profile detected from the experiment	Not provided	Not provided	Not provided	0-1000	1
Aluminium alloy 7075	tension	notched	Velocity profile detected from the experiment	Not provided	Not provided	Not provided	0-1000	1
S2-glass/8553-40	tension	Flat coupon [100/17.8/-]	Displacement-time history load	ABAQUS	4 nodes layered shells S4R	Not provided	0.001-1	2
Woven 7781/F155 E-glass fabric	tension	Flat coupon [100/17.8/-]	Displacement-time history Load at the end of the specimen	ABAQUS	4 nodes layered shells S4R	Not provided	0.001-1	2
S2-glass/8553-40	Compress.	Bar cube [9x9x9]	Displacement-time history load	ABAQUS	8 nodes 3D solid	Not provided	1000	2
GF/epoxy	Impact test	plate	-	PAM-CRASH	Mindlin-Reissner shell	User defined subroutine	n.a.	3
Tufnol grade 10G/40 glass/epoxy	3 point bend	80x15x3	Displacement-time history load	OASYS LS-DYNA3D	8 nodes solid element	Chang-Chang Failure model (no strain rate effect)	0-2.7	4

References: 1. Essam-el Magd, 1999; 2. Thiruppukuzhi and Sun, 2001; 3. Johnson at al., 2001; 4. Okoli and Ainullotfi, 2002.

3.7 Summary of Data from Literature

Table 3-3 reports the summary of the data available from the literature.

Table 3-3: Summary of data from the literature

Material	SR [s^{-1}]	E	σ_U	ε_u
UD glass/epoxy Rotem and Lifshitz, 1971	0-5	slightly improved	slightly improved	slightly improved
UD glass/epoxy Barrè et al., 1996; Daniel and Liber, 1978; Pardo et al., 2002; Rozicky, 2000; Tay et al., 1995	0-30	improved 50%	improved 3 times	-
UD glass/epoxy Wang et al., 2005 (no off-axis)	0-50	unvaried	increased up to 50 %	increased up to 50%
UD glass/epoxy Thiruppukhuzhi and Sun,1998, 2001	500	improved	decreased	decreased
UD carbon/epoxy Daniel and Liber, 1978	0-27	unvaried	unvaried	-
UD Kevlar/epoxy Daniel and Liber, 1978	0-27	increased 20%	increased 20%	Slightly improved
Woven S2-glass/ Vinyl ester Akil et al.,2003	0-500	improved	improved	improved
Woven E-glass/epoxy Harding, 1993	0-1000	Significant improvement	Significantly improvement	improved
Woven E-Glass/ polyamide Todo et al., 2000	0-10	Improved	improved	improved
Woven Carbon/ polyamide Todo et al., 2000	0-10	improved	improved	improved
Woven Glass /epoxy Belingardi and Vadori, 2002	0-100	unvaried	unvaried	unvaried
Woven Glass /epoxy Harding, 1987	0-1000	Increased up to 55%	increased	increased
Woven Carbon /epoxy Harding, 1987	0-1000	Increased up to 55%	increased	increased

4 Research Approach Adopted

4.1 Solution Methodology

The ultimate goal of this work was to investigate under a strain-rate approach the response of a sailing yacht sandwich hull panel, made of E-glass/epoxy, subject to slam loads. A DK46 sailing yacht was used as a case study. Bearing this in mind the research was developed in the following steps.

The strain-rate properties of unidirectional E-glass/epoxy composite material were investigated under rates of strain typically experienced by sailing yacht structures. The material was characterized statically and dynamically as in axis and off-axis configurations; a servo-hydraulic Instron machine was used for this purpose. A specific test set-up was adopted and appropriate test rig was designed and manufactured in order to get the desired results. As a result, stress-strain curves at different strain rates and for different fibre orientations were obtained.

Once the knowledge on the dynamic properties of the material has been acquired, a systematic methodology was proposed to describe the strain-rate behaviour of the material by LS-DYNA explicit finite element code. This methodology was subsequently applied to examine the response of a hull panel subject to a slam load. The slam load was determined by means by of a fluid-structure interaction simulation. ALE (Arbitrary Lagrangian-Eulerian) method, within the LS-DYNA code, was used to for this purpose.

A strain-rate analysis was carried out on the panel assessing stresses at a ply level. A static numerical analysis by use of ANSYS commercial package was also performed and a relative comparison with the dynamic analysis was carried out.

Figure 4-1 schematizes how the work was developed.

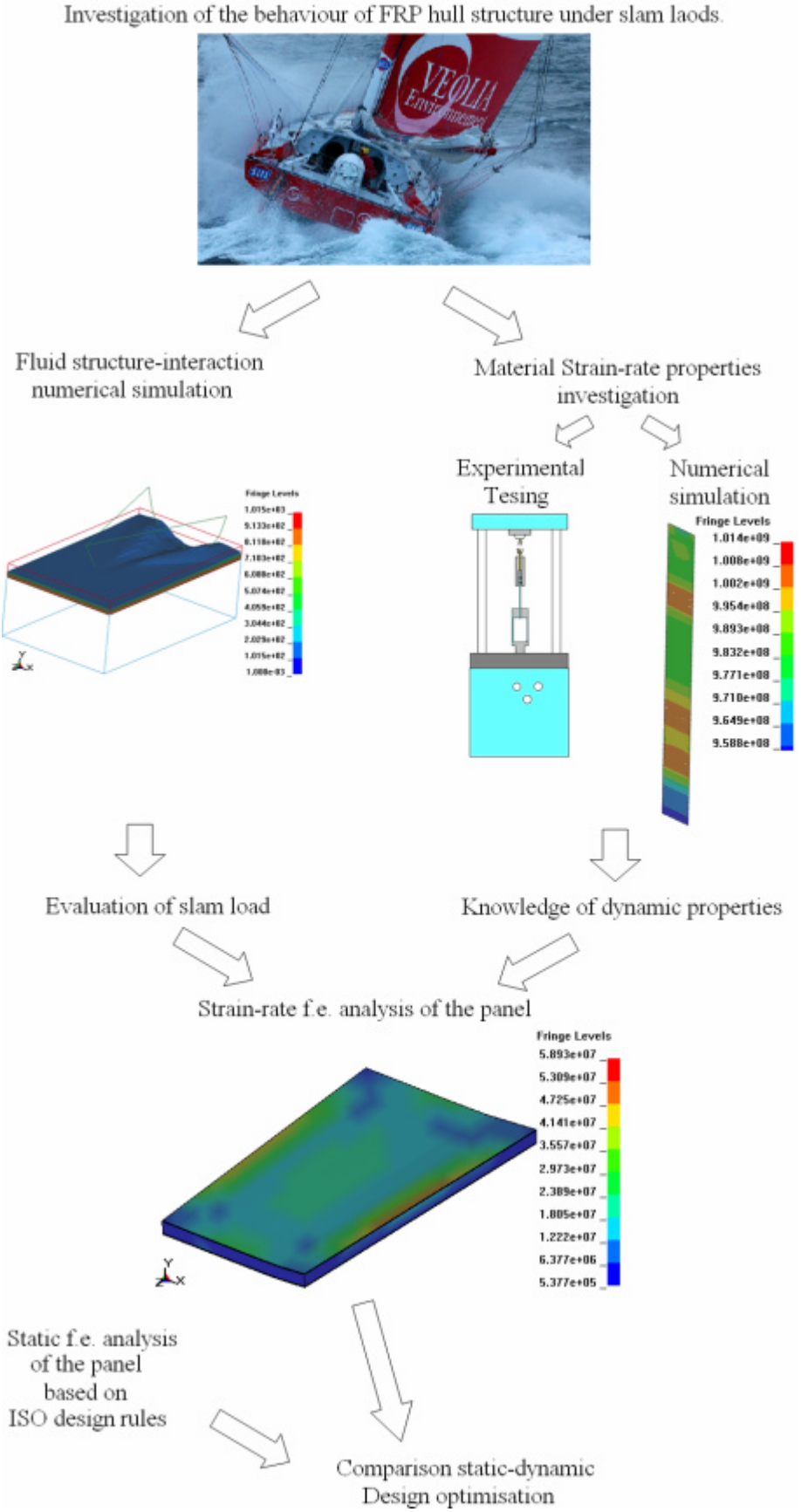

Figure 4-1: Scheme of the research methodology adopted

5 Experimental Assessment Procedure of Materials Behaviour

5.1 Introduction

The purpose of the experimental campaign was to determine the tensile static and dynamic properties of E-glass/epoxy, to be used in the strain-rate based analysis of a sandwich hull panel, whose skins are made of the material under investigation. It can be argued that in a hull sandwich panel under pressure loads, the inner skin undergoes tensile deformations while the outer skin undergoes compressive deformations. Besides, depending on the curvature of the panel sometimes both skins can be under compression. Ideally, the dynamic properties of the material both in compression and tension should be known. The testing equipment adopted for the experimental campaign consisted of a hi-velocity servo-hydraulic machine which allows only for the investigation of the tensile mechanical properties in the strain-rate range of interest. A different machine set-up, not available among the resources of this work, should have been adopted to explore the dynamic compressive properties in the same strain-rate range.

In light of these considerations, the numerical investigation of the hull panel was led by assuming that the behaviour of E-glass/epoxy was the same in tension and compression and it was described by the properties found in the tensile testing.

This assumption was acceptable considering that Rozicky, 2000 did not note a significant difference in tensile and compressive response while testing the same material statically and at lower strain-rates.

The experimental testing has been developed according to the following three points:

1. Choice of the material and type of test to adopt;

2. Results expected;

3. Instrumentation to be used in order to obtain the desired results;

The why of each choice is discussed in the next paragraphs.

5.2 Materials under investigation

The material under investigation was unidirectional E-glass/epoxy pre-preg, namely unidirectional E-fibre glass pre-impregnated with epoxy resin, provided by SP Systems (UK). The pre-impregnated concept allows for the right control of the resin weight such that an optimum fibre-matrix ratio is achieved. The resin system code was SE 84 HT. The pre-preg resin content was 37% by weight. The total areal weight was 476 g/m^2.

The choice of the material was made because unidirectional E-glass/epoxy is widely adopted in the yacht industry, and is one of the most preferred materials particularly when performances and lightweight structures are sought. As an example, the hull panel of a DK46, made of this material, is considered as object of the study in chapter 8.

5.2.1 Material variables

The overall behaviour of composite materials is a function of both the properties of each individual component (type of matrix and fibres) and the way they are assembled together. Theoretically, understanding the dependence of every single component on the strain-rate is a way to determine the overall strain-rate dependence of the composite material. This could be achieved by conducting separately strain-rate tests on the matrix, the fibres and the whole assembly. As shown in the literature review, this approach can be laborious and time consuming due to the difficulty related to tests set-up, especially for fibres. In addition, according to the published works (Rotem, 1971), it usually leads to conflicting results.

In light of these considerations in this work it was preferred to investigate experimentally the overall behaviour of the composite.

5.3 Type of Test adopted and results to be obtained

As well established in the review, the choice of the type of test to adopt is mainly related to the mechanical properties to be investigated and the strain-rate range of interest. Bearing in mind the hull panel case study, in order to perform a strain-rate numerical simulation of a sailing-yacht GRP hull panel, it has to be known how the

stiffness and the ultimate values of stress and strain vary depending on the strain-rate, in the strain-rate range of interest, usually 0-80 s^{-1} for fast sailing-boats. The test better suited to determining these properties was a tensile test by use of a servo-hydraulic machine.

By means of tensile tests it was possible to obtain the stress-strain curves at different strain rates, namely the mechanical properties (modulus of elasticity, ultimate strength and ultimate strain) of E-glass/epoxy. Different off-axis configurations, typically adopted in the lay-up of sailing-yacht hull constructions, were analyzed in order to assess the strain-rate dependence on the load application-fibre angle.

5.4 Testing Equipment

For the experimental campaign, a servo-hydraulic Instron machine, capable of performing tests up to 20 m/s, was used. The testing speed is referred to the speed of the ram of the machine. In order to obtain the strain-rate values intended to explore, some issues concerned with the general set-up of the experiment and the operation of the machine have to be considered. As understood in the review, strain-rate experiments may need to be designed according to the results desired. Consequently, understanding in detail how the machine works, it is one of the key aspects of the experimental testing.

5.4.1 Transmission of the Load

The novel feature of the machine used was a fast jaws grip system. This system works such that the lower part of the specimen is pulled once the actuator reaches the velocity set in the experiment. The transmission of the load occurs by means of friction. Figure 5-1 shows a sketch of the whole machine and describes how it works.

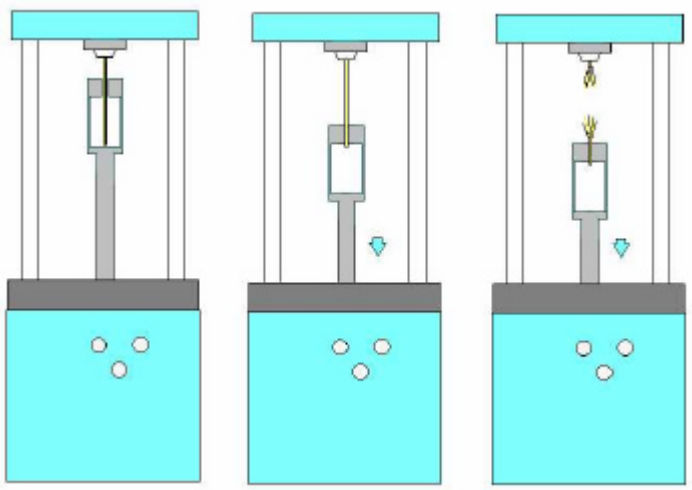

Figure 5-1: Standard Machine Set-up

Figure 5-2 illustrates in detail how the machine runs. In the set up phase the actuator is placed in a position, let's call it x = 0. The gauge length will be given by the summation of the length of the specimen above the actuator at t = 0 and the run (fixed at 180mm for design reasons) the actuator needs to accelerate at the wanted velocity. Therefore the test begins at $t = t_o$ when the jaws clutch the specimen and start to pull it until failure occurs at $t = t_1$.

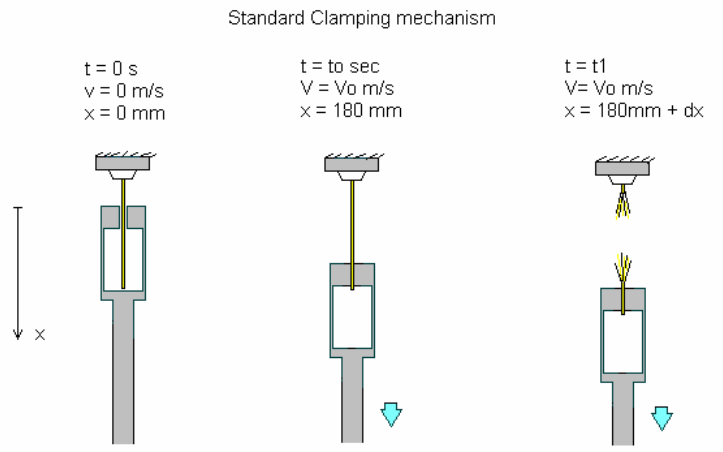

Figure 5-2: Scheme of Clamping System

This system is interesting and innovative but shows some limits, since it does not take into account some fundamental issues concerned with this research.

Firstly the fast jaws work very well with metals but they do not manage to clamp composites properly. This is due to the irregular surface of the composite itself and to the coarse surface of the grips designed specifically to clutch metals.

Secondly, this device needs a run of 180 mm to accelerate before clamping the specimen at the needed velocity. This length has to be added to the gauge length of the specimen. Consequently the total length of the specimen is a function of the machine system. This has to be avoided since the geometry of the specimen influences the strain-rate response of the material. As a result of this, the geometry is a design parameter to be chosen according to the results expected, and it is essential to avoid a coupling with the machine configuration.

In the following paragraph it is discussed why a different clamping system is needed.

5.4.2 Design of specific testing equipment parts

Assuming that the geometry of the specimen is designed according to the reasons explained above, it is evident that the clamping system had to be redesigned. It was necessary to devise a new clamping system such that the load transmission did not occur through friction on the specimen surface itself. For both economical and practical reasons, as redesigning the whole machine would have been out of the purpose of this work, the idea was to optimise the design of the existing mechanism through the adoption of a new part. The purpose was achieved linking in series the composite specimen to a metal stripe; the metal stripe was then pulled by the standard fast jaws and at the same time ensured the transmission of the motion to the composite specimen. The link was realized by means of two plates. Composite specimen and metal stripe were inserted between the plates that presented a coarse surface in the inner side for better gripping. A set of bolts adequately tightened ensured the right clamping conditions. The metal stripe was linked to the plates through a couple of pins placed in adequate holes. Figure 5-3 shows a drawing of the plates that were designed while figure 5-4 shows the new configuration of the clamping system.

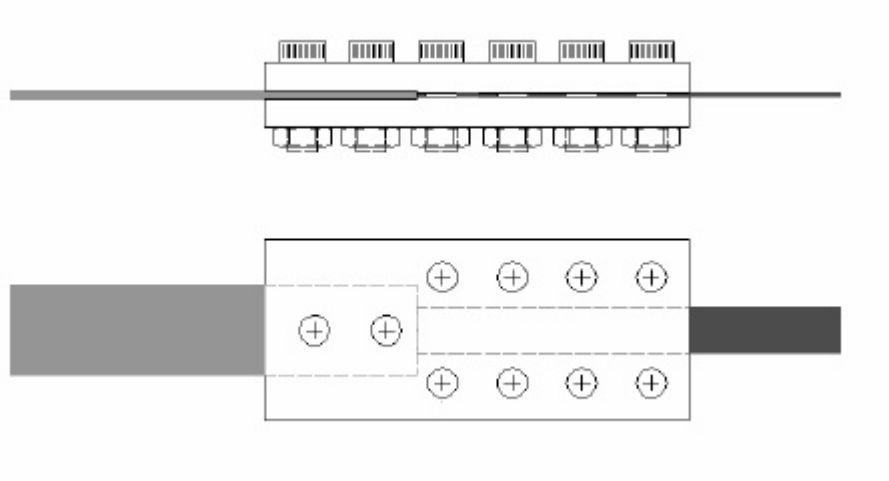

Figure 5-3: Clamping plates devised

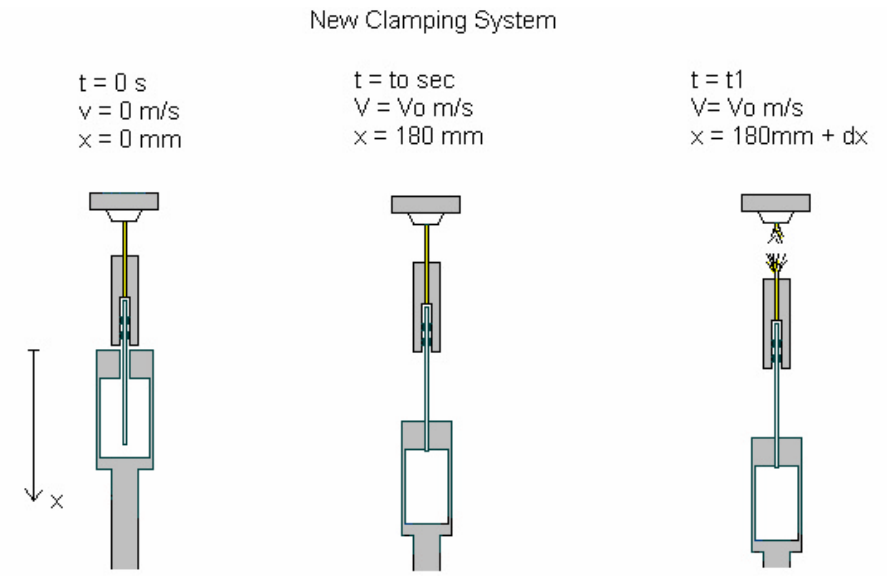

Figure 5-4: Scheme of the new clamping system devised

The plates were made of steel hardened by heat treatment. The total cross section area dimensions were chosen such that the parts behaved as a rigid body, such that no energy dissipation occurred during the testing process. Figure 5-5 depicts the final set-up adopted and schematizes the different phases in a test.

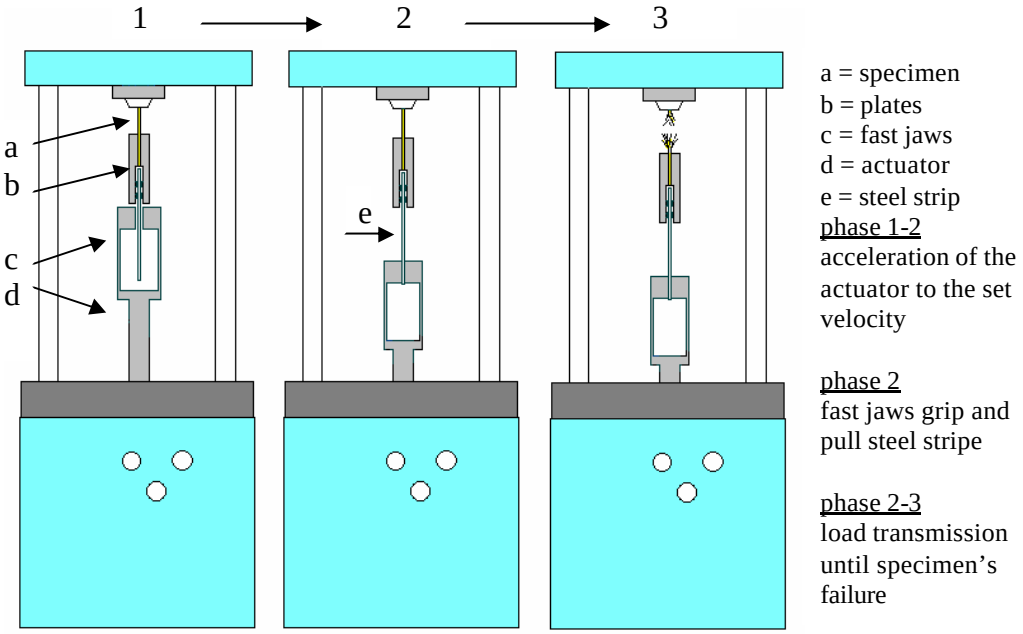

Figure 5-5: New Machine Set-up

The reliability of the new clamping system was verified practically and with a preliminary dynamic f.e. analysis of the experiment, considering the material dynamic properties of the metal parts. The intention was to verify that in the worst scenario (highest actuactor velocity), failure took place in the composite specimen rather than in the metal stripe or the plates. One half of the parts was modelled thanks to the symmetry (figure 5-6). The simulation confirmed that the metal parts were well below their yield stress and the failure took place in the composite specimen (figure 5-7). A more detailed description of the numerical modelling approach followed and the software used is given in Chapter 7.

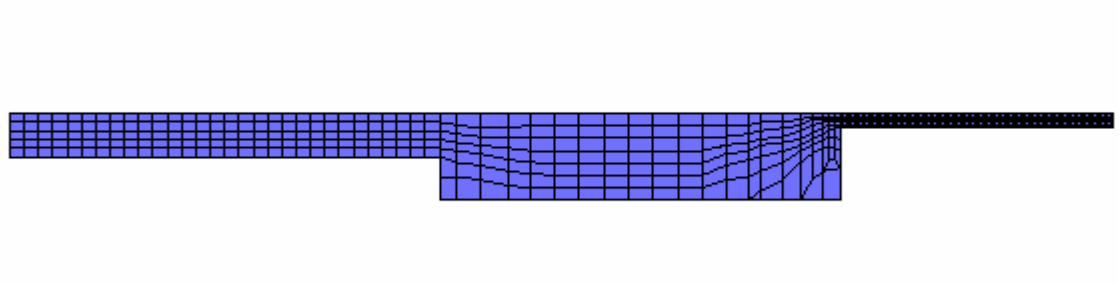

Figure 5-6: Finite element model of specimen plates and metal strip

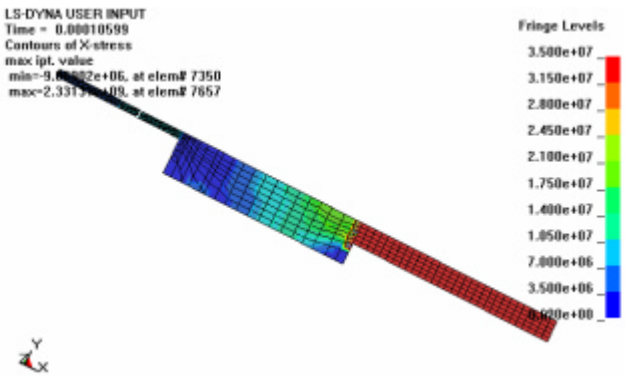

Figure 5-7: Stress Distribution in the plates

5.4.3 Advantages of Specific Clamping System

The advantages of a new clamping system to perform strain-rate testing by means of a servo-hydraulic machine can be summarized in the following points:

1) Simpler specimen configuration;

2) Higher strain rates achieved;

3) More constant distribution of the strain rate along the specimen length;

4) Smoother load signal from the load cell;

5) Easier set up and acquisition data;

These key advantages are discussed in detail in the following paragraphs.

5.5 Selection and Design of test specimen

The geometry of the specimen is a crucial aspect in strain-rate testing. The reasons why a certain configuration was chosen are shown to be strictly related to the need of designing a new clamping system.

It was established that in the general test configuration the specimen was clamped in one end and pulled through the other end at a certain velocity, almost constant during the test duration. This was possible thanks to a feedback control system of the testing machine which regulates the hydraulic pressure of the lower ram according to the force measured from the load cell.

In preliminary studies, many tests on specimens of different length and parallel numerical simulations were carried out by the author. From these, the conclusion of "the shorter the better" has been drawn in complete agreement with the literature (Pardo et al., 2002; Baguelin et al., 1991).

First of all, the shorter the specimen the higher the strain-rate, and the more constant is the strain-rate distribution along its length. The latter because the waves propagation and reflection occurring into the material reaches the equilibrium earlier (Clements et al., 1996). It is fundamental to perform a test with a constant strain rate distribution since the strain, and therefore the strain-rate, is measured only in one point of the gauge length.

The reason why a higher strain-rate is obtained can be found referring to a simplified formula according to which the strain-rate is a function of the ratio velocity/specimen's length. It is clear that theoretically for a given velocity the value of the strain-rate can be doubled just by halving the length.

$$\dot{e} = \frac{V}{L} \qquad \text{(eq.5.1).}$$

The minimum length of the specimen will be dictated by the space needed to glue the strain-gauge on it and the space needed to set the specimen on the machine (practically, the space to handle the span to tighten the grip's bolts).

Three specimens with different lengths respectively 105, 165 and 225 mm were examined in preliminary f.e.m. simulations aimed at assessing and verifying the

strain-rate along the specimen length. The strain-rates in each position of the specimens and at each time step were measured as the derivative of the strain values with respect to the time.

In figure 5-8, the correspondent strain-rate profile along the length was plotted for five different time steps. By looking at the plots it can be noticed that:

a) The shorter the specimen the higher the strain-rate in a section;

b) The longer the specimen the more the strain-rate fluctuates in every section.

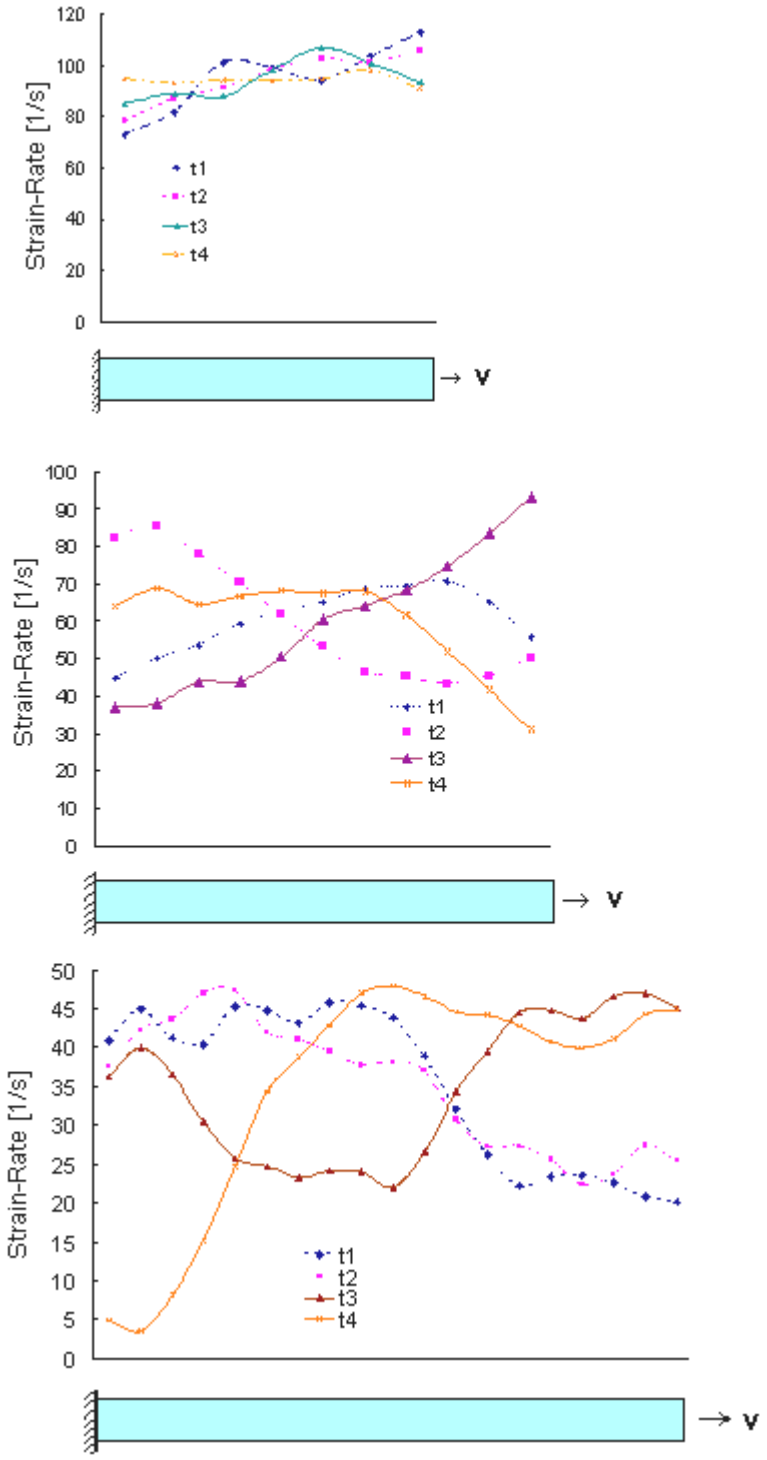

Figure 5-8: Strain-Rate along the specimen length at different time steps for three different specimen lengths

5.5.1 Geometry variables

Once the criterion for the choice of the length was established, the two other dimensions were examined.

The use of particular specimen profiles like the dog-bone shape could have been convenient to drive the failure in a precise zone. Unfortunately for u.d. composites a crack starts in the curves of the specimen and propagates in the matrix parallel to the fibres direction. Therefore a very simple rectangular shape was believed to be the most suitable geometry to use for u.d. specimen under tensile loading. The width of the specimen as well as the thickness influence the maximum load needed to break the material. The thickness of the specimen depends on the number of layers of the laminate. The width had to take into account the space needed to place the strain-gauge. These variables were chosen such that the breaking load was well below the maximum load performable by the machine (about 100KN), since in this condition the load cell happens to be in resonance with subsequent noises in the measurements (Instron manual, 2001). A 1 mm thickness obtained by using four layers and a 10 mm width ensured the compliance with this condition.

Tabs were also adopted to improve the grip as the direct contact of the grips with the composite surface may cause indentation and consequent microcracks that could drive the failure unexpectedly. Hence, by using tabs the risk of damaging the composite surface during the tightening procedure was avoided as the load was distributed and transmitted uniformly to the specimen.

A material with a modulus of elasticity close to the modulus of the specimen was adopted for the tabs in order to avoid discontinuity in the stress distribution. Aluminium was the most suitable material for this purpose. The tabs were glued using epoxy resins.

Geometry and relative dimensions are reported in Figure 5-9 and Table 5-1.

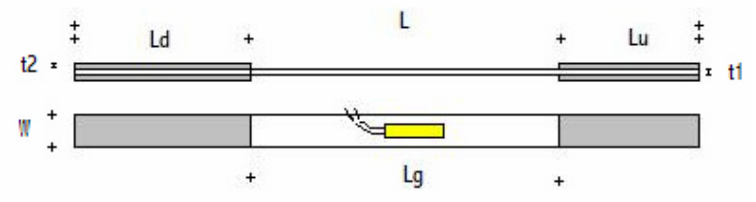

Figure 5-9: Specimen geometry

Table 5-1: Specimen Dimensions

L	Lu	Ld	Lg	W	t1	t2
195mm	45mm	55mm	95mm	10mm	1mm	1mm
Tabs dimensions						
Lu	Ld	t2	W			
55mm	45mm	0.7mm	10mm			

5.5.2 Laminate reinforcement Configuration

Three laminate configurations were considered such that the angles obtained between the direction of the fibres and the direction of the application of the load were 0º, 15º and 30º. The purpose of this choice was to investigate the influence of the fibres direction on the strain-rate behaviour of the laminate.

As explained before the choice of the range 0-30º lies in structural considerations related to yacht constructions. When designing high performance boat structures, unidirectional plies are preferably aligned with the predicted highest load direction, offering in this way their best mechanical properties. Practically, diverse lay-up configurations are adopted, depending on the area of the hull and the dimensions of the panel, to obtain structures capable to withstand complex loading scenarios. A ±30º lay-up is commonly adopted in conjunction with 0º and woven laminates in sailing yacht panels. Figure 5-10 depicts the specimen configurations.

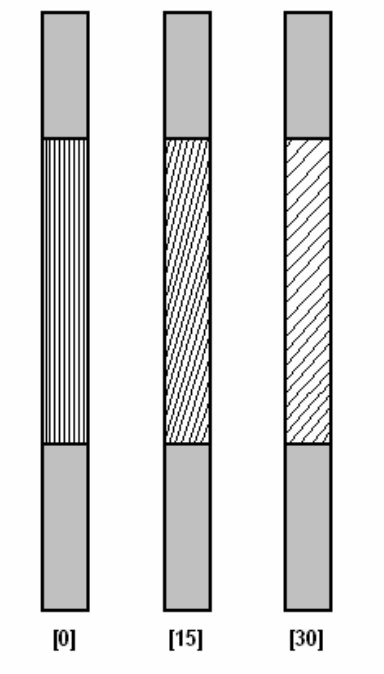

Figure 5-10: Fibres configurations tested

5.5.3 Manufacturing Procedure

A panel was manufactured by laying up four plies and then cured in an oven with a vacuum bag technique for 12 hours at 90 C°. This process produced 1m x 1m plates with a thickness of 1mm.

Specimens were cut out from the plates in the desired geometry by use of a circular saw. The length of the specimen was 195 mm, the width 10 mm, and the thickness 1 mm. Aluminium tabs 1mm thick were glued on the specimen ends leaving a 95mm gauge length. A total of twenty-four specimens were used in the experimental study. Considerable effort and care was spent to ensure dimensional accuracy and prevent delamination. Figure 5-11 depicts the manufacturing equipment used in the vacuum beg technique.

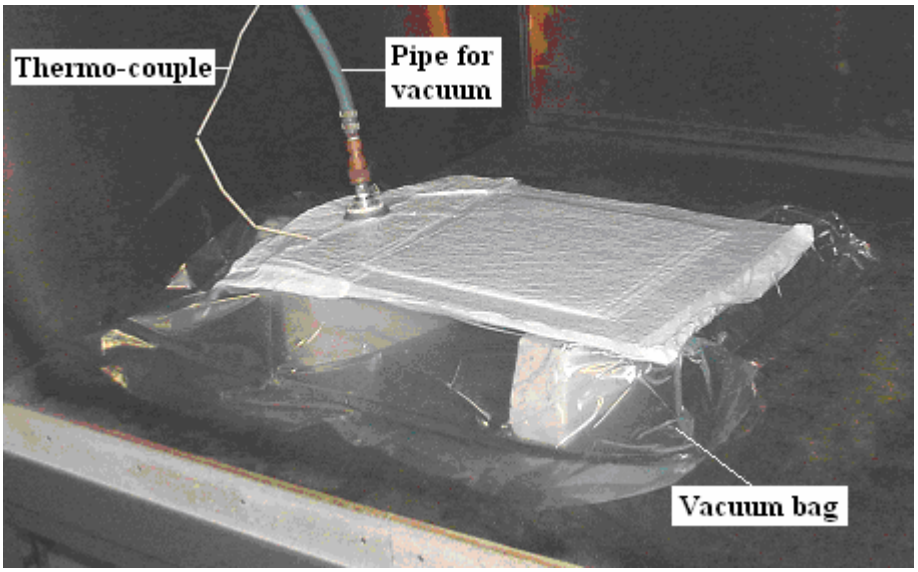

Figure 5-11: Vacuum bagging technique for plate manufacturing

5.6 Static testing

Static testing was necessary in order to assess and compare the mechanical properties investigated in the high strain-rate testing. Quasi-static tests were carried out by use of a universal servo-hydraulic 8802 Instron machine. The tests were performed according to the ASTM rules about composite materials. For the $[0]_4$ specimen the Young's modulus was found to be 42.1GPa, while the values of the ultimate strength and strain were found to be 805 MPa and 1.92% respectively. For the $[15]_4$ specimen the Young's modulus was found to be 30.9 GPa, while the values of the ultimate strength and strain were found to be 135 MPa and 0.53% respectively. For the $[30]_4$ specimen the Young's modulus was found to be 18.5 GPa, while the values of the ultimate strength and strain were found to be 40.3 MPa and 0.24% respectively.

5.6.1 Geometry of specimen

Figure 5-12 shows a picture and a sketch of the geometry of the specimen adopted in the static testing. The relative dimensions suggested by ASTM are also reported.

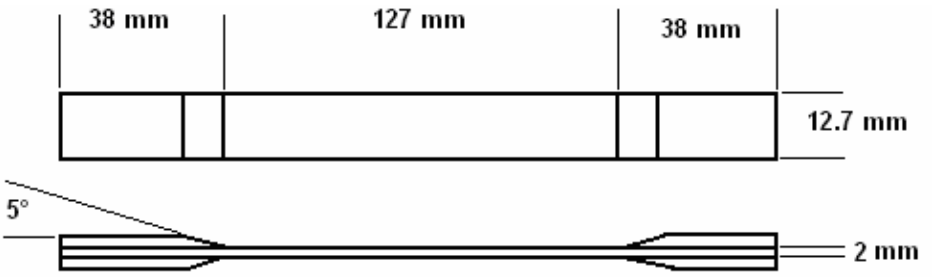

Figure 5-12: Specimen adopted for static tests

5.6.2 Experimental Stress-Strain Curves for $[0]_4$, $[15]_4$, $[30]_4$

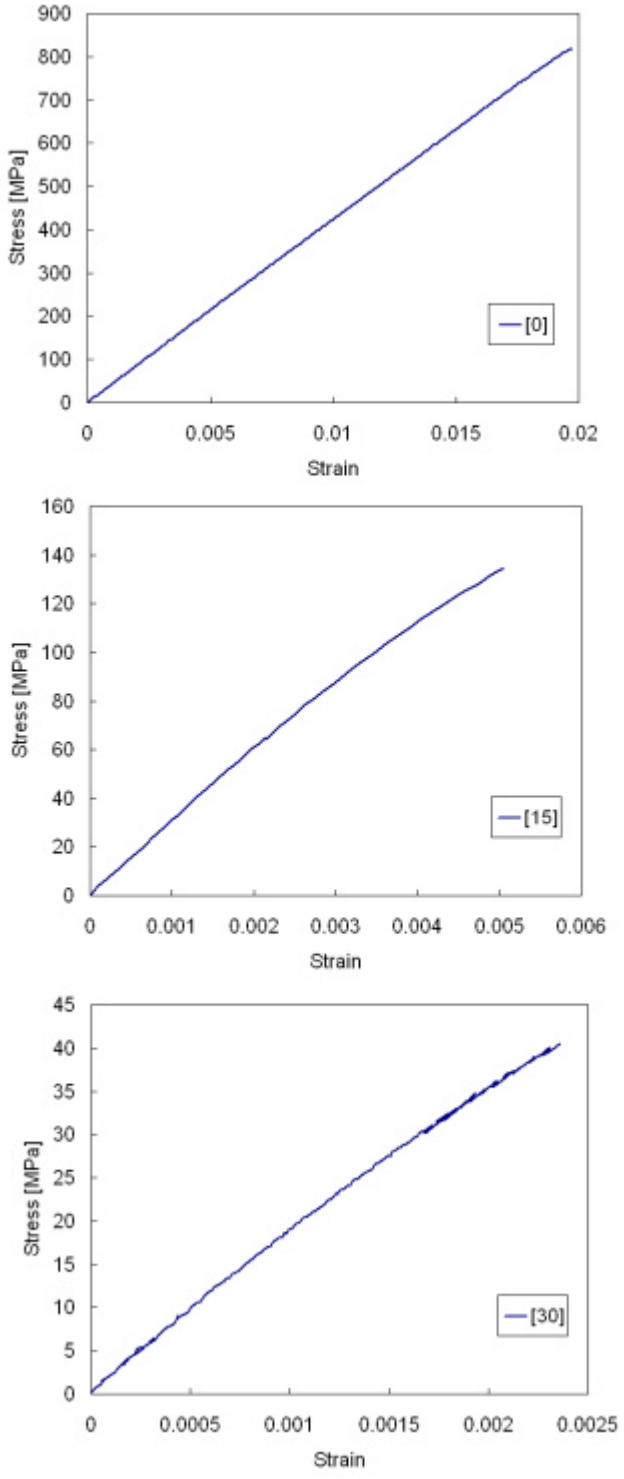

Figure 5-13: Static stress strain curves

Table 5-2: *Mechanical Properties obtained from Static Tests*			
Fibre Orientation [Deg]	**Young's Modulus [GPa]**	**Ultimate Strain**	**Ultimate Strength [MPa]**
0	42.1	0.0192	805
15	30.9	0.0053	135
30	18.5	0.0024	40.3

A comparison between experimental and theoretical Young's modulus versus fibre orientation angle was performed in order to assess the reliability of the results obtained from the experimental testing campaign.

The theoretical formula adopted which derives from the plane stress constitutive is:

$$E_J = \frac{E_1}{\left[m^4 + m^2 n^2 \left(-2\nu_{12} + \frac{E_1}{G_{12}} \right) + n^4 \frac{E_1}{E_2} \right]} \qquad \text{(eq.5.2)}$$

Where, m and n are respectively the cosine and sine of the angle formed between fibre direction and application of the load, ν_{12} is the Poisson's ratio, E_1 and E_2 are respectively the Young's modulus in the direction of the fibres and the direction perpendicular to the fibres, and G_{12} is the shear modulus.

Since this testing campaign did not include testing [90] and [±45] specimens necessary to determine the values of ν_{12}, E_2, and G_{12}, experimental data obtained from such tests conducted in research works led by Rozycki, 2000 on the same material have been considered.

The values considered for ν_{12}, E_2, and G_{12}, were 0.299, 10.3GPa and 4.43GPa respectively.

The theoretical and experimental curves are plotted in figure 5-14 showing a slight discrepancy likely to be due to the assumed value of $?_{12}$, E_2, and G_{12}.

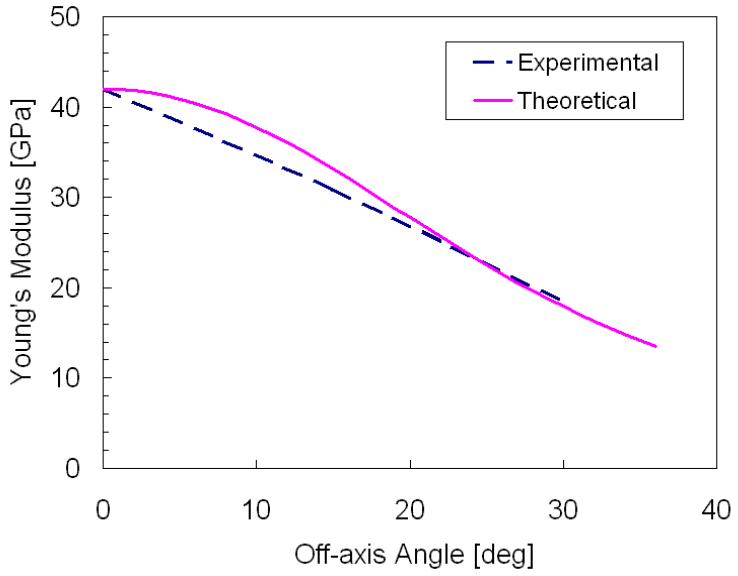

Figure 5-14: Comparison theoretical-experimental static Young's Modulus versus fibre's angle

5.7 Strain-rate Testing: "Material Characterization"

The purpose of the strain-rate experimental testing was to characterize the behaviour of unidirectional E-glass/epoxy in a certain strain-rate range considering the dependence on the load-fibre angle. As explained earlier, the angle of interest for the case study ranges between 0º and 30º. Three set of tests on $[0]_4$, $[15]_4$, and $[30]_4$ laminates, were therefore performed.

5.8 Results for $[0]_4$

(a) Experimental curves

Three experiments were performed at 5 m/s, 10 m/s, 15m/s. The respective strain-rates detected were 38.6 s^{-1}, 64 s^{-1} and 75 s^{-1}. The following graph reports the stress-strain curves obtained along with the static one.

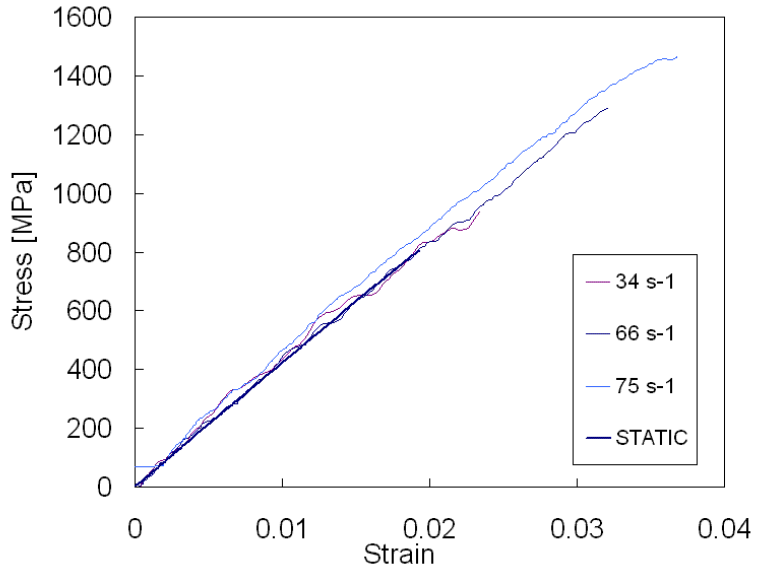

Figure 5-15: Stress-Strain curves at different strain-rates

(b) Response and failure mechanisms

Figure 5-15 reports the stress-strain curve detected at different strain rates. Noticeably due to the considerations on the designs of both the equipment and the specimen, the results are free from noise with no need to filter them. From the experimental testing the following observations were noticed:

a) A significant increase of the strength to failure increasing the strain-rate (it is remarkable that the ultimate strength varies from 805 MPa in the static case to nearly 1500 MPa at 75 s^{-1});

b) A significant increase of the strain to failure with increasing strain-rate;

c) The stress-strain curves are linear with no significant dependence of the Young modulus on the strain-rate.

As suggested by Wang et al., 2005 these results might find an explanation in the following consideration about fibres. It is very probable that there is a variation of strength and stiffness amongst different fibres. When the material is loaded statically, the weakest fibres in the material undergo rupture immediately. This effect is delayed when the material is loaded dynamically due to wave effects travelling in the material. In this case, the stress is more uniformly distributed across the section, and therefore among all the fibres; this results in the weakest fibres being able to withstand the load longer. This phenomenon enables the composite to stretch more and to withstand higher loads. From the experimental observations it can be noticed that while the strain-rate influences the strength and the strain to failure it does not alter the essential linearity of stress-strain response.

Therefore, for u.d. specimens under tensile load applied parallel to the direction of reinforcement, the mechanical response is determined mainly by the fibres, which are known to have a much higher stiffness and strength than the matrix. The rate dependence of the matrix therefore is relatively unimportant.

By looking at the specimen after failure in figure 5-16, it can be seen that no clear breakage zone is identifiable. The failure process takes place in a very complex way in, a very short time period and in different places of the specimen leading to the so called christmas tree shape of the broken specimen.

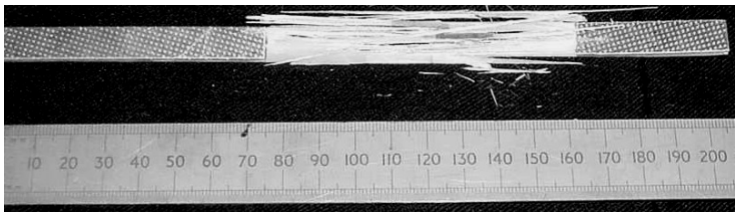

Figure 5-16: Specimen after failure

(c) Comparison with Data from the Literature

Some considerations about the results obtained can be done by comparing this work with some published evidence. Figure 5-17 reports the plots of the normalized ultimate strength versus the strain rate, namely the ultimate strength at a given strain-rate divided by the correspondent static value, for three different research works. In Wang et al., 2005 and Rozycki, 2000 the same material as the one tested in this study was studied while a polyester matrix was adopted in Rotem and Lifshitz, 1971 instead. No variation in the Young's modulus was noticed in this work in agreement with works of Wang et al. and Rotem and Lifshitz, 1971. However, a significant increase of the Young's modulus up to 20% was found in the range 0-44 s^{-1} in the work of Rozycki, 2000. Besides for the latter, the ultimate values of strain and stress reached a maximum at 25 s^{-1} and then decreased. Similarities are noticed in the trend with the work of Wang et al., 2005.

It may be argued that the discrepancies noticed could be due to the different test set-up and the geometry of the specimen chosen. As already stated the length of the specimen and the transmission of the load play an important role in the dynamic effects created in the phenomenon. Since no detailed information on the test set-up adopted in other works are available, a meaningful comparison was only possible with Wang and al., 2005 work. It is important to point out that the same machine was used in both studies but a different set-up arrangement was adopted. As a consequence of the set-up choice, the specimen geometry has had to be designed accordingly. In the arrangement used in Wang et al., 2005 the fast-jaws system clamps the specimen once the actuator reaches the velocity set in the test.

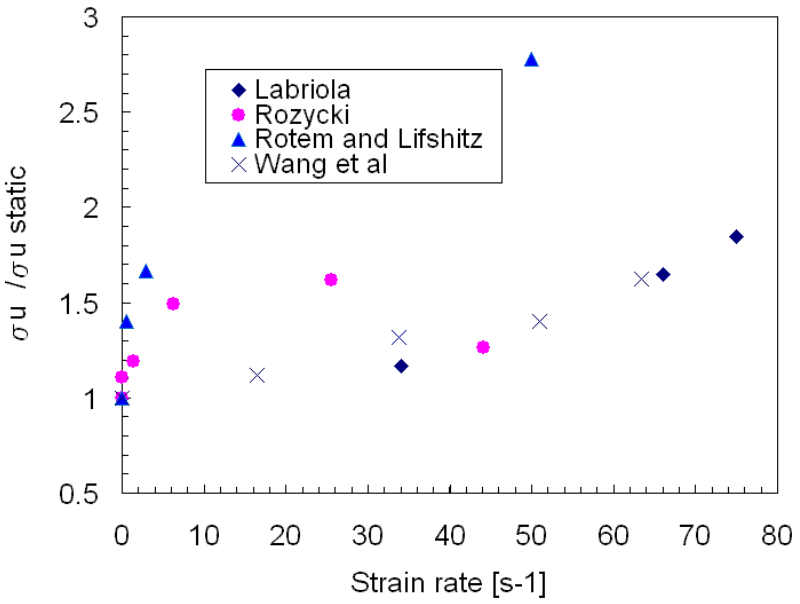

Figure 5-17 : Normalized Ultimate Strength versus strain-rate for different works

The specimen used by Wang et al., 2005 has a longer gauge length, since the run the actuator needs to accelerate to reach the set velocity has to be taken into account, and provided with special tabs to optimise the load transmission. This set-up entails a direct impact on the specimen which results in a load signal acquisition not free from noise. A longer specimen also leads to lower strain-rates. From figure 5-17 it can be seen that the highest strain-rate value achieved by Wang et al., 2005 is 62 s^{-1} and it was achieved using the same actuator velocity.

In this work, as already discussed previously, a particular test arrangement was devised. The advantages can be found in a smoother signal acquisition and a shorter specimen which allows to reach higher strain-rates with the same actuator velocity.

(d) Mechanical properties evolution

In figure 5-18 the ultimate strain and the ultimate strength versus the strain-rate are reported.

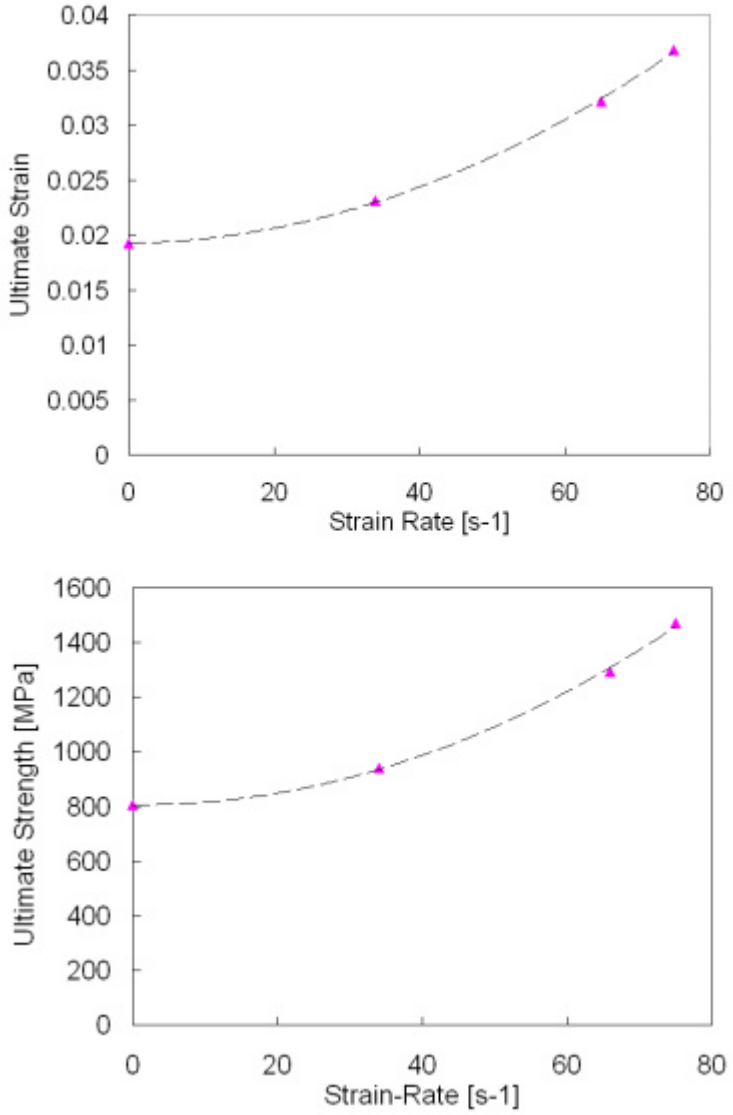

Figure 5-18: Ultimate strength and strain versus strain-rate

5.9 Results for $[15]_4$

(a) Experimental curves

Three experiments were performed at 5 m/s, 10 m/s and 15m/s. The respective strain-rates detected were 29 s^{-1}, 48 s^{-1} and 52 s^{-1}. Figure 5-19 depicts the stress-strain curves obtained along with the static one.

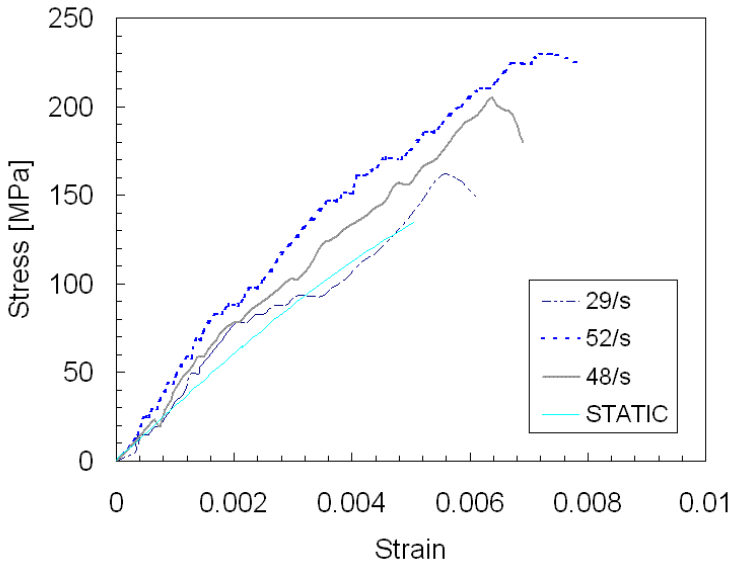

Figure 5-19: Stress-Strain curve at different strain rate for $[15]_4$

(b) Response and failure mechanisms

From the experimental testing the following three observations were noticed:

a) A significant increase of the strength to failure with increasing the strain-rate (up to 64%);

b) A significant increase of the strain to failure with increasing strain-rate (up to 54%);

c) A significant increase of the Young's modulus (up to 33%).

As can be seen in figure 5-20 the failure occurs by shear preserving the fibre orientation. In this case the composite sensitivity on the strain-rate seems to be driven by the resin behaviour as found by Gilat et al., 2002 while testing carbon/epoxy specimens.

Figure 5-20: $[15]_4$ Specimen after failure

(c) Mechanical properties evolution

Figure 5-21 reports the plots of the Young's modulus, ultimate strain and ultimate strength versus the strain-rate.

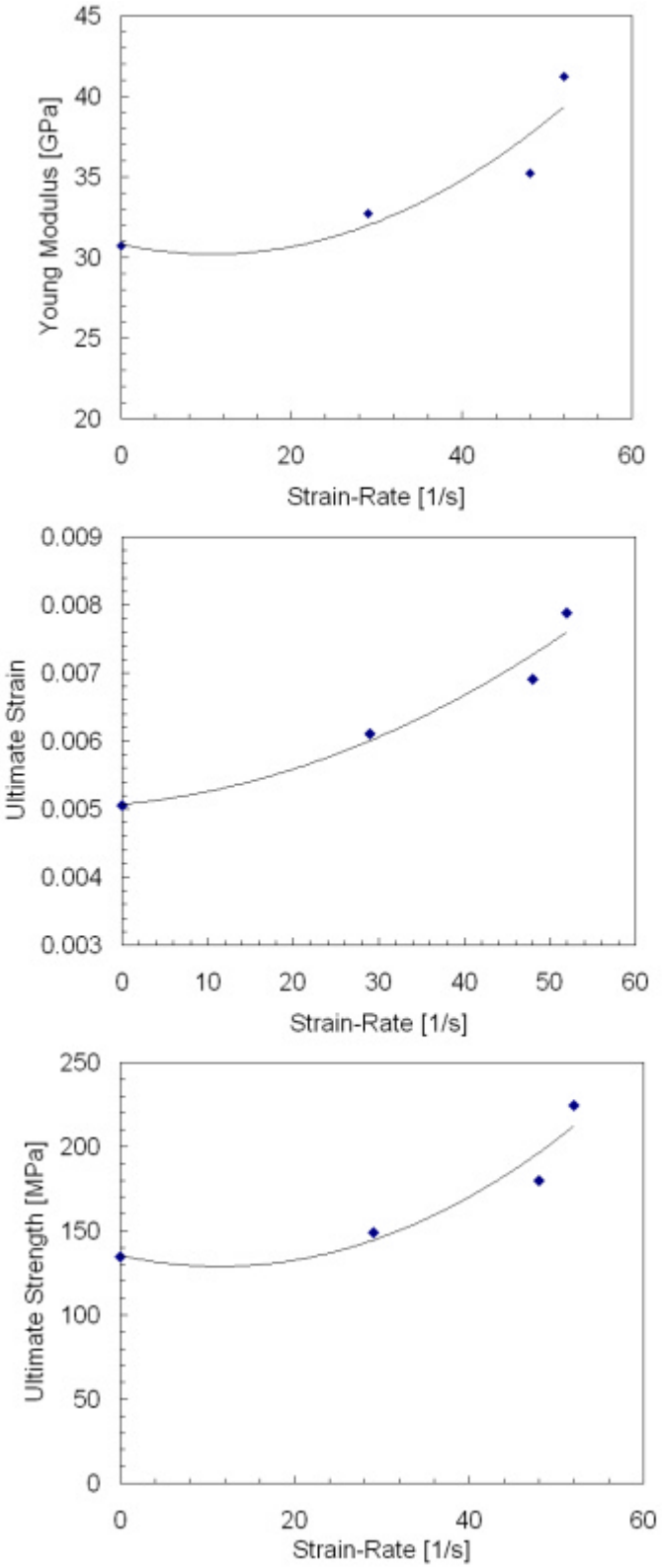

Figure 5-21: Mechanical properties evolution for [15] [4]

5.10 Results for $[30]_4$

(a) Experimental curves

Three experiments were performed at 5 m/s, 10 m/s and 15 m/s. The respective strain-rates detected were 23 s^{-1}, 32 s^{-1} and 48 s^{-1}. In the following graph the stress-strain curves obtained along with the static one are depicted.

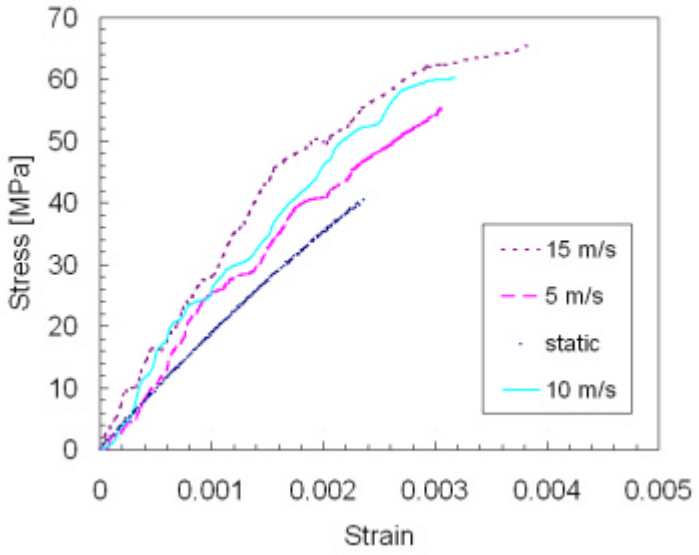

Figure 5-22: Stress-Strain curve at different strain rate for $[30]_4$

(b) Response and Failure Mechanism

From the experimental testing, the following three observations were noticed:

a) A significant increase of the strength to failure with increasing the strain-rate (up to 60%);

b) A significant increase of the strain to failure with increasing strain-rate (up to 65%);

c) A significant increase of the Young's modulus (up to 55%). The curves could be approximately described by a bilinear trend as shown in figure 5-23 for the test at 15m/s. This consideration was used in chapter 8 for the numerical modelling of the experiments.

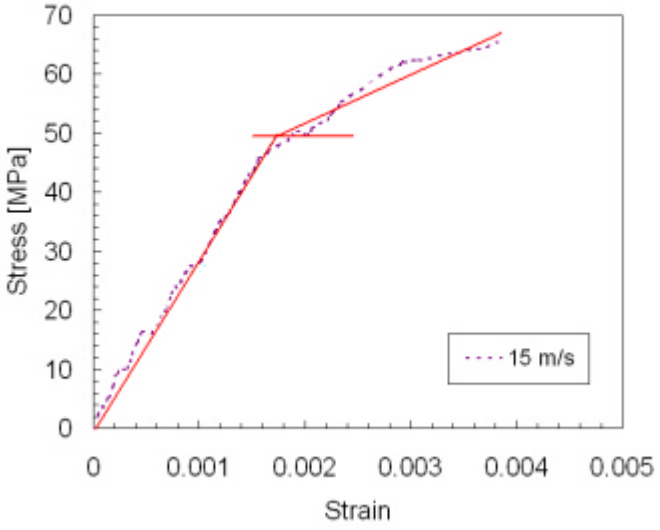

Figure 5-23: Bilinear trend approximation for test at 15m/s

As can be seen in figure 5-24, the failure occurs by shear preserving the fibre orientation as for the previous case. Once again the composite sensitivity on the strain-rate seems to be driven by the resin behaviour, in accordance with what Gilat et al. found.

It is interesting to note that a more significant effect of the strain rate on the maximum stress is observed as the off-axis angle increases. For the same rate $48s^{-1}$, the ultimate stress increases 87% for 30º laminates versus 34% for 15º ones. This seems to be in trend with what Gilat et al. observed, namely that the highest dependence of the maximum stress and strain on the strain-rate was observed for 45º laminates.

Figure 5-24: $[30]_4$ Specimen after failure

(d) Mechanical properties evolution

Figure 5-25 reports the plots of the Young's modulus, ultimate strain and ultimate strength versus the strain rate.

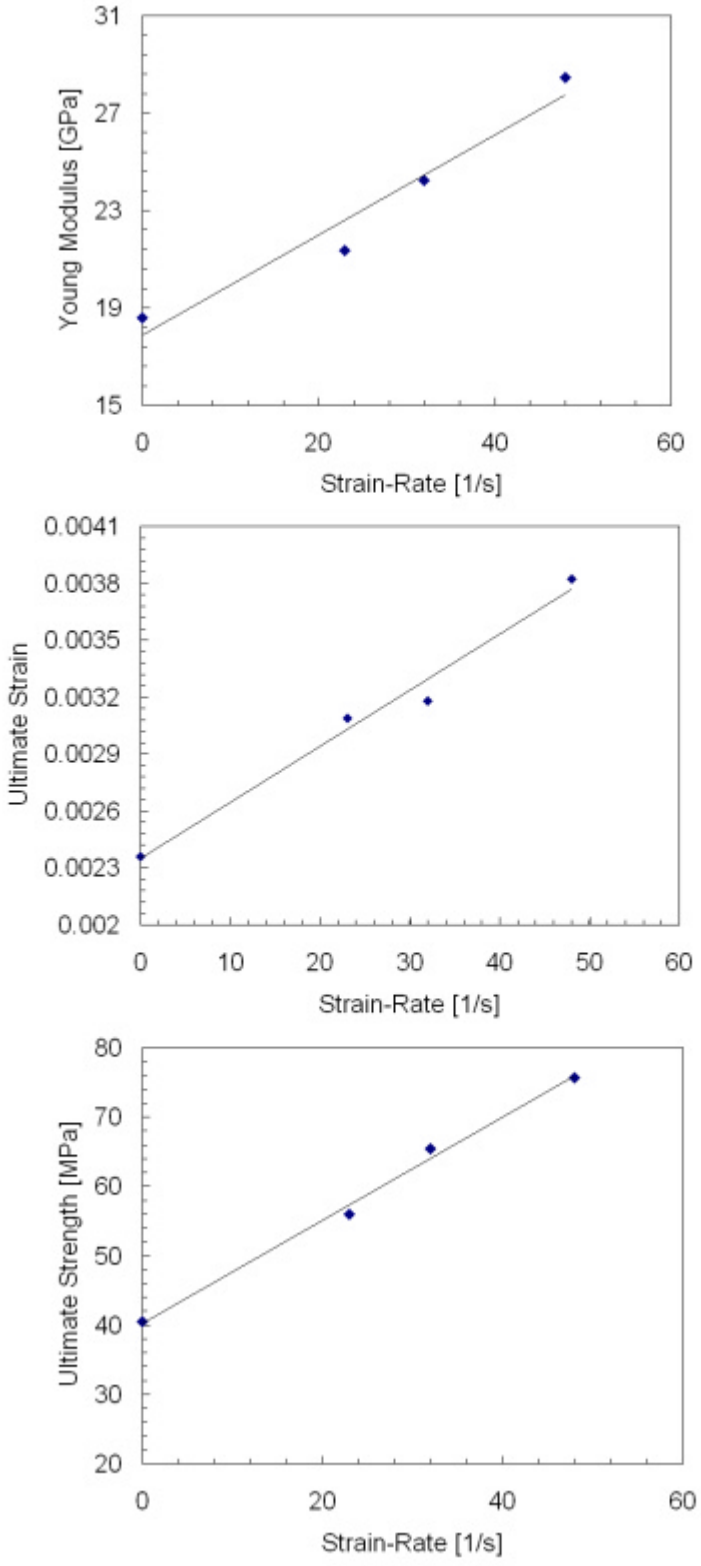

Figure 5-25: Mechanical properties evolution for [30] [4]

5.11 Comparison between different fibre orientation specimens

Figure 5-26 reports the plots of the stress-strain curves for the three configurations tested, both in the static case and at a given strain-rate (34 s^{-1} for 0º, 48 s^{-1} for 15º and 30º configurations). It is noted that by increasing the rate of the strain the curves become closer. This is due to the improvement of the elastic modulus, which is more significant as the angle between fibres and load application direction increases, owing to the improvement of the resin's mechanical properties.

Figure 5-27 reports the Young's Modulus, the ultimate strength and the ultimate strain versus the fibres' angle at different strain-rates. It also shows that the ultimate strength and strain at a given fibre-load application angle increase as the rate of the strain increases.

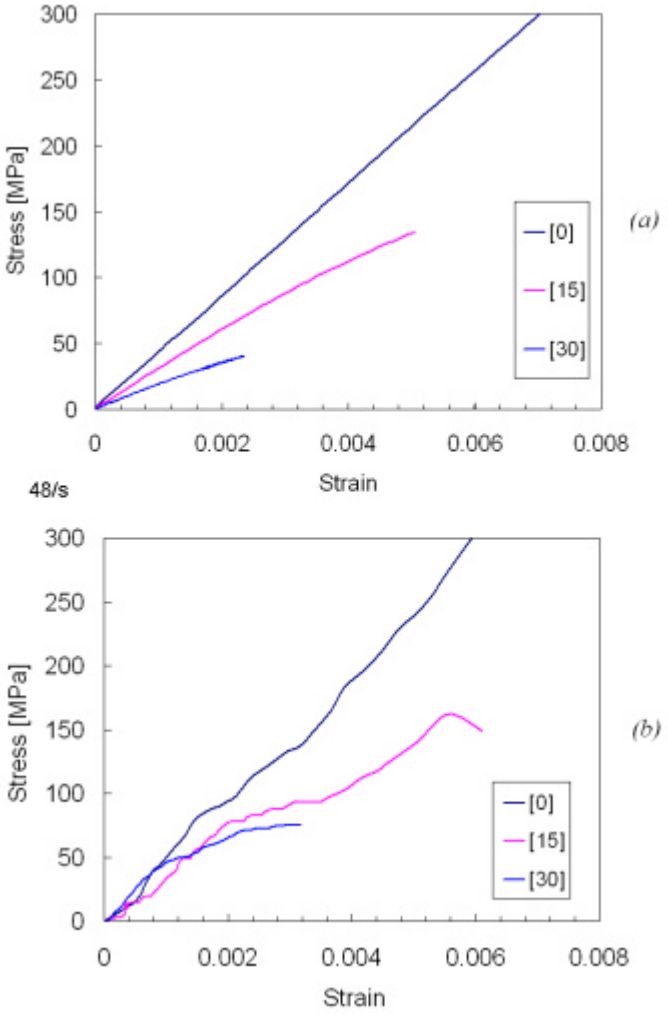

Figure 5-26: Fibre orientation influence in static (a) and at a given strain-rate (b)

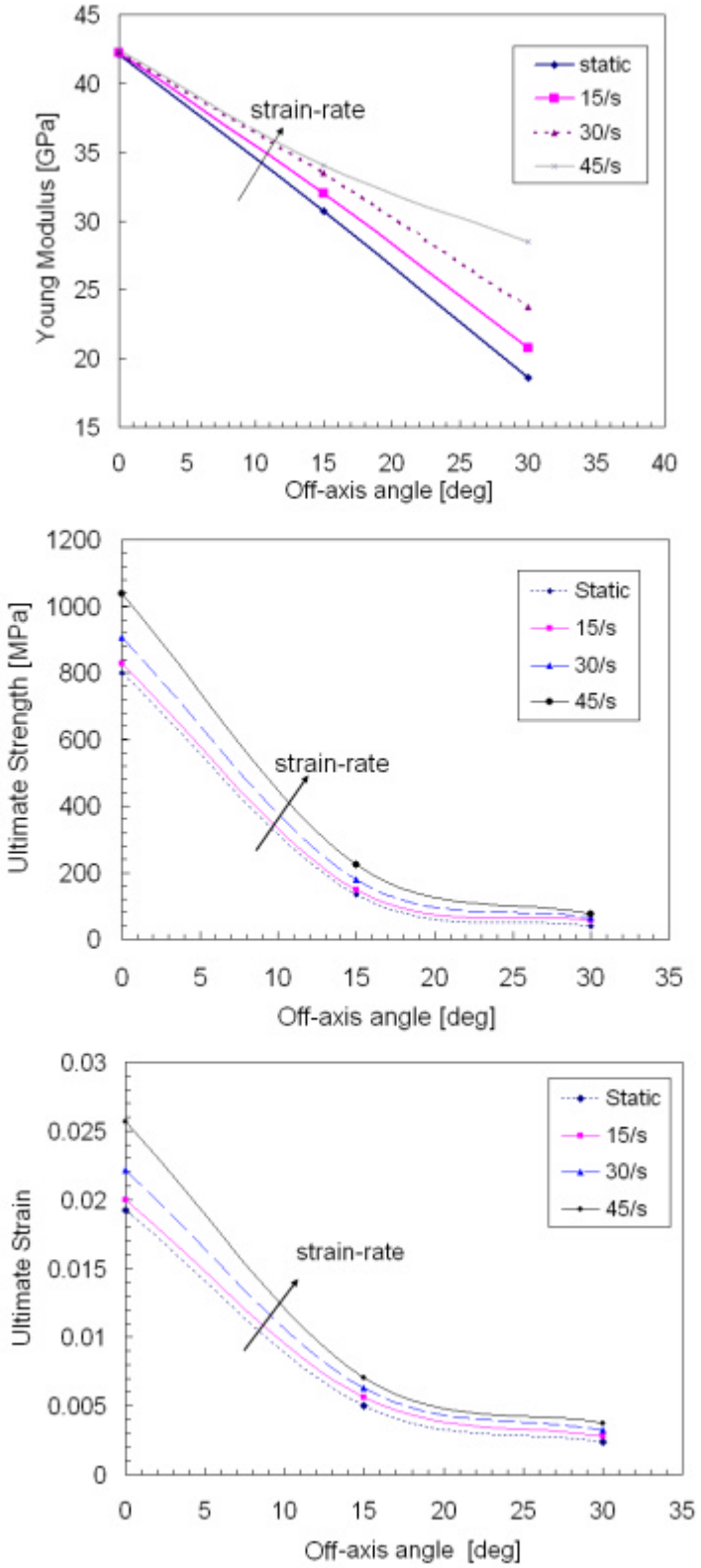

Figure 5-27: Off-axis mechanical properties evolution at different strain-rates

Table 5-3: Summary of the mechanical properties obtained from the experiments

Mechanical Properties for $[0]_4$			
Strain-Rate	**Young's Modulus [GPa]**	**Ultimate Strain**	**Ultimate Strength [MPa]**
0	41.2	0.0192	805
34	41.2	0.0231	942
66	41.2	0.0321	1295
75	41.2	0.0368	1470
Mechanical Properties for $[15]_4$			
Strain-Rate	**Young's Modulus [GPa]**	**Ultimate Strain**	**Ultimate Strength [MPa]**
0	30.7	0.00505	134.5
29	32.7	0.00610	149.2
48	35.2	0.00691	180.0
52	41.2	0.00787	224.5
Mechanical Properties for $[30]_4$			
Strain-Rate	**Young's Modulus [GPa]**	**Ultimate Strain**	**Ultimate Strength [MPa]**
0	18.6	0.00235	40.49
23	21.37	0.00308	55.91
32	24.25	0.00317	65.48
48	28.46	0.00382	75.68

6 Theoretical Assessment of Material Behaviour

6.1 Introduction

Several researchers have attempted to idealise the strain rate dependent behaviour of diverse composite materials using a network of Hookean springs and Newtonian dashpots connected in series or parallel as discussed in the literature review. In general, these models are too simple to accurately describe the behaviour of real materials. More complicated models are difficult to analyse because of considerable difficulty in determining the various constants from experiments.

Based on the output of the experimental campaign, ideally an analytical model should be found that is capable of describing the strain-rate behaviour of unidirectional E-glass/epoxy under diverse off-axis loads. This could be then implemented in an f.e.m. code, allowing the dynamic response of general structures made of E-glass/epoxy to be investigated. In the following paragraphs an approach is presented to model part of the experimental results, and it is highlighted the need of further development of theoretical models for E-glass/epoxy.

6.2 Theoretical modellisation of the observed experiments

6.2.1 Empirical failure criterion for $[0]_4$

According to the experimental results, the constitutive relationship useful to describe the overall behaviour of the material can still be $\sigma = \varepsilon E$. This is because the dependence of the Young's Modulus on the strain rate is negligible. An empirical equation capable of predicting the ultimate tensile strength of GFRP is proposed below.

From the experimental observations it was established that the ultimate strength and strain are functions of the strain-rate. The ultimate strain varies with the strain-rate as described in figure 5-18. The function which best describes the trend of the ultimate strain versus strain-rate relationship is parabolic:

$$\varepsilon_U = a \cdot \dot{\varepsilon}^2 + b \cdot \dot{\varepsilon} + c \qquad \text{(eq.6.1)}$$

where *a*, *b*, and *c* are parameters determined experimentally, whose values are:

$a = 6 \cdot 10\text{-}6\ s^2$;

$b = 9 \cdot 10\text{-}6$ s;

$c = 0.0192$.

The ultimate strength at a given strain rate can therefore be obtained simply substituting eq.6.1 in

$$s_U(\dot{e}) = E \cdot e_U(\dot{e}) \qquad \text{(eq. 6.2)}$$

Rearranging:

$$s_U(\dot{e}) = E \cdot (a \cdot \dot{e}^2 + b \cdot \dot{e} + c) \qquad \text{(eq. 6.3)}$$

gives the ultimate strength at a certain strain rate.

Figure 6-1 shows a comparison between the predicted increment in failure strength found by use of this empirical criterion and the one made by use of a visco-elastic model developed by Wang et al., 2005 for the same material and by use of the same machine but different test set-up. Both the models well describe the respective trend of the experimental data but seem not to be in accordance with each other. Wang et al., 2005 was developed in the range 0-64 s^{-1} while 0-74 s^{-1} is the range which the current failure criterion refers to. Each model takes the coefficients values from the related experimental observations which are a function of the particular test set-up and specimen geometry adopted. As a consequence, each model will be a function of both the test set-up and geometry adopted.

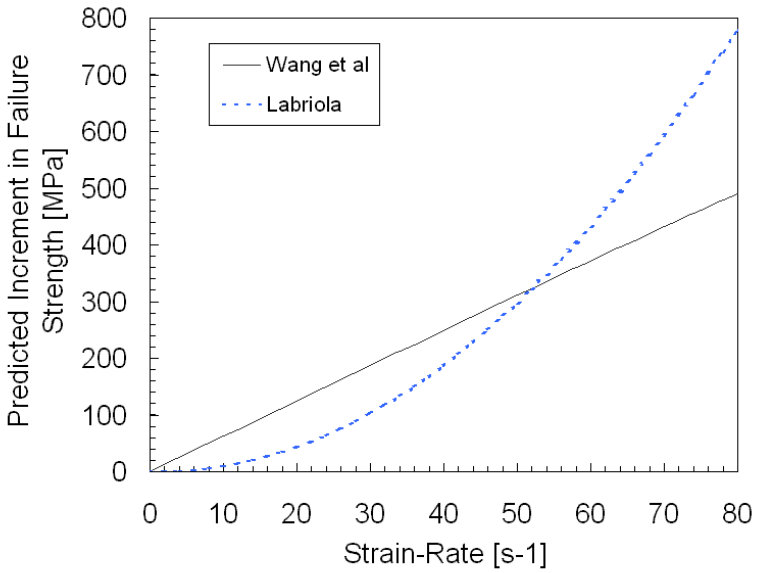

Figure 6-1: Comparison between predicted increment in failure strength models

7 Numerical Modelling of the Observed Experiments

7.1 Introduction

The goal of the numerical modelling of the experiments was to establish a systematic methodology to describe the strain-rate behaviour of E-glass/epoxy material. Once the validity of the modelling approach was demonstrated, this was shown to be applicable to the investigation of more general problems where the same type of material is deployed. Particularly, as an ultimate objective of this thesis, this approach was used to investigate the behaviour of the skins of a sailing-yacht sandwich hull panel under slam loads.

Ideally, an analytical model capable of describing the strain-rate behaviour of unidirectional E-glass/epoxy under diverse off-axis loads should be considered and implemented in the code utilized. The author proposed an approach, based on assumptions explained later on, which considers the rate dependence of the material properties found in the experimental testing, and compensates for the lack of availability of such a model.

7.2 Choice of the F.e.m. Code

The use of FEA in structural design has become common practice when a quest for time, costs and performance optimization is required. Two commercial software packages were adopted in the present work. ANSYS implicit solver was used for the comparative static analysis of the hull panel. LS-DYNA was used for dynamic analysis of the experiments, of the hull panel, and for the fluid-structure interaction problem. LS-DYNA was chosen as it is a well suited general purpose finite element code for dynamic analysis. Unlike ANSYS, the main solution methodology of LS-DYNA is based on explicit time integration. Explicit analysis refers to the numerical method used to represent and solve the time derivatives in the momentum and energy equations. The advantage of using this methodology can be found in the following considerations as discussed in NAFEMS, 2006. In an implicit solution, global equilibrium is achieved by iteration, after which local element variables are evaluated. The solution is therefore calculated iteratively at every discrete time step. Providing equilibrium can be achieved, there is no limit to

the size of the time step that can be used. Hence, implicit schemes are termed "unconditionally stable". Achieving global equilibrium at each time step involves matrix factorisation however, which is computationally intensive. Analyses that are well-suited to implicit solution techniques are static, low-speed dynamic or steady-state transport analyses.

By contrast, explicit solution techniques evaluate local variables directly, without the need for global equilibrium calculations, hence without iteration and without solving a system of linear algebraic equations. The dynamic explicit approach has the characteristic of less memory requirement and computational efficiency since the need for a consistent stiffness matrix is obviated. Nevertheless this integration scheme is only "conditionally stable", that is, only very small time steps lead to a stable solution. The time step, dt, must be less than a critical value or computational errors will grow resulting in a bad solution. The critical time step time must be less than the length of time it takes a signal travelling at the speed of sound in the material to traverse the distance between the node points. The critical time step for this problem can be calculated by $dt_{max} = dL / c$, where c is the speed of the sound and dL is the distance between two nodes. More details are reported in Appendix 1. Problems well suited to explicit solution are simultaneous large displacement and contact problems, rapidly changing or discontinuous loading, and rigid body motion.

7.3 Validation

Method validation is possibly the most important aspect of the finite element method, with some typical tests described by NAFEMS, 1984.

Patch testing was found to be the easiest method of validation. It can be interpreted as a check which ascertained whether a pattern of elements subjected to a constant strain reproduce exactly the constitutive behaviour of material, and result in correct stresses when it becomes infinitesimally small. If so, it can be argued that the finite element model represents the real material behaviour, and in the limit, as the size of the elements decreases would therefore reproduce exactly the behaviour of the real structure.

7.4 Modelling variables

The most common problem that faces the analyst is choosing the correct mesh density as well as understanding the implication of different mesh density (Cook et al., 1989). A too coarse mesh, chosen to save time modelling, can lead to an overestimate of the stress. A mesh that is too fine, to improve accuracy, increases modelling time and can lead to false results. One of the key requirements is that the selected displacement pattern for the elements is able to produce consistent stress fields inside the elements (Zienkiewicz and Taylor, 2000).

With this information in mind the specimen gauge length has been modelled by use of four node shell elements. The choice of shell elements has been dictated by the thickness of the specimen. A large number of solid elements would have been necessary to respect their aspect ratio, compromising the computational efficiency. The shape and the number of elements were chosen with the critical time step requirement for explicit solver in mind. A fine mesh with square shaped shells was then obtained. The element formulation was Belytschko and Tsay, 1981 which is based on a combined co-rotational and velocity-strain formulation (see Appendix 1). These kinematical assumptions ensure optimal computational efficiency.

The boundary conditions were imposed such that one end of the specimen was clamped and a prescribed motion was applied to the nodes at the opposite end through an input velocity-time curve. The velocity-time curve was determined by following a trial and error procedure with the main purpose being to get a similar strain-rate in the gauge section. As schematically illustrated in figure 7-1, the velocity profile was chosen such that by applying a constant velocity v_{fem} to the free end of the specimen in the finite element model, the strain-rate detected in the gauge section was the same to the one recorded in the experiment where the velocity v_{act} was applied at the actuator. Figure 7-2 depicts a scheme of the f.e. model.

7.5 Constitutive material model

A material model (MAT.19 in LS-DYNA's library) with strain-rate dependence options developed for isotropic materials was used to describe the behaviour of the composite under investigation (Appendix 1). The strain-rate effects are accounted for using Cowper and Symonds developed for metals. In MAT.19 the yield strength, Young's modulus, tangent modulus and the failure (either with a maximum stress or strain criterion), can be input as a function of the strain-rate. For 0º specimens for which the stress-strain curve is linear up to failure, this model was used considering the yield strength coinciding with the ultimate strength of the composite material. The failure was modelled using the ultimate stress versus strain-rate curve detected in the experiments. The Young's modulus strain-rate dependence option was not utilized since no significant variation was observed in the experiments.

It is argued that a isotropic material model in the element formulation is valid in this context since the structure is a slender one with high aspect ratio, with response in the long span direction being dependent principally on the material properties in that direction. The implicit assumption is that Poisson's effect owing to properties in the transverse direction are neglected. This is in accordance with Okoli and Smith, 2000 findings.

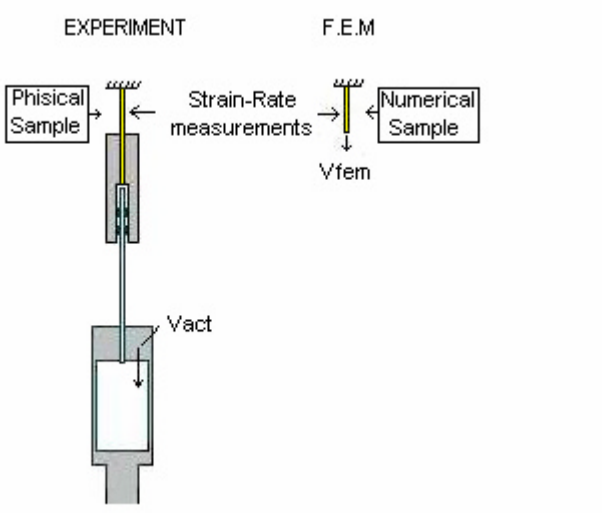

Figure 7-1: Correlation scheme of physical and numerical model

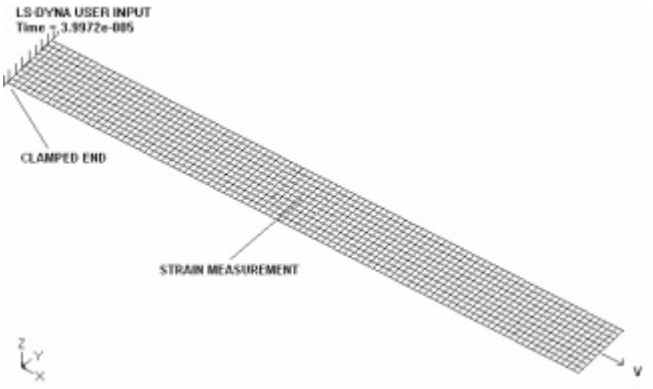

Figure 7-2: Scheme of the f.e.m. model

7.5.1 Numerical simulation of $[0]_4$ laminates

The force-time, strain-time and the resulting stress-strain graphs are reported both for the numerical and experimental cases. Figure 7-3 depicts the stress distribution at 34 s^{-1} when failure starts to take place. Elements are deleted when they reach the ultimate strength and these are graphically represented in white. The graphs in figure 7-4 show a comparison between the experimental and numerical variables for the same value of the strain rate. The numerical stress-strain curve was plotted calculating the force in the same way as for the real experiment to achieve an accurate comparison. The force was measured in the nodes of the clamped end and the strain reading was taken in the gauge length. The numerical curves seem to reflect the behaviour observed in the experiments. This confirms the validity of the assumption made on the use of the material model developed for metals.

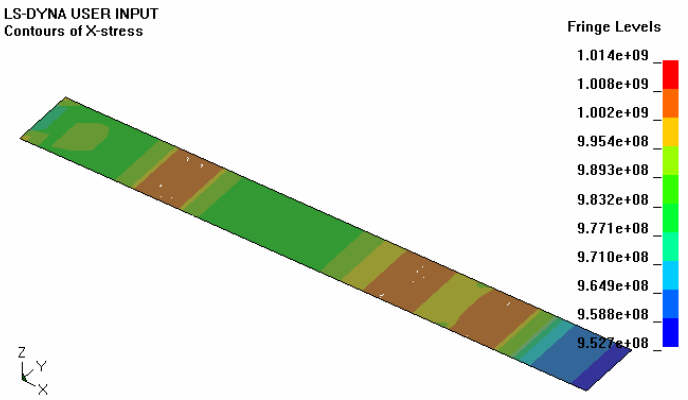

Figure 7-3: Stress Distribution for $[0]_4$ @ 34 s^{-1}

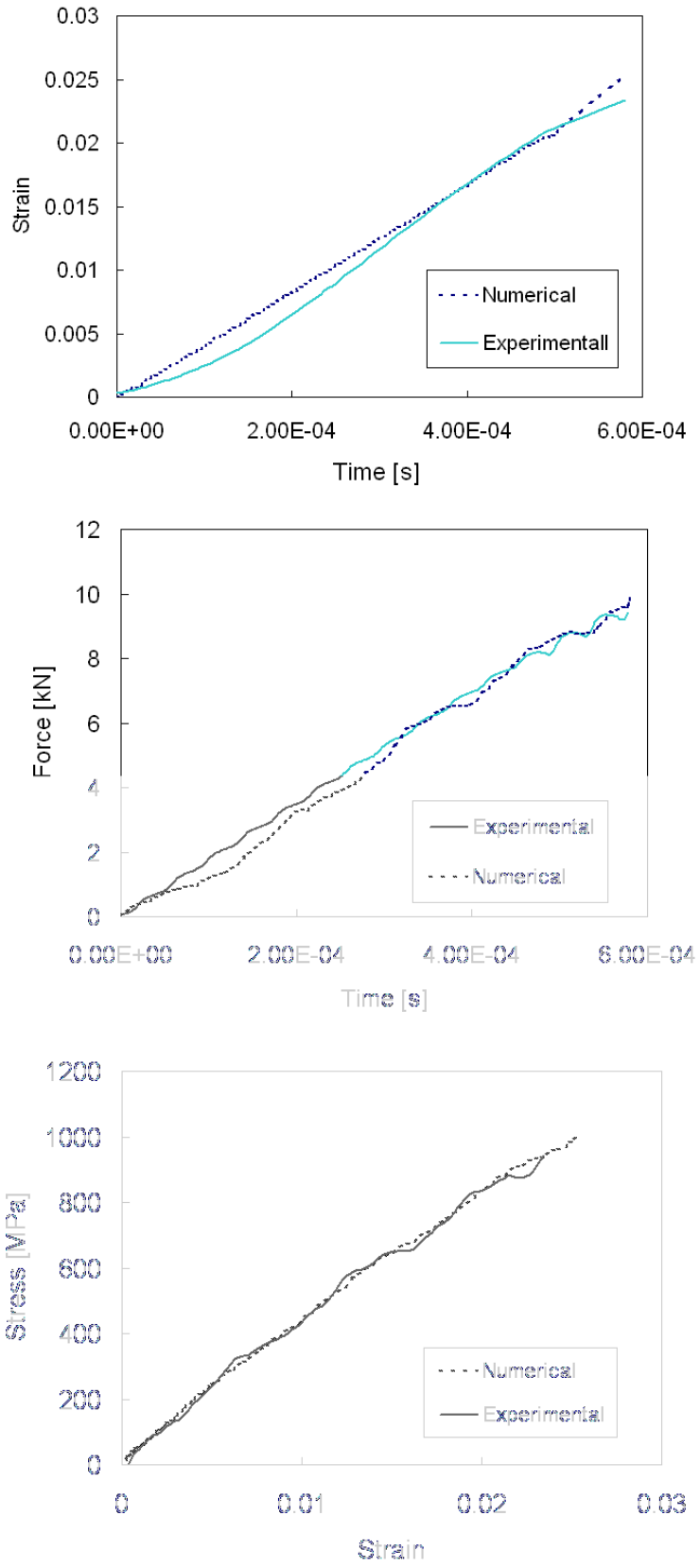

Figure 7-4: Comparison Numerical-Experimental for $[0]_4$ @ 34 s^{-1}

7.5.2 Numerical Simulation for Off-Axis Configurations

The numerical analysis of the 15º and 30º specimens was based on the same material model and assumptions used for the 0º case. The stress-strain behaviour for 30º specimens was approximated to be bi-linear. The yield stress has been identified from the experimental curves at different rates, and the strain-rate dependence of the Young modulus, the tangent modulus and the ultimate strength has been considered.

The force-time, strain-time and the resulting stress-strain graphs are reported both for the numerical and experimental cases. Graphs shown in figures 7-5 and 7-6 depict the comparisons between the experimental and numerical variables at a given strain-rate respectively in the 15º case and 30º case.

7.5.3 Curves Analysis

By looking at the graphs, experimental and numerical curves seem to be in accordance especially for the 0º tests.

It may be argued that the assumption made on the material model is more realistic in the 0º case. In contrast for off-axis configurations, the response dependence on the transverse properties can be more significant. Nevertheless, the numerical curves produced still match reasonably well the relative experimental ones. Discrepancies are noted as the off-axis angle increases and may be due to the assumptions made.

As a conclusion, the approach used in this chapter is suitable for modelling unidirectional composite materials when the applied load direction is known a priori. Ideally, a constitutive material model for orthotropic materials, allowing for incorporation of the strain-rate effects, should be considered to predict the behaviour of more complex structures and loading scenarios.

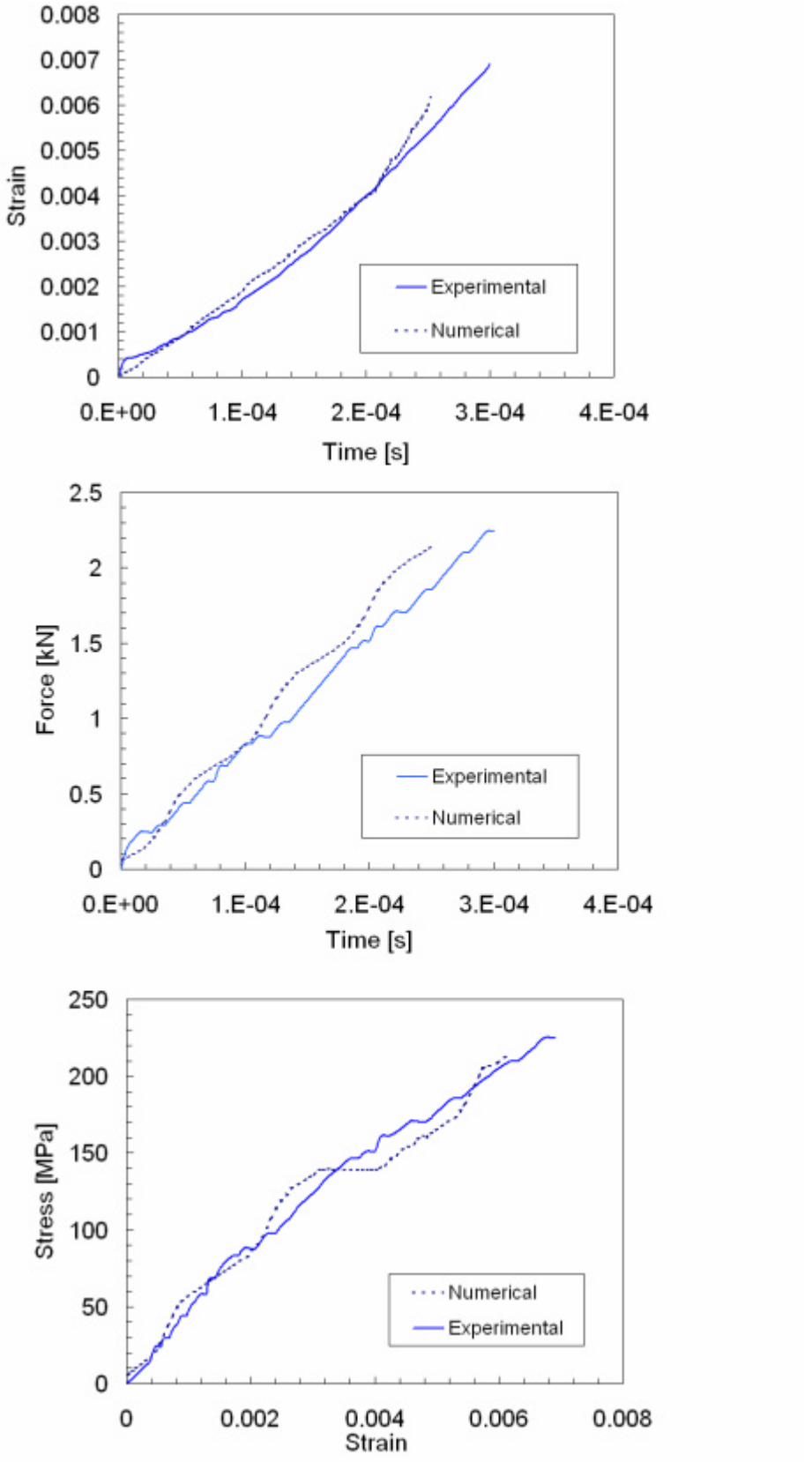

Figure 7-5: Comparison Numerical Experimental for [15]$_4$ @ 52 s^{-1}

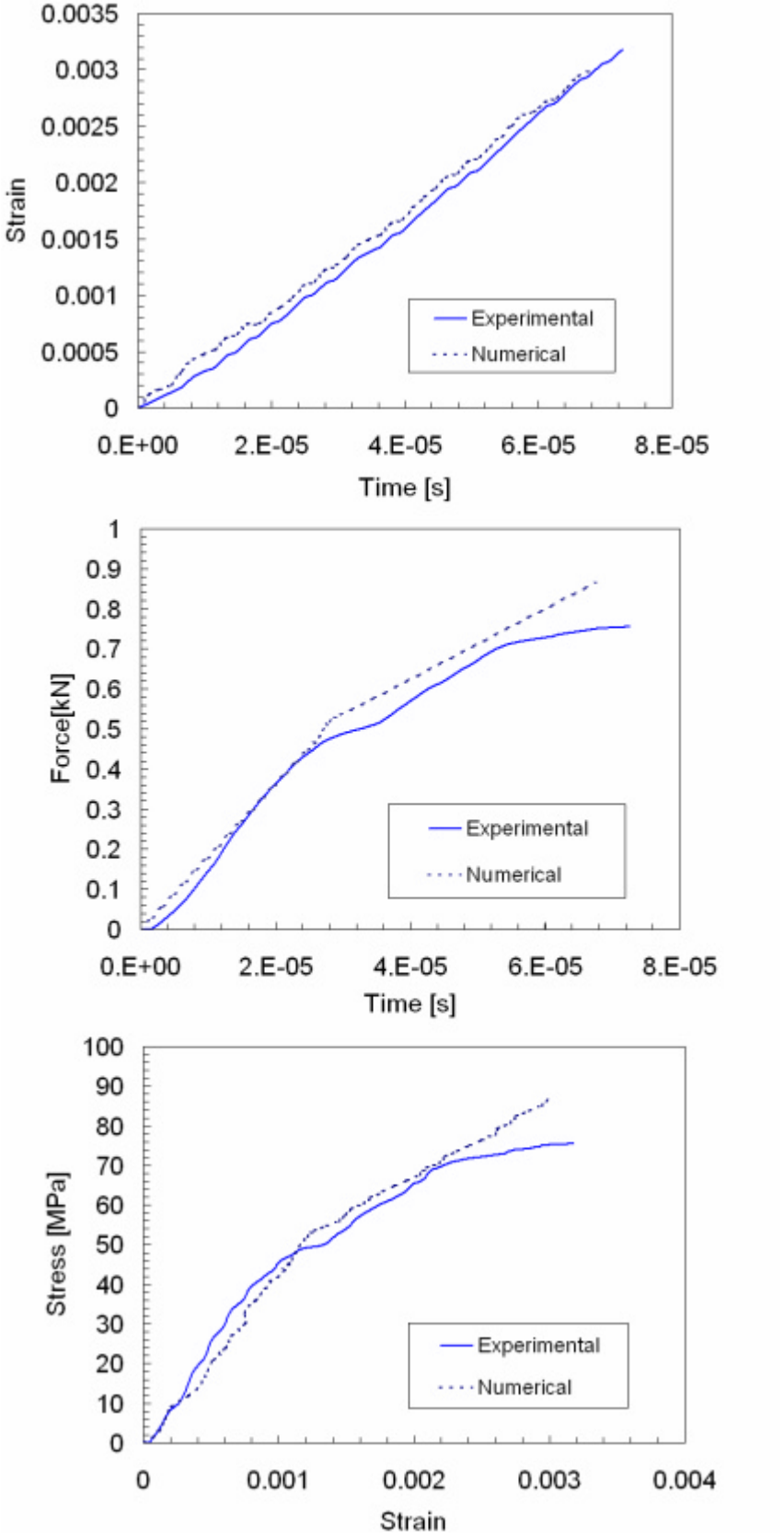

Figure 7-6: Comparison Numerical Experimental for $[30]_4$ @ 48 s^{-1}

8 Theoretical investigation of a Hull Panel under slam loads

8.1 Introduction

This chapter presents a theoretical investigation of a sandwich hull panel under slam loads bearing in mind the knowledge acquired on the dynamic properties of E-glass/epoxy developed in chapters 5, 6 and 7. Stresses and deformations were evaluated considering their dependence on the strain-rate. With this in mind, a theoretical study was conducted on an E-glass/epoxy sandwich panel cored with SAN (Styrene Acrilo-Nitrile) polymeric foam, using the DK46 sailing-yacht as a case study. As described previously, a sandwich panel is one made of two stiff strong skins separated by a lightweight core material. The bending and the in-plane stresses are mainly carried by the faces, whereas the shear stresses are taken by the core (Zenkert, 1995). In the experimental part the in-plane dynamic properties of E-glass/epoxy material were investigated as these are the key properties of interest in sandwich structures where composites are deployed in the skins. Polymeric foams usually do not show significant dependence on the strain-rate at the strain-rate ranges concerned with this application (Saha et al., 2005; Mahfuz et al., 2006). It was therefore viable to limit the strain-rate analysis of such sandwich panel to the skins. The purpose of the investigation was to understand, by comparing the results with static based approaches, how the dynamic mechanical properties of the materials influenced the overall panel response. This analysis allows for a better understanding of the response of sailing yacht structures under slam loads and eventually for their design to be improved.

This study was conducted in the following steps:

a) Firstly, a finite element analysis, simulating the hull-water impact typical in a slamming phenomenon, was carried out on the yacht under consideration in order to evaluate the pressure-time distribution over the hull panel, namely the slam load.

b) Dynamic numerical simulation of the sandwich panel under investigation was performed at a ply level. The panel was subject to the pressure-time load evaluated

in point a). The strain-rate characteristics of the material assessed in the experimental testing were considered. Consequently a strain-rate analysis was carried out and the stress distribution evaluated.

c) A static f.e.m. analysis of the panel, based on ISO design rules, was run to assess the stress in each ply.

d) A comparison between dynamic and static results was proposed and discussed.

8.2 Determination of Slam Loads by fluid-structure interaction simulation

The aim of this simulation was to assess the time-pressure distribution on the area of the hull affected by the slamming phenomenon. This was achieved by using the fluid-structure interaction modelling capabilities available in LS-DYNA. The suitability of the software to model these kind of problems has already been investigated and validated by Le Sourne et al., 2003 by successfully modelling experimental drop tests performed on cylinder and v-shaped bodies by Zhao et al., 1997.

8.2.1 Modelling Approach

Experimental observations led by Manganelli et al., 2003 showed that the hull experiences the highest slamming pressure in the flat bottomed area located in front of the keel. For this reason, only the part of the hull from the keel to the bow was modelled. Figure 8-1 shows the hull metal grid structure with the contour of the panel under examination indicated by the number 1. Perfect bonding was ensured between the grid and the hull such that a fixed edges condition could be assumed for the panel.

Figure 8-1: Grid structure and panel under investigation

A purely Lagrangian approach to model both hull structure and water, was initially considered since it may capture the initial impact accurately. But as the structure moves into the fluid, high element distortion takes place leading to numerical instability.

For this reason, the ALE (arbitrary Lagrangian-Eulerian) method within LS-DYNA explicit finite element code was used. Olovsson and Souli, 2000, 2001 and Souli et al., 2003 demonstrated to be a suitable method to describe fluid-structure interaction problems. The feature of this method is to adopt two mesh types in the analysis. The Lagrangian mesh, associated with the typical finite element analysis is used to model the material impacting the fluid. This mesh deforms as it responds to the loading and the boundary conditions in the analysis. The Eulerian mesh is used to model the fluids, water and air in this study, and remains fixed throughout the analysis tracking material as it moves through the mesh.

The hull was modelled with shell Lagrangian elements whereas the water and the air were modelled by solid Eulerian elements. Similar size was adopted for fluid and structural elements to ensure the best coupling quality as verified by Olovsson and Souli, 2001. An air region was considered to accommodate the splash effect of the water. Polynomial equations of state were considered to describe the fluids behaviour (Appendix 1). To avoid reflection of the pressure waves by the walls of the virtual tank, an outflow boundary condition was considered.

The hull part, excluding the panel, was modelled as a rigid body. Elements which are rigid are bypassed in the element processing and no storage is allocated for

storing history variables; consequently, the rigid material type is very cost efficient (Benson and Hallquist, 1986).

The panel was modeled as an elastic material and the elastic modulus and thickness of the elements were chosen such that the same bending stiffness of the laminate under investigation was obtained. The same approach was followed by Manganelli et al., 2003 in experimental drop tests on a racing sailing-yacht open 60.

Figure 8-2 depicts the fluid-structure model.

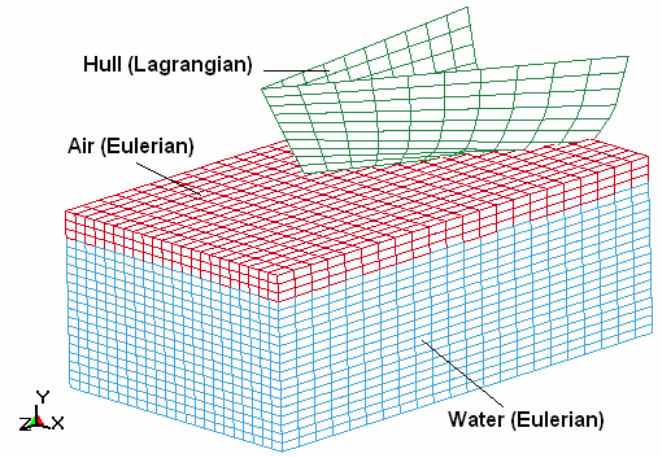

Figure 8-2: Scheme of the fluid-structure model

The boundary conditions considered were vertical impact velocity and forward velocity (2.3 m/s and 4.3 m/s respectively). These values were determined considering those measured by Manganelli and Wilson, 2001 on a full scale Open 60 racing yacht during an ocean race in severe sea conditions. The values were scaled down to account for the dimensions and the performances of the hull studied.

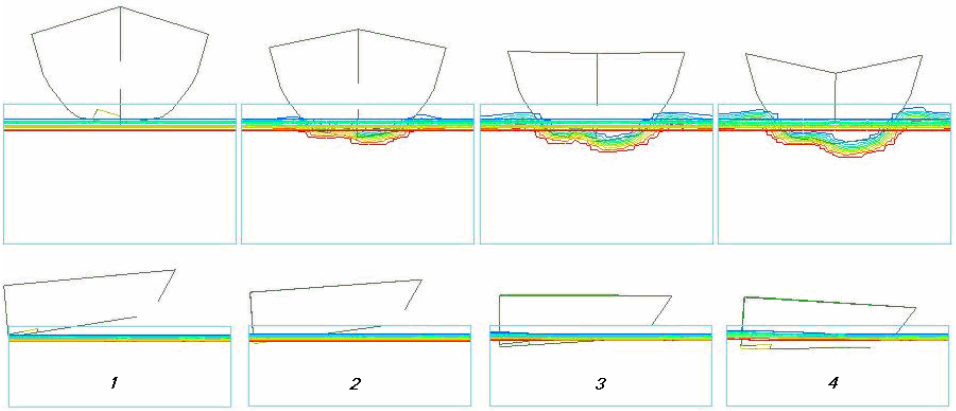

Figure 8-3: Water entry of the hull in four different time step

The simulation was run for 0.15 seconds. The pressure on the whole panel was calculated as the average pressure acting on each element of the panel. Results of pressure-time distribution are reported in figure 8-4. The peak pressure acts for less then 3 msec and is detected when the hull first touches the water (step 1 figure 8-3). The pressure then stabilizes to values close to 100 kPa and drops as the boat looses its vertical velocity.

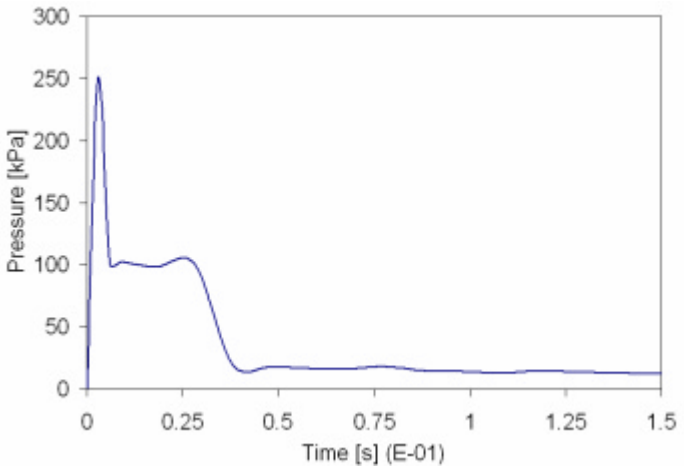

Figure 8-4: Slam pressure-time distribution

Similar pressure-time trends were found by Hentinen and Holm in slamming experimental tests on a full scale 9.4 m long sailing yacht and by Manganelli et al. in experimental scale model testing of an Open 60. The peak pressure values found by Hentinen and Holm, 1994 and Manganelli et al., 2003 were respectively lower and higher than the one detected in this work. This was in accordance with the

different dimensions of the boats considered, confirming that the modelling approach followed leads to significant results.

The pressure-time distribution curve calculated, emulating the effect of the impact hull bottom-water surface, was then used in the dynamic analysis of the sandwich panel under examination.

8.3 Strain-rate analysis of the panel under slam pressure

8.3.1 Modelling of the panel

Dimensions and geometry were obtained by the designer who provided the needed CAD drawings. These were imported in LS-DYNA allowing the panel to be modelled layer by layer (figure 8-5). The sandwich was composed of a five plies outer skin and five plies inner skin. The skins were made of a combination of woven and unidirectional E-glass/epoxy layers. The unidirectional layers formed an angle of 0º, +30º and -30º with the shorter span of the panel. The core material utilized was SAN (styrene acrilonitrile) polymeric closed cell foam. Material stack sequence is reported in table 8-1. Solid elements were used as the most suitable to describe three dimensional stresses and deformation fields (Norrie and Devries, 1978). These elements can be modelled as isotropic, orthotropic or anisotropic.

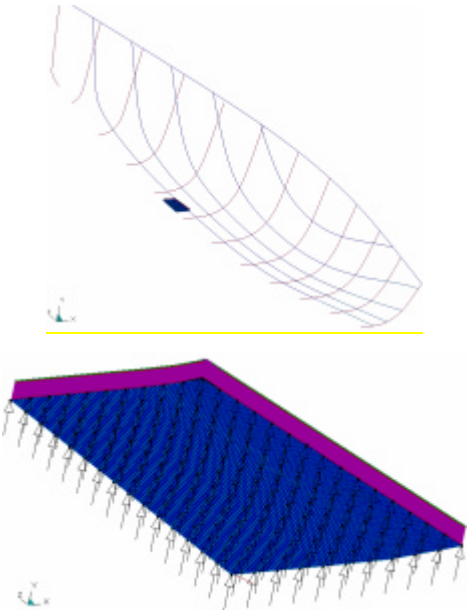

Figure 8-5: Sandwich panel modelling

Layers (outer skin)		Layers (inner skin)	
N	**Type**	**N**	**Type**
1	Woven	6	UD +30
2	UD 0	7	UD 0
3	UD +30	8	UD -30
4	UD 0	9	UD 0
5	UD -30	10	Woven

Table 8-1: Panel stacking sequence

Due to the rectangular aspect of the panel, cylindrical bending takes place under lateral pressure (Smith, 1990). Practically, the predominant response can be considered along the direction of the shorter span. It is argued that under this hypothesis, the material model used in chapter 7 is still suitable to describe the response of the layers made of unidirectional E-glass/epoxy forming an angle of $\pm 30^{o}$ with the direction of the shorter span (x direction in figure 8-6). This assumption is most viable in central sections of the panel.

Belingardi and Vadori, 2002 verified that woven E-glass/epoxy strain-rate sensitivity is negligible at rates of strain concerned with this application. It was therefore practical to model the woven layers by using an orthotropic material model based on their static material properties. The same material model was used to describe unidirectional layers forming a 0^{o} angle with the shorter span. As verified in the experiments, the modulus of elasticity was not affected by the strain-rates. As a result the static constitutive equation was still valid to describe their behaviour.

It has to be pointed out that the numerical investigation of the hull panel was led by assuming that the behaviour of E-glass/epoxy was the same in tension and compression as already discussed in chapter five. It can be disputed that in a sandwich panel under lateral loads, the inner skin undergoes tensile deformations while the outer skin undergoes compressive deformations. In addition, both skins may be under compression depending on the curvature of the panel. Ideally, the dynamic properties of the material both in compression and tension should be known while modelling composite structure problems. The assumption made was

practical considering that Rozicky, 2000 did not note significant difference between tensile and compressive response while testing the same material statically and at lower strain-rates.

8.4 Results analysis

The simulation was run for 0.05 seconds as after this time the pressure stabilizes towards the hydrostatic pressure (figure 8-4).

From the general response of the panel to the applied time-pressure load, no reaction to the initial peak load was noted. The duration of the peak is so small (around 3 msec) that the panel does not have the time to perceive the load and deform accordingly. This was in agreement with experimental observations by Hentinen and Holm, 1994 and Manganelli et al., 2003.

In-plane strain-rate values were computed in the composite skins. Strain-rates top values achieved in the composite skins ranged between 25 s^{-1} and 40 s^{-1}. The highest values were found in the centre of the outer skin part of the panel in the short span direction, whereas in the long span direction they were found to be around four times lower. The maximum strain-rate values registered in the inner skin varied between 5 s^{-1} and 28 s^{-1} (figure 8-6). Figure 8-6 and 8-7 show the strain-rate values in the shorter span direction, for a 30º layers in the inner and outer skin respectively, in six different positions from the edge towards the centre of the panel. These layers are the most crucial as they are the closest to their ultimate failure. In Particular, layer 8 at -30º in the inner skin was the closest to its ultimate strength.

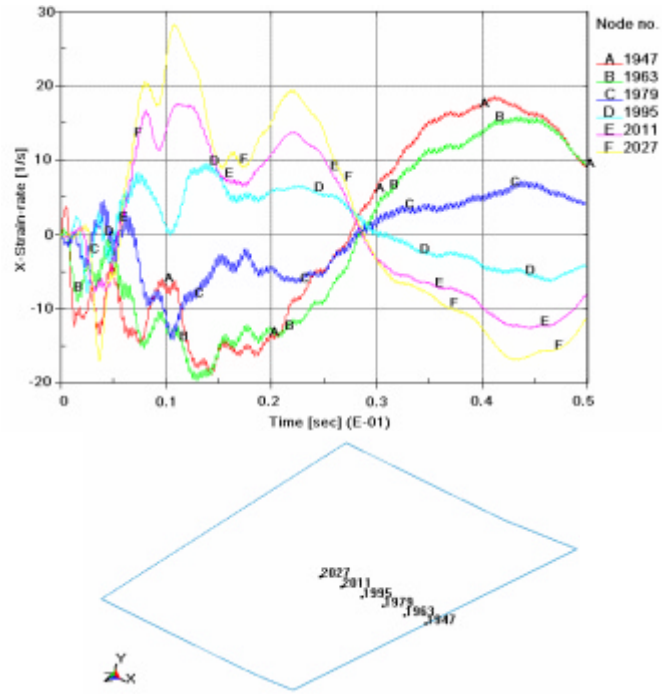

Figure 8-6: Strain-rate for ply 8 at -30º at different position in x direction

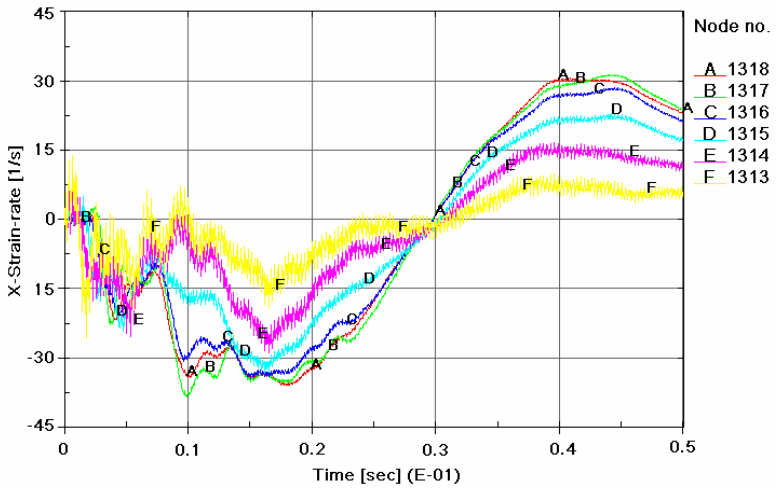

Figure 8-7: Strain-rate for ply 3 at +30º at different position in x direction

The highest stresses and strain were also found to be in the short span direction in accordance with the cylindrical bending effect. Figures 8-8 and 8-9 report the von-Mises versus time plots for the same plies as per figure 8-6 and 8-7, in six different positions from the edge towards the centre of the panel. The highest von-Mises stress was detected in the centre of the panel for the outer skin layers and was mainly due to the compressive deformation of the outer skin in the short span

direction. For the inner layer, the highest stress was in proximity of the clamped edge. Figure 8-10, 8-11 and 8-12 report the stress plots for all the plies and the core.

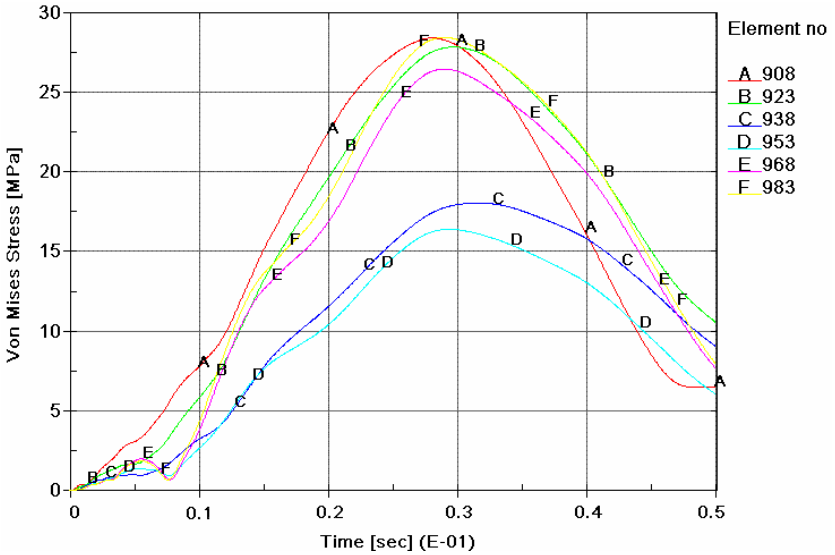

Figure 8-8: Von-Mises Stress for ply 8 at -30º in different elements in x direction

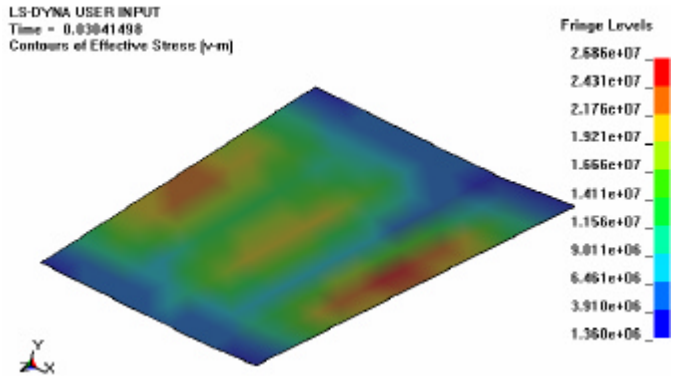

Figure 8-9: Von-Mises Stress plot for ply8 at -30º

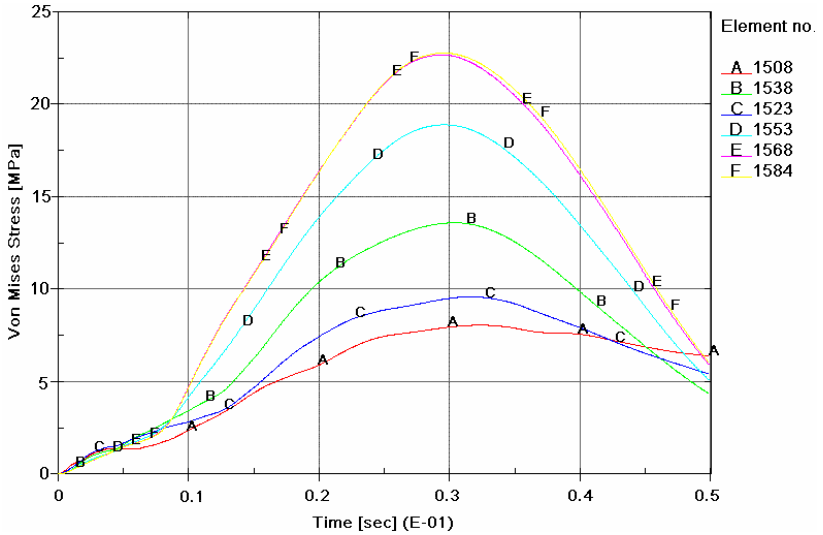

Figure 8-10: Von-Mises Stress for ply 3 at +30º in different elements in x direction

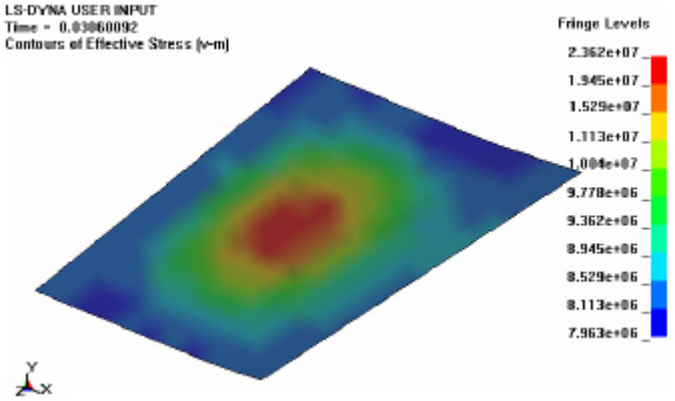

Figure 8-11: Von-Mises Stress plot for ply 3 at +30º

Figure 8-12: Von-Mises stress plots for plies 10, 9, 8, and 7.

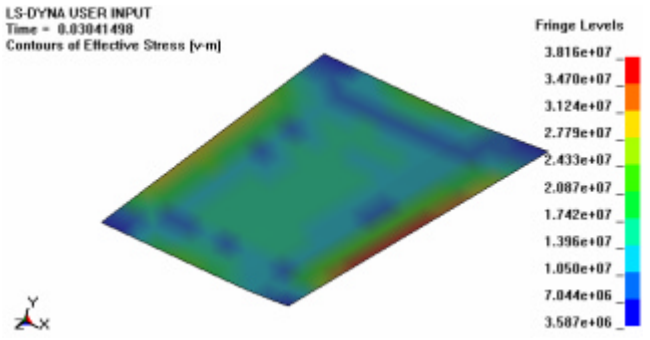

ply 10 (woven) inner skin

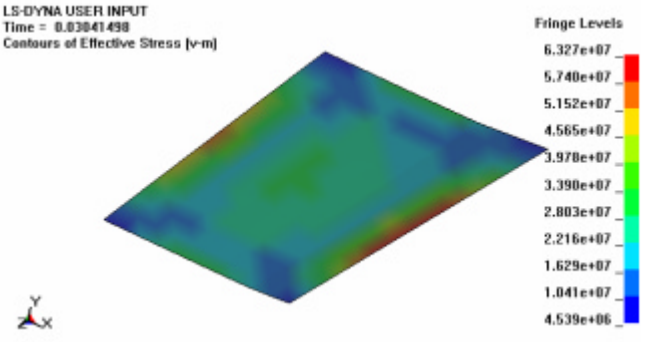

ply 9 (0°) inner skin

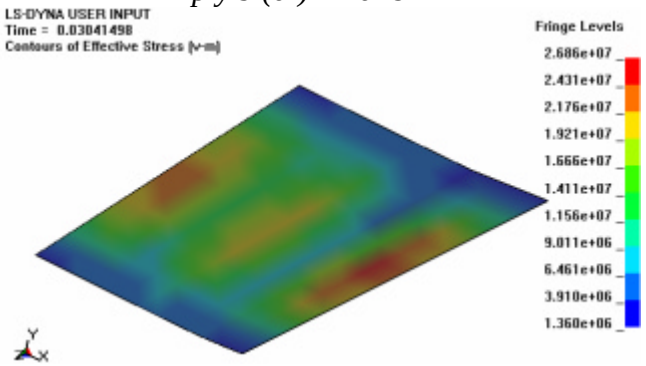

ply 8 (-30°) inner skin

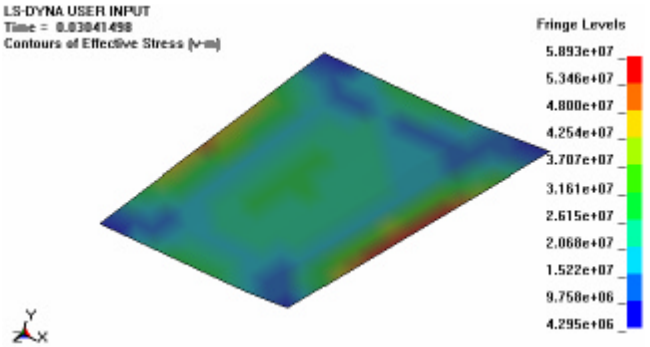

ply 7(0°) inner skin

Figure 8-13: Von-Mises plots for plies 6, 5, 4 and core

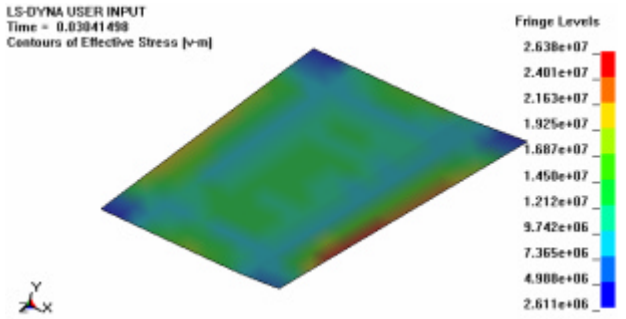

ply 6 (+30º) inner skin

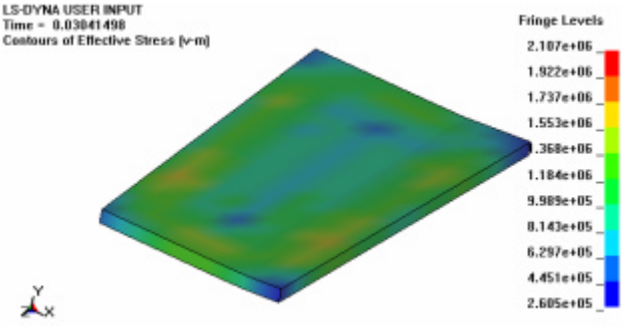

Core

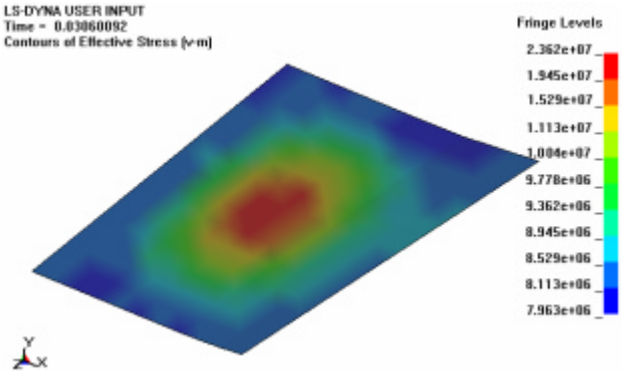

ply 5 (-30º) outer skin

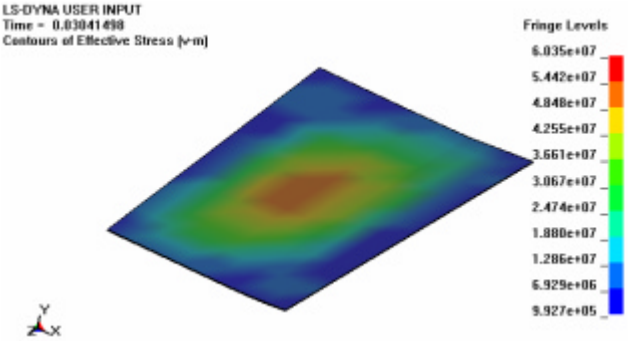

ply 4 (0º) outer skin

Figure 8-14:Von-Mises plots for plies 3, 2 and 1

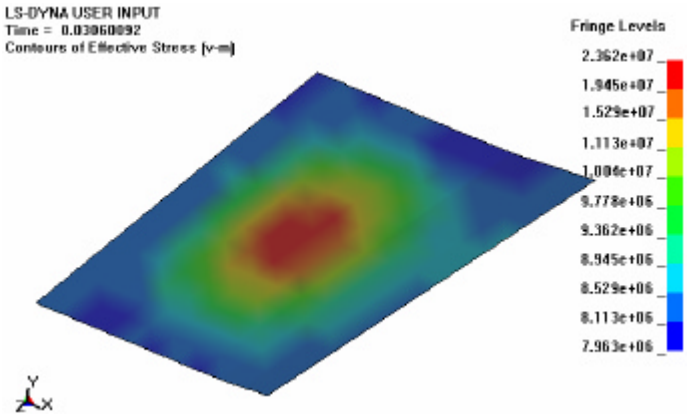

ply 3(+30º) outer skin

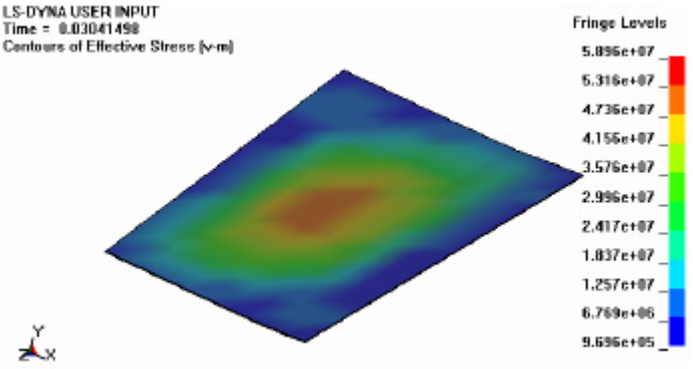

ply 2 (0º) outer skin

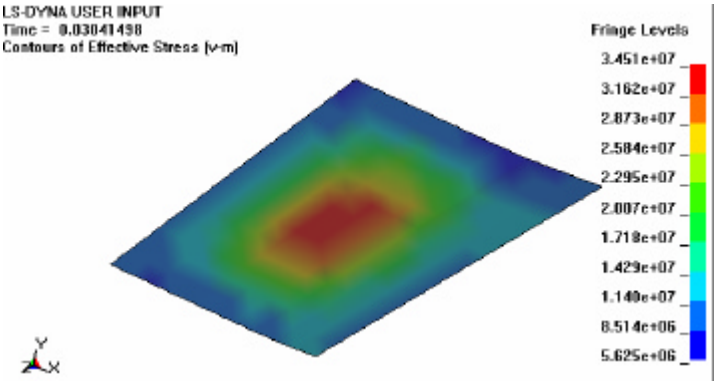

ply 1 (woven) outer skin

By looking at the strain-rate time and stress plots for ±30 deg layers, it is noted that after the peak load, both stress and strain-rate start to increase. When the applied pressure load starts to decrease (t = 0.025 s), stress and strain reach their peak values, while the strain-rate goes to zero (being the derivative of the strain with respect to the time). The strain-rate restarts to rise as the panel recovers its initial shape. In light of this, it can be said that during the loading and unloading phases a stiffening effect is noted for layers at 30º, as they deform at rates of strain up to $36s^{-1}$, values for which their Young's modulus was found to improve. As a result, the difference in stiffness between adjacent 0º and 30º layers is reduced and consequently it is the interlaminar stress. This can represent an important aspect regarding fatigue issues. All boats are subject in their lifetime to repetitive slamming loads which result in cyclic interlaminar stresses in the skins of their sandwich structures. The reduction of the difference in Young's modulus between diverse off-axis unidirectional layers, due to strain-rate effects, may result in improved fatigue behaviour. Numerous sandwich core failures observed during the end of Whitbread race took place during conditions which were not as heavy as those encountered during the whole race. This demonstrates that depending on their intensity and their frequency of occurrence, slamming loads can produce a structural failure either due to fatigue or because of the maximum stress being exceeded.

8.5 Comparison with Static Analysis

As anticipated in chapter two, nowadays boats are designed following the ISO standards rules which are based on a static approach. The following rules were applied to the yacht under consideration to calculate the dimensioning pressure load. Subsequently a static f.e. analysis was run on the panel by using ANSYS implicit finite element code. Finally results were compared with the dynamic analysis.

ISO standards state that the sailing craft bottom pressure (P_{bs}) is the greatest of:

$$P_{bs} = P_{bsbase} \cdot k_s \cdot k_l \cdot f_w \qquad \text{(eq.8.1)}$$

$$P_{bs} = 10 \cdot T_c + 0.83 \cdot L_H \cdot f_w \qquad \text{(eq.8.2)}$$

Where

$$P_{bsbase} = 36 \cdot T_c + 1.8 \cdot L_{WL} + 19.4 \qquad \text{(eq.8.3)}$$

T_c is the maximum draft of the canoe body, L_H the length of the hull and f_w a design category factor. According to this equation, the pressure value relative to the DK46 panel under investigation was calculated to be 46.8 kN/m^2. This pressure was applied to the panel for a static numerical simulation by use of ANSYS. The panel was modelled in three dimensions layer by layer by means of SOLID45, 8 nodes element. Composite layers were modelled by a linear orthotropic material model, whereas the core material was modelled by an isotropic material model. A first linear static simulation was run as a trial to assess if the structure was characterized by large deflections. The deflection of the panel registered was very small ($1.17*10^{-3}$m) if compared to the thickness of the panel, showing the absence of geometric nonlinearities and confirming that a linear analysis was adequate in this case. Maximum von-Mises stresses are reported in table 8.1 for both the static and the dynamic simulations. Relative plots are reported in Appendix 2.

Layers		**Von Mises Stress [MPa]**	
N	**Type**	**ANSYS**	**DYNA**
1	Woven	13.9	34.5
2	UD 0	37.8	58.9
3	UD +30	14.9	23.8
4	UD 0	37.9	60.4
5	UD -30	14.2	23.4
Core	SAN	1.5	2.1
6	UD +30	16.9	26.3
7	UD 0	38.9	58.9
8	UD -30	17.1	26.8
9	UD 0	39.0	63.2
10	Woven	21.9	38.2

Table 8-2: Comparison static and dynamic Von-Mises stresses

8.6 Discussion

By comparing the results from static and dynamic simulations, the following considerations can be drawn. The static analysis was carried out considering the slam pressure as an equivalent static load. In comparison, for the dynamic analysis a real pressure-time curve obtained by f.s.i. simulation was used. Stresses in the dynamic case were found to be higher than those predicted by the static case. The deflection was noted to be $1.82*10^{-3}$m in the dynamic and $1.17*10^{-3}$ m in the static case. The static analysis shows that the panel is built with a safety factor of 2.3 whereas the dynamic analysis shows a factor of 1.49. As a conclusion, the static approach design was thought to be more conservative than it really is. From a deeper look into the f.e.m. dynamic analysis the following observation can be suggested. The panel theoretical study showed that where laminates are used in conjunction with off-axis layers, the advantageous strain-rate properties of unidirectional composites along their fibre direction are not utilized. This is because their Young's modulus is not strain-rate sensitive. In other words, the laminate does not benefit from their improvement in ultimate strength as other layers reach their ultimate limit earlier. On the contrary, when used in off-axis lay-up they benefit from a stiffness improvement which is more tangible as the off-axis angle increases. As a result, the difference in stiffness between adjacent 0º and 30º layers is reduced and consequently the interlaminar stress is also reduced. Interlaminar movements are therefore more limited and crack initiation and propagation can be delayed. This can represent an important aspect regarding fatigue issues. All boats are subject in their lifetime to repetitive slamming loads which result in cyclic interlaminar stresses in the skins of their sandwich structures. The reduction of the difference in Young's modulus between diverse off-axis unidirectional layers due to the strain-rate effects, may result in improved fatigue behaviour as the relative movement between different layers is reduced.

Based on the static and dynamic f.e.m. comparative study, it can be said that from a performance point of view, there is room for improvement in terms of lighter structures to be designed. From the comparison between static and dynamic f.e.m. observations, it was noted that the structural design can be optimised using a

methodology based on the following fundamental steps. Firstly, the slam loads to be used in dimensioning the structure have to be predicted by fluid-structure interaction simulations. Then a first design trial has to be conducted and subsequently stresses have to be assessed by dynamic numerical simulation considering the strain-rate properties of the materials used. In this way the margin from the stress to failure of the structure is evaluated. Further design trials can be conducted by varying dimensions or lay-up sequence until a minimum safety factor is achieved.

Depending on their intensity and their frequency of occurrence, slamming loads can produce a structural failure either due to fatigue or because of the maximum stress being exceeded. The design methodology proposed, based on the knowledge of the dynamic properties and the use of f.e.m. tools, focused on investigating structural failures due to the maximum stress being exceeded. Nevertheless, in light of the considerations on interlaminar stress dependence on the strain-rate, it is suggested that fatigue failure should be investigated adopting a similar methodology. The knowledge of unidirectional E-glass/epoxy dynamic properties should be extended to more off-axis configuration for a full characterization of their behaviour. An adequate constitutive model capable of describing the strain-rate behaviour of unidirectional E-glass/epoxy under diverse off-axis loads should be considered and implemented in the code utilized to obtain more accurate results.

9 Conclusions and further work

9.1 Summary

This project aimed to provide a comprehensive overview of the dynamic response of a GRP sailing yacht sandwich hull panel subjected to slam loads. The overarching aim was to assess the influence of the dynamic properties of the materials utilized on the overall response of the panel. This was achieved as described in the following summary.

An experimental strain-rate campaign was conducted to assess the dynamic properties of unidirectional E-glass/epoxy. Within this campaign, a novel approach was proposed to conduct tensile strain-rate testing on composite materials by means of a servo-hydraulic machine fitted with a test rig purposely designed by the author. The material behaviour was characterized under diverse configurations used in yacht construction and over a strain-rate range typical of boats applications. Unidirectional E-glass/epoxy were noted to improve their ultimate strength and strain to failure more than two times the static value in all the configuration tested. In particular, an increase of up to 55% of the Young modulus was noted for off-axis configurations.

A systematic methodology was then proposed to describe the strain-rate behaviour of the material by LS-DYNA explicit finite element code. This methodology was subsequently applied to examine the response of a hull panel to a slam load.

The ALE (arbitrary Lagrangian-Eulerian) method, within LS-DYNA code, was used to model the fluid-structure interaction slam problem and to assess the relative entity of the load to be applied in the panel analysis. A static finite element analysis was also carried out based on the loads suggested by ISO design rules. ANSYS implicit finite element code was utilized for this purpose. Results were compared with the dynamic approach presented and the conservativeness of the static method was highlighted.

9.2 Modelling uncertainties

Representation of the experimental results in the numerical studies saw some assumptions and restrictions.

A constitutive model developed for isotropic materials which accounted for the strain-rate effects was used to describe the behaviour of unidirectional E-glass/epoxy observed in the experiments. It was argued that an isotropic material model in the element formulation was valid in this context since the structure was slender with high aspect ratio, with response in the long span direction being dependent principally on the material properties in that direction. The implicit assumption was that Poisson's effect owing to properties in the transverse direction were neglected. The use of this model was limited to describe the dynamic behaviour of the laminates only in the direction for which the properties of composites were observed. The skins of the sandwich panel were modeled by using this approach, with the argument that the predominant deformations were in the direction of the shorter panel span, with which the layers formed 0º and 30º angles as for the tested configurations. This approach is applicable only for panels having high long/short span aspect ratio. Ideally, an orthotropic material model capable of describing the strain-rate behaviour of unidirectional E-glass/epoxy under diverse off-axis loads should be considered and implemented in the code utilized.

Mechanical properties of E-glass/epoxy properties were assumed to be similar in tension and compression. This assumption was based on Rozicky's observations from testing the same material in tension and compression at low strain-rates.

Strain-rate properties of woven E-glass/epoxy were not part of the materials investigated experimentally in this research. It was generally verified (Belingardi and Vadori) for woven E-glass/epoxy that their strain-rate sensitivity is negligible at rates of strain concerned with this application. It was therefore practical to model the woven layers of the panel by using an orthotropic material model based on static material properties.

9.3 Conclusions and further work

The following conclusions were drawn after this study.

Developing the knowledge of both the dynamic properties of the materials and the use of tools such as explicit finite element codes was shown to be a valid approach to optimise the design of sailing structures under slam loads. A first step to account for composite strain-rate dependence in dynamic analysis by using LS-DYNA explicit finite element code was proposed. The use of ALE method within LS-DYNA code was verified to be suitable for the characterization of the slam loads.

From the comparison between static and dynamic f.e.m. observations it was established that the structural design can be optimised by following a methodology based on these fundamental steps. Firstly, the slam loads to be used in dimensioning the structure have to be predicted by f.s.i. simulations. Then a first design trial has to be conducted and subsequently stresses have to be assessed by dynamic numerical simulation considering the strain-rate properties of the materials used. In this way the margin from the stress to failure of the structure is evaluated. Further design trials can be conducted by varying dimensions or lay-up sequence until a minimum safety factor is achieved.

The panel theoretical study showed that where laminates are used in conjunction with off-axis layers, the advantageous strain-rate properties of unidirectional composites along their fibre direction are not utilized. This is because their Young modulus is not strain-rate sensitive. In other words, the laminate does not benefit from their improvement in ultimate strength as other layers reach their ultimate limit earlier. On the contrary, when used in off-axis lay-up they benefit from a stiffness improvement which is more tangible as the off-axis angle increases. As a result, the difference in stiffness between adjacent 0º and 30º layers is reduced and consequently it the interlaminar stress is also reduced. Interlaminar movements are therefore more limited and crack initiation and propagation can be delayed. This can represent an important aspect regarding fatigue issues. All boats are subject in their lifetime to repetitive slamming loads which result in cyclic interlaminar stresses in the skins of their sandwich structures. The reduction of the difference in Young modulus between diverse off-axis unidirectional layers due to the strain-

rate effects, may result in improved fatigue behaviour as the relative movement between different layers is reduced.

Depending on their intensity and their frequency of occurrence, slamming loads can produce a structural failure either due to fatigue or because of the maximum stress being exceeded. The design methodology proposed, based on the knowledge of the dynamic properties and the use of f.e.m. tools, focused on investigating structural failures due to the maximum stress being exceeded. Nevertheless, in light of the considerations on interlaminar stress dependence on the strain-rate, it is suggested that fatigue failure should be investigated adopting a similar methodology.

The knowledge of unidirectional E-glass/epoxy dynamic properties should be extended to more off-axis configurations for a full characterization of their behaviour. An adequate constitutive model capable of describing the strain-rate behaviour of unidirectional E-glass/epoxy under diverse off-axis loads should be considered and implemented in the code utilized.

APPENDIX 1: LS-DYNA governing equations and material models

Preliminaries

Consider the body shown in Figure A1-1. We are interested in time-dependent deformation in which a point in b initially at X*a* (*a* = 1, 2, 3) in a fixed rectangular Cartesian coordinate system moves to a point x*i* (*i* = 1, 2, 3) in the same coordinate system. Since a Lagrangian formulation is considered, the deformation can be expressed in terms of the convected coordinates Xa, and time t

$$x_i = x_i(X_a, t) \qquad \text{(eq.A1.1)}$$

At time t = 0 we have the initial conditions

$$x_i(X_\alpha, 0) = X_\alpha \qquad \text{(eq.A1.2)}$$

$$\dot{x}_i(X_\alpha, 0) = V_i(X_\alpha) \qquad \text{(eq.A1.3)}$$

where Vi defines the initial velocities.

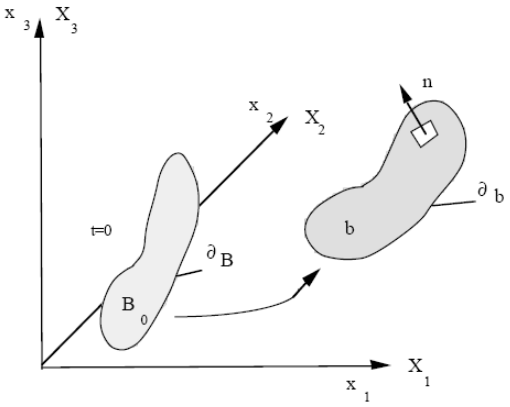

Figure A1-1: Notations

Governing equations

We seek a solution to the momentum equation:

$$\sigma_{ij,j} + \rho f_i = \rho \ddot{x}_i \qquad \text{(eq.A1.4)}$$

satisfying the traction boundary conditions:

$$\sigma_{ij} n_i = t_i(t) \qquad \text{(eq.A1.5)}$$

on boundary ∂b1, the displacement boundary conditions

$$x_i(X_\alpha, t) = D_i(t) \tag{eq.A1.6}$$

on boundary ∂b2, the contact discontinuity

$$\left(\sigma_{ij}^{+} - \sigma_{ij}^{-}\right) n_i = 0 \tag{eq.A1.7}$$

Here σ_{ij} is the Cauchy stress, ρ is the current density, *f* is the body force density, $\ddot{x}$ is acceleration, the comma denotes covariant differentiation, and nj is a unit outward normal to a boundary element of *∂b*.

Mass conservation is trivially stated

$$\rho V = \rho_0 \tag{eq.A1.8}$$

where V is the relative volume, i.e., the determinant of the deformation gradient matrix, Fij,

$$F_{ij} = \frac{\partial x_i}{\partial X_j} \tag{eq.A1.9}$$

and ρ0 is the reference density. The energy equation

$$\dot{E} = V s_{ij} \dot{\varepsilon}_{ij} - (p + q)\dot{V} \tag{eq.A1.10}$$

is integrated in time and is used for equation of state evaluations and a global energy balance. In Equation (A.1), sij and p represent the deviatoric stresses and pressure,

$$s_{ij} = \sigma_{ij} + (p + q)\delta_{ij} \tag{eq.A1.11}$$

$$p = -\frac{1}{3}\sigma_{ij}\delta_{ij} - q = -\frac{1}{3}\sigma_{kk} - q \tag{eq.A1.12}$$

respectively, q is the bulk viscosity, δij is the Kronecker delta (δij = 1 if i = j; otherwise δij = 0) and $\dot{\varepsilon}_{ij}$ is the strain rate tensor. The strain rates and bulk viscosity are discussed later.

We can write:

$$\int_v \left(\rho \ddot{x}_i - \sigma_{ij,j} - \rho f\right)\delta x_i d\upsilon + \int_{\partial b_1} \left(\sigma_{ij} n_j - t_i\right)\delta x_i ds$$

$$+\int_{\partial b_3}\left(\sigma_{ij}^{+}-\sigma_{ij}^{-}\right)n_j\delta x_i ds=0 \qquad \text{(eq.A1.13)}$$

where δx_i satisfies all boundary conditions on ∂b_2, and the integrations are over the current geometry. Application of the divergence theorem gives

$$\int_{\upsilon}\left(\sigma_{ij}\delta x_i\right)_{,j}\,d\upsilon=\int_{\partial b_1}\sigma_{ij}n_j\delta x_i ds+\int_{\partial b_3}\left(\sigma_{ij}^{+}-\sigma_{ij}^{-}\right)n_j\delta x_i ds \qquad \text{(eq.A1.14)}$$

and noting that

$$(\sigma_{ij}\delta x_i)_{,j}\;\sigma_{ij,j}\delta x_i=\sigma_{ij}\delta x_{i,j} \qquad \text{(eq.A1.15)}$$

leads to the weak form of the equilibrium equations:

$$\delta\pi=\int_{\upsilon}\rho\ddot{x}_i\,\delta x_i d\upsilon+\int_{\upsilon}\sigma_{ij}\delta x_{i,j}d\upsilon-\int_{\upsilon}\rho f_i\delta x_i d\upsilon-\int_{\partial b_1}t_i\delta x_i ds=0 \qquad \text{(eq.A1.16)}$$

a statement of the principle of virtual work.

We superimpose a mesh of finite elements interconnected at nodal points on a reference configuration and track particles through time, i.e.,

$$x_i\left(X_\alpha,t\right)=x_i\left(X_\alpha\left(\xi,\eta,\zeta\right),t\right)=\sum_{j=1}^{k}\phi_j\left(\xi,\eta,\zeta\right)x_i^j(t) \qquad \text{(eq.A1.17)}$$

where ϕ_j are shape (interpolation) functions of the parametric coordinates (ξ,η,ζ), k is the number of nodal points defining the element, and is x_{ij} the nodal coordinate of the jth node in the ith direction.

Summing over the n elements we may approximate $\delta\pi$ with

$$\delta\pi=\sum_{m=1}^{n}\delta\pi_m=0 \qquad \text{(eq.A1.18)}$$

and write

$$\sum_{m=1}^{n}\left\{\int_{\upsilon_m}\rho\ddot{x}_i\Phi_i^m d\upsilon+\int_{\upsilon_m}\sigma_{ij}^m\Phi_{i,j}^m d\upsilon-\int_{\upsilon_m}\rho f_i\Phi_i^m d\upsilon-\int_{\partial b_1}t_i\Phi_i^m ds\right\}=0 \qquad \text{(eq.A1.19)}$$

where

$$\Phi_i^m = \left(\phi_1, \phi_2, ..., \phi_k\right)_i^m \qquad \text{(eq.A1.20)}$$

In matrix notation Equation (A.19) becomes

$$\sum_{m=1}^{n}\left\{\int_{\upsilon_m} \rho \mathrm{N}^t \mathrm{N}\, a\, d\upsilon + \int_{\upsilon_m} \mathrm{B}^t \sigma\, d\upsilon - \int_{\upsilon_m} \rho \mathrm{N}^t \mathrm{b}\, d\upsilon - \int_{\partial b_1} \mathrm{N}^t \mathrm{t}\, ds\right\}^m = 0 \qquad \text{(eq.A1.21)}$$

where N is an interpolation matrix, σ is the stress vector

$$\sigma^{\mathrm{t}} = (\sigma_{xx}, \sigma_{yy}, \sigma_{zz}, \sigma_{xy}, \sigma_{yz}, \sigma_{zx}) \qquad \text{(eq.A1.22)}$$

B is the strain-displacement matrix, a is the nodal acceleration vector

$$\begin{bmatrix} \ddot{x}_1 \\ \ddot{x}_2 \\ \ddot{x}_3 \end{bmatrix} = \mathrm{N} \begin{bmatrix} a_{x_1} \\ a_{y_1} \\ \vdots \\ a_{y_k} \\ a_{z_k} \end{bmatrix} = \mathrm{N}\, a \qquad \text{(eq.A1.23)}$$

b is the body force load vector, and t are applied traction loads.

$$b = \begin{bmatrix} f_x \\ f_y \\ f_z \end{bmatrix}, \quad t = \begin{bmatrix} t_x \\ t_y \\ t_z \end{bmatrix} \qquad \text{(eq.A1.24)}$$

Solid Elements

For a mesh of 8-node hexahedron solid elements, Equation (A1.17) becomes:

$$x_i(X_\alpha,t) = x_i\left(X_\alpha(\xi,\eta,\zeta),t\right) = \sum_{j=1}^{8}\phi_j(\xi,\eta,\zeta)x_i^j(t) \qquad \text{(eq.A1.25)}$$

The shape function ϕ_j is defined for the 8-node hexahedron as

$$\phi_j = \frac{1}{8}\left(1+\xi\xi_j\right)\left(1+\eta\eta_j\right)\left(1+\zeta\zeta_j\right) \qquad \text{(eq.A1.26)}$$

where ξ_j, η_j, ζ_j take on their nodal values of (±1, ±1, ±1) and x_{ij} is the nodal coordinate of the *j*th node in the *i*th direction (see Figure A1.2).

For a solid element, N is the 3 × 24 rectangular interpolation matrix give by

$$\mathrm{N}(\xi,\eta,\zeta) = \begin{bmatrix} \phi_1 & 0 & 0 & \phi_2 & 0 & \cdots & 0 & 0 \\ 0 & \phi_1 & 0 & 0 & \phi_2 & \cdots & \phi_8 & 0 \\ 0 & 0 & \phi_1 & 0 & 0 & \cdots & 0 & \phi_8 \end{bmatrix} \qquad \text{(eq.A1.27)}$$

σ is the stress vector

$$\sigma^t = (\sigma_{xx}, \sigma_{yy}, \sigma_{zz}, \sigma_{xy}, \sigma_{yz}, \sigma_{zx}) \qquad \text{(eq.A1.28)}$$

B is the 6 × 24 strain-displacement matrix

$$\mathrm{B} = \begin{bmatrix} \frac{\partial}{\partial x} & 0 & 0 \\ 0 & \frac{\partial}{\partial y} & 0 \\ 0 & 0 & \frac{\partial}{\partial z} \\ \frac{\partial}{\partial y} & \frac{\partial}{\partial x} & 0 \\ 0 & \frac{\partial}{\partial z} & \frac{\partial}{\partial y} \\ \frac{\partial}{\partial z} & 0 & \frac{\partial}{\partial x} \end{bmatrix} \mathrm{N} \qquad \text{(eq.A1.29)}$$

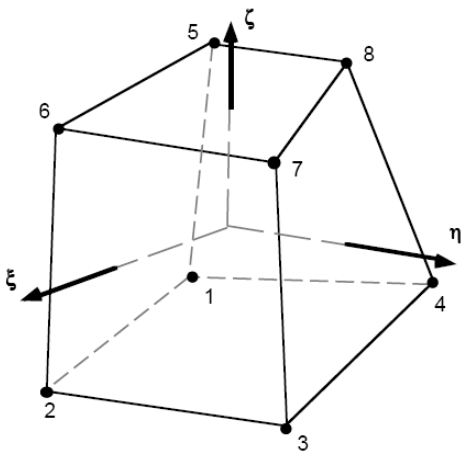

Node	ξ	η	ζ
1	-1	-1	-1
2	1	-1	-1
3	1	1	-1
4	-1	1	-1
5	-1	-1	1
6	1	-1	1
7	1	1	1
8	-1	1	1

Figure A1-2: 8 node solid hexahedron element

In order to achieve a diagonal mass matrix the rows are summed giving the kth diagonal term as

$$m_{kk} = \int_{\upsilon} \rho \phi_k \sum_{i=1}^{8} \phi_i d\upsilon = \int_{\upsilon} \rho \phi_k d\upsilon \qquad \text{(eq.A1.30)}$$

since the basis functions sum to unity.

Terms in the strain-displacement matrix are readily calculated. Note that

$$\begin{aligned}
\frac{\partial \phi_i}{\partial \xi} &= \frac{\partial \phi_i}{\partial x}\frac{\partial x}{\partial \xi} + \frac{\partial \phi_i}{\partial y}\frac{\partial y}{\partial \xi} + \frac{\partial \phi_i}{\partial z}\frac{\partial z}{\partial \xi} \\
\frac{\partial \phi_i}{\partial \eta} &= \frac{\partial \phi_i}{\partial x}\frac{\partial x}{\partial \eta} + \frac{\partial \phi_i}{\partial y}\frac{\partial y}{\partial \eta} + \frac{\partial \phi_i}{\partial z}\frac{\partial z}{\partial \eta} \\
\frac{\partial \phi_i}{\partial \zeta} &= \frac{\partial \phi_i}{\partial x}\frac{\partial x}{\partial \zeta} + \frac{\partial \phi_i}{\partial y}\frac{\partial y}{\partial \zeta} + \frac{\partial \phi_i}{\partial z}\frac{\partial z}{\partial \zeta}
\end{aligned} \qquad \text{(eq.A1.31)}$$

which can be rewritten as

$$\begin{bmatrix} \frac{\partial \phi_i}{\partial \xi} \\ \frac{\partial \phi_i}{\partial \eta} \\ \frac{\partial \phi_i}{\partial \zeta} \end{bmatrix} = \begin{bmatrix} \frac{\partial x}{\partial \xi} & \frac{\partial y}{\partial \xi} & \frac{\partial z}{\partial \xi} \\ \frac{\partial x}{\partial \eta} & \frac{\partial y}{\partial \eta} & \frac{\partial z}{\partial \eta} \\ \frac{\partial x}{\partial \zeta} & \frac{\partial y}{\partial \zeta} & \frac{\partial z}{\partial \zeta} \end{bmatrix} \begin{bmatrix} \frac{\partial \phi_i}{\partial x} \\ \frac{\partial \phi_i}{\partial y} \\ \frac{\partial \phi_i}{\partial z} \end{bmatrix} = J \begin{bmatrix} \frac{\partial \phi_i}{\partial x} \\ \frac{\partial \phi_i}{\partial y} \\ \frac{\partial \phi_i}{\partial z} \end{bmatrix} \qquad \text{(eq.A1.32)}$$

Inverting the Jacobian matrix, J, we can solve for the desired terms

$$\begin{bmatrix} \frac{\partial \phi_i}{\partial x} \\ \frac{\partial \phi_i}{\partial y} \\ \frac{\partial \phi_i}{\partial z} \end{bmatrix} = J^{-1} \begin{bmatrix} \frac{\partial \phi_i}{\partial \xi} \\ \frac{\partial \phi_i}{\partial \eta} \\ \frac{\partial \phi_i}{\partial \zeta} \end{bmatrix} \qquad \text{(eq.A1.33)}$$

Belytschko-Lin-Tsay Shell

The Belytschko-Lin-Tsay shell element ([Belytschko and Tsay 1981], was implemented in LS-DYNA as a computationally efficient alternative to the Hughes-Liu shell element. For a shell element with five through-the-thickness integration points, the Belytschko-Lin-Tsay shell elements requires 725 mathematical operations compared to 4066 operations for the under integrated Hughes-Liu element. The selectively reduced integration formulation of the

Hughes-Liu element requires 35,367 mathematical operations. Because of its computational efficiency, the Belytschko-Lin-Tsay shell element is usually the shell element formulation of choice. For this reason, it has become the default shell element formulation. The Belytschko-Lin-Tsay shell element is based on a combined co-rotational and velocitystrain formulation. The efficiency of the element is obtained from the mathematical simplifications that result from these two kinematical assumptions. The co-rotational portion of the formulation avoids the complexities of nonlinear mechanics by embedding a coordinate system in the element. The choice of velocity strain, or rate of deformation, in the formulation facilitates the constitutive evaluation, since the conjugate stress is the more familiar Cauchy stress. We closely follow the notation of Belytschko, Lin, and Tsay in the following development.

Co-rotational Coordinates

The midsurface of the quadrilateral shell element, or reference surface, is defined by the location of the element's four corner nodes. An embedded element coordinate system (see Figure A1-3) that deforms with the element is defined in terms of these nodal coordinates. Then the procedure for constructing the co-rotational coordinate system begins by calculating a unit vector normal to the main diagonal of the element:

$$\hat{e}_3 = \frac{s_3}{\|s_3\|} \qquad \text{(eq.A1.34)}$$

$$\|s_3\| = \sqrt{s_{31}^2 + s_{32}^2 + s_{33}^2} \qquad \text{(eq.A1.35)}$$

$$\mathrm{s}_3 = \mathrm{r}_{31} \times \mathrm{r}_{42} \qquad \text{(eq.A1.36)}$$

where the superscript caret $(\hat{\cdot})$ is used to indicate the local (element) coordinate system. It is desired to establish the local x axis $\hat{x}$ approximately along the element edge between nodes 1 and 2. This definition is convenient for interpreting the element stresses which are defined in the local $\hat{x}$–$\hat{y}$ coordinate system. The procedure for constructing this unit vector is to define a vector s_1 that is nearly parallel to the vector r_{21}, viz.

$$s_1 = r_{21} - (r_{21} \cdot \hat{e}_3)\hat{e}_3 \qquad \text{(eq.A1.37)}$$

$$\hat{e}_1 = \frac{s_1}{\|s_1\|} \qquad \text{(eq.A1.38)}$$

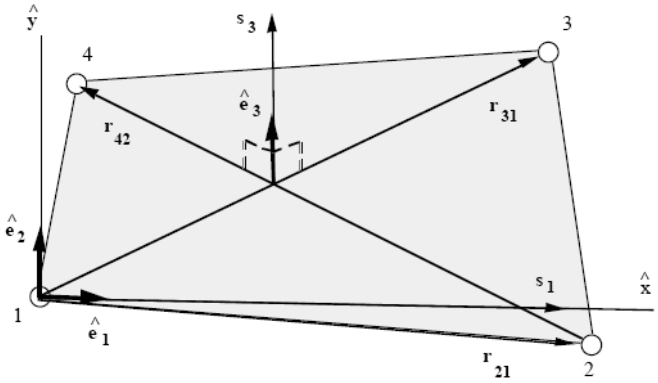

Figure A1-3: element coordinate system

The remaining unit vector is obtained from the vector cross product

$$\hat{e}_2 = \hat{e}_3 \times \hat{e}_1 \qquad \text{(eq.A1.39)}$$

If the four nodes of the element are coplanar, then the unit vectors e1 and e2 are tangent to the midplane of the shell and e3 is in the fiber direction. As the element deforms, an angle may develop between the actual fiber direction and the unit normal e3. The magnitude of this angle may be characterized as

$$\left|\hat{e}_3 \cdot f - 1\right| < \delta \qquad \text{(eq.A1.40)}$$

where f is the unit vector in the fiber direction and the magnitude of d depends on the magnitude of the strains. According to Belytschko et al., for most engineering applications acceptable values of d are on the order of 10-2 and if the condition presented in Equation A1.21 is met, then the difference between the rotation of the co-rotational coordinates e and the material rotation should be small.

The global components of this co-rotational triad define a transformation matrx between the global and local element coordinate systems. This transformation operates on vectors with global components A = (Ax, Ay, Az) and element coordinate components and is defined as;

$$\{A\} = \begin{Bmatrix} A_x \\ A_y \\ A_z \end{Bmatrix} = \begin{bmatrix} e_{1x} & e_{2x} & e_{3x} \\ e_{1y} & e_{2y} & e_{3y} \\ e_{1z} & e_{2z} & e_{3z} \end{bmatrix} \begin{Bmatrix} \hat{A}_x \\ \hat{A}_y \\ \hat{A}_z \end{Bmatrix} = [\mu]\{\hat{A}\} = [q]^T\{\hat{A}\}$$

(eq.A1.41)

where eix, eiy, eiz are the global components of the element coordinate unit vectors. The inverse transformation is defined by the matrix transpose, i.e.;

$$\{\hat{A}\} = [\mu]^T\{A\}$$

(eq.A1.42).

Simplified Arbitrary Lagrangian-Eulerian

Arbitrary Lagrangian-Eulerian (ALE) formulations may be thought of as algorithms that perform automatic rezoning (Winslow 1966, 1990). Users perform manual rezoning by

1. Stopping the calculation when the mesh is distorted,

2. Smoothing the mesh,

3. Remapping the solution from the distorted mesh to the smooth mesh.

An ALE formulation consists of a Lagrangian time step followed by a "remap" or "advection" step. The advection step performs an incremental rezone, where "incremental" refers to the fact that the positions of the nodes are moved only a small fraction of the characteristic lengths of the surrounding elements. Unlike a manual rezone, the topology of the mesh is fixed in an ALE calculation. An ALE calculation can be interrupted like an ordinary Lagrangian calculation and a manual rezone can be performed if an entirely new mesh is necessary to continue the calculation.

The accuracy of an ALE calculation is often superior to the accuracy of a manually rezoned calculation because the algorithm used to remap the solution from the distorted to the undistorted mesh is second order accurate for the ALE formulation while the algorithm for the manual rezone is only first order accurate.

In theory, an ALE formulation contains the Eulerian formulation as a subset. Eulerian codes can have more than one material in each element, but most ALE implementations are simplified ALE formulations which permit only a single material in each element. The primary advantage of a simplified formulation is its reduced cost per time step. When elements with more than one material are permitted, the number and types of materials present in an element can change dynamically. Additional data is necessary to specify the materials in each element and the data must be updated by the remap algorithms.

The range of problems that can be solved with an ALE formulation is a direct function of the sophistication of the algorithms for smoothing the mesh. Early ALE codes were not very successful largely because of their primitive algorithms for smoothing the mesh. In simplified ALE formulations, most of the difficulties with the mesh are associated with the nodes on the material boundaries. If the material boundaries are purely Lagrangian, i.e., the boundary nodes move with the material at all times, no smooth mesh maybe possible and the calculation will terminate. The algorithms for maintaining a smooth boundary mesh are therefore as important to the robustness of the calculations as the algorithms for the mesh interior.

The cost of the advection step per element is usually much larger than the cost of the Lagrangian step. Most of the time in the advection step is spent in calculating the material transported between the adjacent elements, and only a small part of it is spent on calculating how and where the mesh should be adjusted. Second order accurate monotonic advection algorithms are used in LS-DYNA despite their high cost per element because their superior coarse mesh accuracy which allows the calculation to be performed with far fewer elements than would be possible with a cheaper first order accurate algorithm.

The second order transport accuracy is important since errors in the transport calculations generally smooth out the solution and reduce the peak values in the history variables. Monotonic advection algorithms are constructed to prevent the transport calculations from creating new minimum or maximum values for the solution variables. They were first developed for the solution of the Navier Stokes equations to eliminate the spurious oscillations that appeared around the shock fronts. Although monotonic algorithms are more diffusive than algorithms that are not monotonic, they must be used for stability in general purpose codes. Many constitutive models have history variables that have limited ranges, and if their values are allowed to fall outside of their allowable ranges, the constitutive models are undefined. Examples include explosive models, which require the burn fraction to be between zero and one, and many elastoplasticity models, such as those with power law hardening, which require a non-negative plastic strain.

The overall flow of an ALE time step is:

1. Perform a Lagrangian time step.
2. Perform an advection step.
    a. Decide which nodes to move.
    b. Move the boundary nodes.
    c. Move the interior nodes.
    d. Calculate the transport of the element-centered variables.
    e. Calculate the momentum transport and update the velocity.

Each element solution variable must be transported. The total number of solution variables, including the velocity, is at least six and depends on the material models. For elements that are modeled with an equation of state, only the density, the

internal energy, and the shock viscosity are transported. When the elements have strength, the six components of the stress tensor and the plastic strain must also be advected, for a total of ten solution variables. Kinematic hardening, if it is used, introduces another five solution variables, for a total of fifteen. The nodal velocities add an extra three solution variables that must be transported, and they must be advected separately from the other solution variables because they are centered at the nodes and not in the elements. In addition, the momentum must be conserved, and it is a product of the node-centered velocity and the element-centered density. This imposes a constraint on how the momentum transport is performed that is unique to the velocity field. A detailed consideration of the difficulties associated with the transport of momentum is deferred until later.

Material Type 19: Strain Rate Dependent Isotropic Plasticity

In this model, a load curve is used to describe the yield strength as a function of effective strain rate, where the latter is:

$$\dot{\bar{\varepsilon}} = \left(\frac{2}{3} \dot{\varepsilon}'_{ij} \; \dot{\varepsilon}'_{ij} \right)^{\frac{1}{2}} \qquad \text{(eq.A1.43)}$$

and the prime denotes the deviatoric component. The yield stress is defined as

$$\sigma_y = \sigma_0 \left(\dot{\bar{\varepsilon}} \right) + E_p \; \bar{\varepsilon}^p \qquad \text{(eq.A1.44)}$$

where ε_p is the effective plastic strain and Ep is given in terms of Young's modulus and the tangent modulus by:

$$E_p = \frac{E \, E_t}{E - E_t} \; . \qquad \text{(eq.A1.45)}$$

Both Young's modulus and the tangent modulus may optionally be made functions of strain rate by specifying a load curve ID giving their values as a function of strain rate. If these load curve ID's are input as 0, then the constant values specified in the input are used. Note that all load curves used to define quantities as a function of strain rate must have the same number of points at the same strain rate

values. This requirement is used to allow vectorized interpolation to enhance the execution speed of this constitutive model.

This model also contains a simple mechanism for modeling material failure. This option is activated by specifying a load curve ID defining the effective stress at failure as a function of strain rate. For solid elements, once the effective stress exceeds the failure stress the element is deemed to have failed and is removed from the solution. For shell elements the entire shell element is deemed to have failed if all integration points through the thickness have an effective stress that exceeds the failure stress. After failure the shell element is removed from the solution.

In addition to the above failure criterion, this material model also supports a shell element deletion criterion based on the maximum stable time step size for the element, Δt_{max}. Generally, Δt_{max} goes down as the element becomes more distorted. To assure stability of time integration, the global LS-DYNA time step is the minimum of the Δt_{max} values calculated for all elements in the model. Using this option allows the selective deletion of elements whose time step Δt_{max} has fallen below the specified minimum time step, Δt_{crit}. Elements which are severely distorted often indicate that material has failed and supports little load, but these same elements may have very small time steps and therefore control the cost of the analysis. This option allows these highly distorted elements to be deleted from the calculation, and, therefore, the analysis can proceed at a larger time step, and, thus, at a reduced cost. Deleted elements do not carry any load, and are deleted from all applicable slide surface definitions. Clearly, this option must be judiciously used to obtain accurate results at a minimum cost.

Material Type 20: Rigid

The rigid material type 20 provides a convenient way of turning one or more parts comprised of beams, shells, or solid elements into a rigid body. Approximating a deformable body as rigid is a preferred modeling technique in many real world applications. For example, in sheet metal forming problems the tooling can properly and accurately be treated as rigid. In the design of restraint systems the occupant can, for the purposes of early design studies, also be treated as rigid. Elements which are rigid are bypassed in the element processing and no storage is

allocated for storing history variables; consequently, the rigid material type is very cost efficient.

Two unique rigid part ID's may not share common nodes unless they are merged together using the rigid body merge option. A rigid body may be made up of disjoint finite element meshes, however. LS-DYNA assumes this is the case since this is a common practice in setting up tooling meshes in forming problems.

All elements which reference a given part ID corresponding to the rigid material should be contiguous, but this is not a requirement. If two disjoint groups of elements on opposite sides of a model are modeled as rigid, separate part ID's should be created for each of the contiguous element groups if each group is to move independently. This requirement arises from the fact that LSDYNA internally computes the six rigid body degrees-of-freedom for each rigid body (rigid material or set of merged materials), and if disjoint groups of rigid elements use the same part ID, the disjoint groups will move together as one rigid body. Inertial properties for rigid materials may be defined in either of two ways. By default, the inertial properties are calculated from the geometry of the constitutent elements of the rigid material and the density specified for the part ID. Alternatively, the inertial properties and initial velocities for a rigid body may be directly defined, and this overrides data calculated from the material property definition and nodal initial velocity definitions. Young's modulus, E, and Poisson's ratio, u, are used for determining sliding interface parameters if the rigid body interacts in a contact definition. Realistic values for these constants should be defined since unrealistic values may contribute to numerical problem in contact.

Material Model 9: Null Material

This material allows equations of state to be considered without computing deviatoric stresses. Optionally, a viscosity can be defined. Also, erosion in tension and compression is possible. For solid elements equations of state can be called through this model to avoid deviatoric stress calculations. A pressure cutoff may be specified to set a lower bound on the pressure. This model has been very useful when combined with the reactive high explosive model where material strength is often neglected. The null material should not be used to delete solid elements.

A optional viscous stress of the form

$$\sigma_{ij} = \mu \dot{\varepsilon'}_{ij} \qquad \text{(eq.A1.46)}$$

is computed for nonzero μ where ε_{ij} is the deviatoric strain rate.

Sometimes it is advantageous to model contact surfaces via shell elements which are not part of the structure, but are necessary to define areas of contact within nodal rigid bodies or between nodal rigid bodies. Beams and shells that use this material type are completely bypassed in the element processing. The Young's modulus and Poisson's ratio are used only for setting the contact interface stiffnesses, and it is recommended that reasonable values be input.

Remarks

1. The null material must be used with an equation of-state. Pressure cutoff is negative in tension.

A (deviatoric) viscous stress is computed for nonzero μ where ε'_{ij} is the deviatoric strain rate. μ is the dynamic viscosity with unit of [Pascal*second].

2. The null material has no shear stiffness and hourglass control must be used with great care. In some applications, the default hourglass coefficient might lead to significant energy losses. In general for fluids, the hourglass coefficient QM should be small (in the range 1.0E-4 to 1.0E-6 in the SI unit system for the standard default IHQ choice).

3. The Null material has no yield strength and behaves in a fluid-like manner.

4. The pressure cut-off, PC, must be defined to allow for a material to "numerically" cavitate. In other words, when a material undergoes dilatation above certain magnitude, it should no longer be able to resist this dilatation. Since dilatation stress or pressure is negative, setting PC limit to a very small negative number would allow for the material to cavitate once the pressure in the material goes below this negative value.

Material Type 1.

This is an isotropic elastic material and is available for beam, shell, solid elements in LS-DYNA. A specialization of this material allows the modeling of fluids.

In this elastic material we compute the co-rotational rate of the deviatoric Cauchy stress tensor as:

$$s_{ij}^{\nabla^{n+½}} = 2G\dot{\varepsilon}_{ij}'^{n+½} \tag{eq.A1.47}$$

and pressure

$$p^{n+1} = -K \ln V^{n+1} \tag{eq.A1.48}$$

where G and K are the elastic shear and bulk moduli, respectively, and V is the relative volume, i.e., the ratio of the current volume to the initial volume.

Equation of State Form 1: Linear Polynomial

This polynomial equation of state, linear in the internal energy per initial volume, E, is given by

$$p = C_0 + C_1\mu + C_2\mu^2 + C_3\mu^3 + \left(C_4 + C_5\mu + C_6\mu^2\right)E \tag{eq.A1.49}$$

in which Ci are user defined constants and

$$\mu = \frac{1}{V} - 1\,. \tag{eq.A1.50}$$

where *V* is the relative volume. In expanded elements, the coefficients of μ^2 are set to zero, i.e.,

$$C_2 = C_6 = 0 \tag{eq.A1.51}$$

The linear polynomial equation of state may be used to model gas with the gamma law equation of state. This may be achieved by setting:

$$C_0 = C_1 = C_2 = C_3 = C_6 = 0 \tag{eq.A1.52}$$

And

$$C_4 = C_5 = \gamma - 1 \tag{eq.A1.53}$$

where γ is the ratio of specific heats. The pressure is then given by:

$$p = (\gamma - 1)\frac{\rho}{\rho_0}E \tag{eq.A1.54}$$

Note that the units of E are the units of pressure.

Equation of State Form 4: Gruneisen

The Gruneisen equation of state with cubic shock velocity-particle velocity defines pressure for compressed material as:

$$p = \frac{\rho_0 C^2 \mu \left[1 + \left(1 - \frac{\gamma_0}{2}\right)\mu - \frac{a}{2}\mu^2\right]}{\left[1 - (S_1 - 1)\mu - s_2 \frac{\mu^2}{\mu+1} - s_3 \frac{\mu^3}{(\mu+1)^2}\right]} + (\gamma_0 + \alpha\mu)E \qquad \text{(eq.A1.55)}$$

where E is the internal energy per initial volume, C is the intercept of the u_s-u_p curve, S_1, S_2, and S_3 are the coefficients of the slope of the u_s-u_p curve, γ_0 is the Gruneisen gamma, and a is the first order volume correction to γ_0. Constants C, S_1, S_2, S_3, γ_0, and a are all input parameters. The compression is defined in terms of the relative volume, V, as:

$$\mu = \frac{1}{V} - 1. \qquad \text{(eq.A1.56)}$$

For expanded materials as the pressure is defined by:

$$p = \rho_0 C^2 \mu + (\gamma_0 + \alpha\mu)E \qquad \text{(eq.A1.57)}$$

APPENDIX 2: Static F.E. Analysis by ANSYS

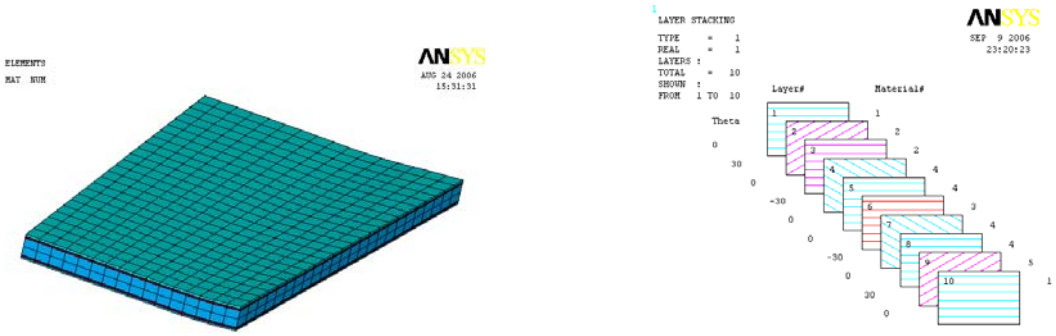

Figure A2-1: Panel Modeling and stacking sequence

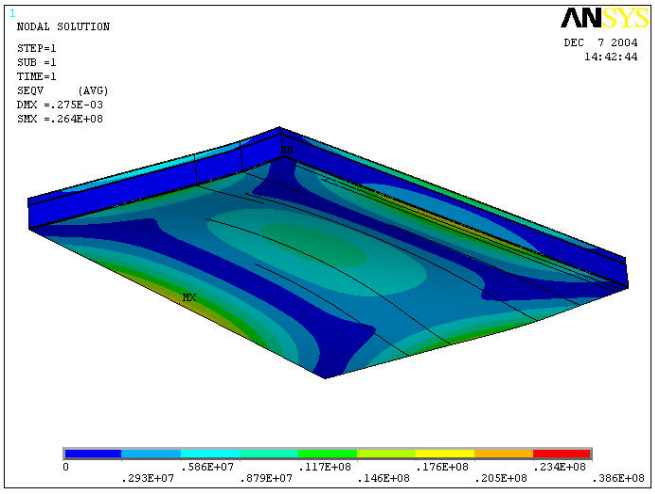

Figure A2-2: von-Mises stress whole panel

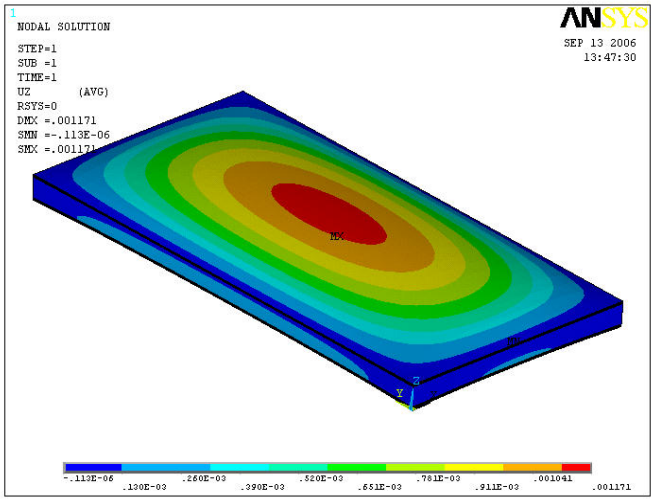

Figure A2-3: Panel deflection

The Stress contour of the most crucial layers are reported.

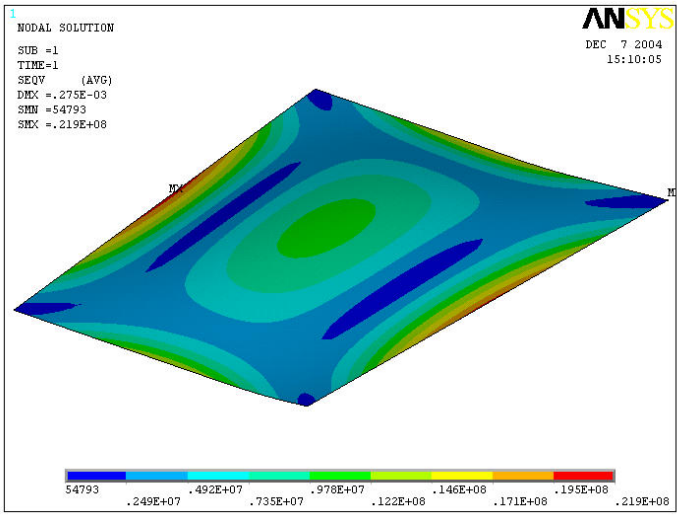

Figure A2-4: Von-Mises Layer 10 (Woven)

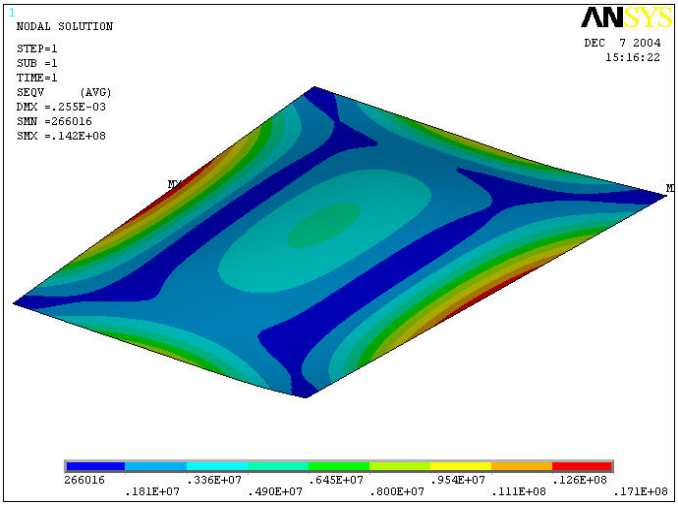

Figure A2-5: Von-Mises Layer 8 (-30º)

SOLID45 3-D ANSYS Structural Solid Element

SOLID45 is used for the three-dimensional modeling of solid structures. The element is defined by eight nodes having three degrees of freedom at each node: translations in the nodal x, y, and z directions. The element has plasticity, creep, swelling, stress stiffening, large deflection, and large strain capabilities. A reduced integration option with hourglass control is available.

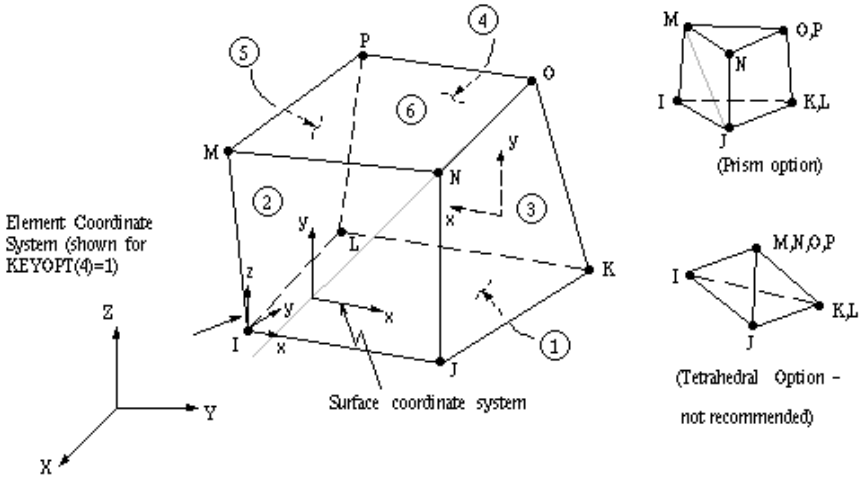

Figure A2-6: Solid 45 3-D Ansys structural element

APPENDIX 3: DK46 Yacht Data

Geometry, dimensions and material stacking sequence of the DK46 sailing yacht have been provided directly by the designer Mark Mills. The geometry has been imported from SolidWorks, commercial 3D modelling package, as an IGS file in Ls-DYNA and subsequently meshed.

Some of the key dimensions are reported beneath.

Length overall (L_{OA}) = 14.1 m

Length water line (L_{WL}) = 12.1 m

Max beam (Bmax) = 4.13 m

Draught (T) = 3m

Ballast 4309 Kg

Displacement 8300 Kg

Table A3-1: Sandwich Panel Materials & Stack Sequence

PLY	***Material***	***Thickness***
PLY 1	RE210P Plain Weave E-Glass cloth	0.208
PLY 2	UT-E500 @ 0	0.52
PLY 3	UT-E500 @ 30	0.52
PLY 4	UT-E500 @ 0	0.52
PLY 5	UT-E500 @ -30	0.52
CORE	Core cell A	25
PLY 6	UT-E500 @ 30	0.52
PLY 7	UT-E500 @ 0	0.52
PLY 8	UT-E500 @ -30	0.52
PLY 9	UT-E500 @ 0	0.52
PLY10	RE210P Plain Weave E-Glass cloth	0.310

The geometry of the panel has been built following these steps.

A drawing of the hull in Solidworks, provided by the designer, has been imported in Max Surf to determine the water lines and subsequently in LS-DYNA. Autocad drawings provided the exact geometry and location of the panel. In this way it was possible to define accurately the position and the geometry of the panel in LS-DYNA. Once the edge of the panel, corresponding to the outer layer, was defined it has been extruded in the y direction to create every single layer the panel was made of.

REFERENCES

ABS, *Guide for classing and building offshore racing yachts*, American Bureau of Shipping, New York, 1994.

Agbossou A., Cohen I. and Muller D., *Effects of interphase and impact strain rates on tensile off-axis behaviour of unidirectional glass fibre composite: experimental results*, Engineering Fracture Mechanics, Vol 52, No 5,pp 923-934, 1995.

Allen R.G., Jones R.R., *A simplified method for determining structural design limit pressures on high performance marine vehicle*, AIAA/SNAME Advanced marine Vehicle Conference, April 1978.

Armenakas A.E. and Garg S.K., *Strength characteristics of glass fibres under dynamic loading*, J. Applied Physics. 41 4, pp. 1657–1664, 1970.

Akil O., Yildirim U., Guden M. and Hall W., *Effect of the strain rate on the compression behaviour of a woven S2-glass fiber reinforced vinyl ester composite*, Polymer testing 22, 883-887, 2003.

ASTM D 3039-76 (reapproved 1989), *Standard test method for tensile properties of fiber-resin composites*, approved August 27, 1976, published October 1976, Annual Book of ASTM Standards, p.118-122, 1976.

Barrè S., Chotard T. and Benzeggagh M.L., *Comparative study of strain rate effects on mechanical properties of glass fibre-reinforced thermoset matrix composites*, Composites Part A 27A , 1169-1181, 1996.

Beguelin P., Barbezat M. and Kausch H., *Mechanical characterization of polymers and composites with a servohydraulic high-speed tensile tester*, Journal of Physics III France 1867-1880, 1991.

Belingardi G. and Vadori R., *Low velocity impact tests of laminate glass-fiber-epoxy matrix composite material plates*, International Journal of Impact Engineering 27 213–229, 2002.

Belytschko T. and Tsay C.S., *Explicit Algorithms for Nonlinear Dynamics of Shells*, AMD-Vol.48, ASME, 209-231, 1981.

Benson D. J. and Hallquist J.O., *A Simple Rigid Body Algorithm for Structural Dynamics Program*, International Journal of Numerical Methods in Engineering, 22, 1986.

Cappello F. and Mancuso A., *Lay-up optimization for the hull of a racing sailing yacht Advances in Engineering Software*, Volume 32, Issue 2, Pages 133-139, 2001.

Claughton A.R., Wellicome J.F. and Shenoi R.A., *Sailing Yacht Design, Practice*, Harlow: Addison Wesley Longman. Chapter 11: Composite engineering of sailing yacht structures, 1998.

Chacravarty U., Mauhfuz H., Saha M and Jeelani S., *Strain rate effects on sandwich core materials: en experimental and analytical investigation*. Acta Materialia, Volume 51, Number 5, pp. 1469-1479(11), March 2003.

Chandra R., Singh S.P. and Gupta K., *Micromechanical damping models for fiber-reinforced composites: a comparative study*, Composites: Part A 33, 787-796, 2002.

Clements B.S., Johnson J.N. and Hixson R.S., *Stress waves in composite materials*, Physical review, volume 54, number 6, Dicember 1996.

Cook R.D., Malkus D.S. and Plesha M.E., *Concepts and Applications of Finite Element Analysis*, 3rd Edition, John Wiley and Sons, 1989.

Coutellier D. and Rozycki P., *Multi-layered multi-material finite element for crashworthiness studies*, Composites Part A, 31, 841-851, 2000

Curry R., *Fiber reinforced plastics sailing yacht: some aspect of structural design*, The 9th CHESAPEAKE sailing yacht symposium, 1987.

Daniel L. and Liber T., *Testing fiber composites at high strain rates*, Proceedings 2nd International Conference on composite materials, pp1003-1018, Toronto 1978.

DNV, *High Speed and Light Craft. Classification Rules for High Speed Light Craft*, Det Norske Veritas Research AS, Veritasveien 1, N-1322 Høvik, Norway, 1991.

El-Magd E., *Simulation of material behaviour under dynamic loading*. Computers and Industrial Engineering 37, 195-198, 1999.

Gilat A., Goldberg R. and Roberts G., *Experimental study of strain-rate-dependent behaviour of carbon/epoxy composite*, Composite Science and Technology 62, 1469-1476, 2002.

Goldberg R.K. and Stouffer D.C., *High Strain Deformation Modeling of a Polymer Matrix Composite*, Part I, Matrix Constitutive Equations. NASA/TM-1998-206969, 1998 (a).

Goldberg R.K. and Stouffer D.C., *High Strain Rate Deformation Modeling of a Polymer Matrix Composite Part II-Composite Micromechanical Model*, NASA TM-1998-208664, 1998 (b).

Goldberg R.K. and Stouffer D.C., *Strain Rate Dependent Modeling of Polymer Matrix Composites*, NASA/TM-1999-209433, 1999.

Goldberg R.K., Roberts G. and Gilat A., *Incorporation of mean stress into the micromechanical analysis of the high strain rate response of polymer matrix composites*, Composites, Part B 34, 2003.

Hagiwara K. and T. Yuhara. *Study on Wave impact loads on ship bow*, Journal of the Society of Naval Architects of Japan, 140: 115-119, December, 1976.

Hamouda A.M.S. and Hashmi M.S.J.. *Testing of composite materials at rates of strain: advances and challenges*, Journal of material processing technology 77 327-336, 1998.

Harding J., *The effect of High Strain Rate on material properties*, Materials at high strain rate, Ed. T.Z.Blazinski. Chapter 4, Material at high strain rates, Elsevier Applied Science, London and New York, pp 133-157, 1987 (a).

Harding J., *Mechanical Properties of Fibre Reinforced Plastics at high rates of strain: testing techniques*, Chapter 4, Material at high strain rates, Ed. T.Z. Blazinski, Elsevier Applied Science, London and New York, pp 158-186, 1987 (b).

Harding J., *Effect of strain rate and specimen geometry on the compressive strength of woven glass-reinforced epoxy laminates*. Composites, vol 24,number 4, 323-332, 1993.

Harding J. and Welsh L.M., *A tensile testing technique for fibre-reinforced composites at impact rates of strain*, Journal of Materials Science, 18, pp. 1810–1826, 1983.

Hayes S.V. and Adams D.F., *Rate sensitive tensile impact properties of fully and partially loaded unidirectional composites*. Journal of Testing & Evaluation, Volume 10, Issue 2, Pages 61-68, ISSN: 0090-3973, March 1982.

Hentinen M. and Holm G., *Load measurement on the 9.4 m sailing yacht sail lab*, Proceedings, 13th International Symposium on "Yacht Design and Yacht Contstruction", Amsterdam, 14-15 November 1994.

Hiley M.J., Dong L. and J. Harding, *Effect of strain rate on the fracture process in interlaminar shear specimens of carbon fibre-reinforced laminates*, Composites Part A: Applied Science and Manufacturing, Volume 28, Issue 2, Pages 171-180, 1997.

Hobbs M. and McEwen M., *Working Load to break load: safety factors in composite structures*, Proceedings 17th International Symposium ion Yacht design and yacht construction, 2002.

Hosur M., J. Alexander, U. Vaidya and S.Jeelani *High Strain rate compression response of carbon/epoxy laminate composites*, Composite Structures 52, 405-417, 2001.

Hsiao H.M. and Daniel I.M., *Strain rate behavior of composite materials*, Composites Part B 29B, 521–533, 1998.

Instron, *VHS 8800 High rate testing machine user manual*, 2001.

ISO/TC, 188/WG 18. ISO/CD 12215-5.17, *Small Craft-Hull Constructions/Scantlings-Part 5: Design Pressures, Allowable Stresses, Scantling Determination*, International Standards Organization-SIS/SMS, Stockholm, 2006.

Jadhav A., Woldesenbet E. and Pang S., *High Strain rate response of balanced angle-ply graphite/epoxy composites*, Composites Part B, Engineering, Volume 34, Issue 4, Pages 339-346, 1 June 2003.

Johnsosn A.F., Pickett A. and Rozycki P, *Computational method for predicting impact damage in composite structures*, Composites Science and Technology 61 2183-2192, 2001.

Karman T., *The impact of seaplane Floats during Landing*, NACA TN 321, 1929.

Le Sourne H., Couty, N. and F. Besnier, *Three dimensional modelization of slamming impacts application to fast ships*, 4th European LS-DYNA Users Conference, 2003.

Larsson L. and Eliasson R.E., *Principles of Yacht design*, Adlard Coles Nautical, ISBN: 07136 5181 4, 2000.

LS-DYNA, *User Manual*, Livermore Software Technology Corporation, 1999.

Mahfuz H., Thomas T., Rangari V. and Jeelani J., *An innovative technique for measuring the high strain rate response of sandwich composites*, Composite Structures 50, 279-285, 2000.

Mahfuz H., Thomas T., Rangari V. and Jeelani J., *On the dynamic response of sandwich composites and their core materials*, Composites Science and Technology, xxx (2006) xxx–xxx (Article in press), 2006.

Manganelli P. and Wilson P.A., *An experimental investigation of slamming on ocean racing yachts*, the 15th Chesapeake sailing yacht symposium, 2001.

Manganelli P., Wagermakers B. and Wilson P.A., *Investigation of slamming loads using slam patches on a scale model of an Open 60' class yacht*, Royal Institution of Naval Architects Transactions Part B1 - International Journal of Small Craft Technology (IJSCT), 145, 47-62. (IJSCT603), 2003.

Marchant A., *Material and structures for high speed motor yachts*, Proceedings 13th International Symposium on Yacht design and Yacht construction, 1994.

Meyers M.R., Murr E.L., Staudhammer K.P. and Huang Z.P., *Shock wave and high-strain rate phenomena in material*, Proceedings of EXPLOMET 90, International Conference on the Materials Effects of Shock-Wave and High-Strain-Rate Phenomena, 1990.

NAFEMS, *Guidelines to Finite Element Practice*, National Association of Finite Element Methods and Standards, Department of Trade Industry UK, ISBN 0-903640-16-3, 1984.

NAFEMS, *Fundamentals of Numerical Techniques for Static, Dynamic and Transient Analyses – Part 2*, NAFEMS, National Association of Finite Element Methods &. Standards, on line publication, 2006.

NBS-VTT, *extended rules 1997*, VTT Manufacturing technology, 1996.

Ninan L., Tsai J. and Sun C. T., *Use of split Hopkinson pressure bar for testing off-axis composites*, International Journal of Impact Engineering, Volume 25, Issue 3, Pages 291-313, March 2001.

Norrie D.H. and Devries G., *An Introduction to Finite Element Analysis*, Academic Press, ISBN, 0 12 521660 2, 1978.

Ojeda R., Prusty B.G. and Salas M., *Finite element investigation on the static response of a composite catamaran under slamming loads*, Ocean Engineering, Vol 31, issue 7, 901-929, May 2004.

Okoli O.I. and Ainullotfi A.L., *Failure in composite laminates: overview of an attempt at prediction*, Composites Part A 33, 315-321, 2002.

Okoli O. and Smith G.F., *Development of a semi-empirical method for obtaining the dynamic Young's modulus in random continuous reinforced glass/epoxy composites*. Journal of Reinforced Plastics and Composites, 19 4, pp. 292–300, 2000 (a).

Okoli O. and Smith G.F., *The effect of strain rate and fibre content on the Poisson's ratio of glass/epoxy composites*, Composite Structures 48, 157-161, 2000 (b).

Olovsson, L. and Souli, M., *ALE and fluid-structure interaction capabilities in LS-DYNA*, Proceedings of 6th International LS-DYNA conference, 9-11 of April 2000.

Olovsson, L. and Souli, M., *Improoved fluid-structure capabilities in LS-DYNA*, Proceedings of 3rd European LS-DYNA conference, 18-19 of June 2001.

Pardo S., Bapsite D., Decpbert F., Fitoussi J. and Joannic R., *Tensile dynamic behaviour of a quasi-unidirectional E-glass/polyester composite*, Composites Science and Technology, 2002.

Peterson P.L, Pangborn R.N. and Pantano C.G., *Static and high strain rate response of glass fiber reinforced thermoplastic,* Journal of Composite Materials, Volume 25, Issue 7, Pages 887-906 ISSN: 00219983, 1991.

Riber H. J., *Response Analysis of Dynamically loaded composite panels,* PhD Theses Submitted at the Technical University of Denmark, June 1997.

Rotem A. and Lifshitz J.M., *Longitudinal Strength of Unidirectional fibrous composites under high rate of loading*, 26th Annual Technical Conference, Reinforced Plastics/Composites Division, The Society of the Plastics Industry, Inc. 1971.

Rozycki P., *Contribution au developpement de lois de comportement pour materiaux composites soumis a l'impact. PhD thesis*, presente a L'Universite de Valenciennes, 2000.

Saha M.C., Mahfuz H., Chakravarty U.K., Uddin M., Kabir M. E. and Jeelani S, *Effect of density, microstructure, and strain rate on compression behavior of polymeric foams*, Materials Science and Engineering A 406, 328–336, 2005.

Savitsky D., *Hydrodynamic Design of Planing Hulls*, Marine Technology, Octorber, 1964.

Sebastiani L., Valdenazzi F., Grossi L. and Kapsenberg G., *A theoretical/experimental investigation of the slamming pressure on fast monohull vessels*, FAST 2001, Southampton, UK September 2001.

Smith C.S., *Design of Marine Structures in Composite Materials*, Elsevier Applied Science, ISBN 1-85166-416-5, London, 1990.

Sohn M.S. and Hu X.Z, *Impact and high strain rate delamination characteristics of carbon-fibre epoxy composites,* Theoretical and Applied Fracture Mechanics 25, 17-29, 1996.

Souli M., Ouahsine A. and Lewin L., *ALE formulation for fluid-structure interaction problems*, Computer Methods in Applied Mechanics and Engneering, 190, 659-675, 2000.

Souli M., *Fluid-Structure Interaction in LS-DYNA": Industrial Applications,* Proceedings 4th European LS-DYNA Users Conference, Ulm, Germany, May 2003.

Tay T., Ang H. and Shim V., *An empirical strain rate-dependent constitutive relationship for glass-fire reinforces epoxy and pure epoxy*, Composite Structures 33, 201-210, 1995.

Thiruppukuzhi S.V. and Sun C.T., *Testing and modeling high strain rate behaviour of polymeric composites,* Composites Part B, 29B, 535-546, 1998.

Thiruppukuzhi S.V. and Sun C.T., *Models for the high strain-rate-dependent behaviour of polymer composites*, Composites Science and Technology 61, 1-12, 2001.

Thomas G., Davis M., Whela J. and Roberts T., *Slamming response of Large high speed Catamaran*, FAST 2001, Southampton, UK, September 2001.

Todo M., Tkahashi K., Beguelin P. and Henning Kausch H., *Strain rate dependence on the tensile fracture behaviour of woven-cloth reinforced polyamide composites*, Composite Science and Technology 60, 763-771, 2000.

Tsai J. and C.T. Sun, *Constitutive model for high strain rate response of polymeric composites*, Composites Science and technology 62, 1289-1297, 2002.

Tsai J. and Sun C. T., *Dynamic compressive strengths of polymeric composites*, International Journal of Solids and Structures, Volume 41, Issues 11-12, Pages 3211-3224, June 2004.

Vinson J.R. and Woldesenbet E., *Fiber Orientation Effects on High Strain Rate Properties of Graphite/Epoxy Composites*, Journal of Composite Materials, Vol.35, No.6, 509-521, 2001.

Vinson J.R., *The Behavior of Sandwich Structures of Isotropic and Composite Materials, Chapter 7: "Dynamic effects on sandwich panels"*. Technomic Publishing Company, ISBN 1-56676-699, 1999.

Vredeveldt A., Hoogeland M. and Janssen G., *Hydrodynamic impact response, a flexible view*, FAST 2001, Southampton, UK, September 2001.

Vural M. and Ravichandran G., *Dynamic response and energy dissipation characteristics of balsa wood: experiment and analysis*, International Journal of Solids and Structures 40, 2147–2170, 2003.

Walley S.M, Field J.E., Pope P.H. and Safford N.A., *The rapid deformation behaviour of various polymers*. Journal de Physique III, France 1, pp. 1889–1925, 1991.

Wang W., Makarov G. and Shenoi R.A., *An analytical model for assessing strain rate sensitivity of unidirectional composite laminates*, Composite Structures, Volume 69, Issue 1, Pages 45-54, June 2005.

Ward W.L., *Sailboat Impact Stresses*, The 8th CHESAPEAKE sailing yacht symposium, 1985.

Winslow A. M., *Equipotential Zoning of Two-Dimensional Meshes*, Journal of Computational Physics, Vol. 149, pp. 153-172, 1966.

Winslow A. M., *Equipotential Zoning of The Interior of a Three-Dimensional Mesh*, Report to LSTC, 1990.

Woldesenbet E. and J.R.Vinson, *Specimen Geometry Effects on the High Strain Rate Testing of Graphite/Epoxy Composites*, AIAA Journal, Vol.37, No.9, 1102-1106, 1999.

Zenkert D., *An Introduction to Sandwich Construction*, Chameleon Press LTD, London, 1995.

Zhao H., *Testing of Polymeric Foams at High and Medium Strain Rates*, Polymer Testing 16, 507-516, 1997.

Zhao R.., Faltinsen O. and Aarsnes J., *Water entry of arbitrary two dimensional sections with and without flow separation*, Proceedings of the Twenty first Symposium of Naval Hydrodynamics, Trondheim (Norway), Ed National Academy Press (Washington), pp 408-423, 1996.

Zheng X.H., Goldberg R.K., Binienda W.K. and Roberts G.D., *LS-DYNA Implementation of Polymer Matrix Composite Model Under High Strain Rate Impact*, 35th International Technical Conference, Dayton, OH, United States, 28 Sep. - 2 Oct. 2003 , 20030901; September 2003.

Zienkiewicz O.C. and Taylor R.L., *The Finite Element Method*, Vol.1: The Basis, 5th edition, Butterworth Heinemann, ISBN 0 7506 5049 4, 2000.